

Universiteit
Leiden
The Netherlands

Seismology of magnetars

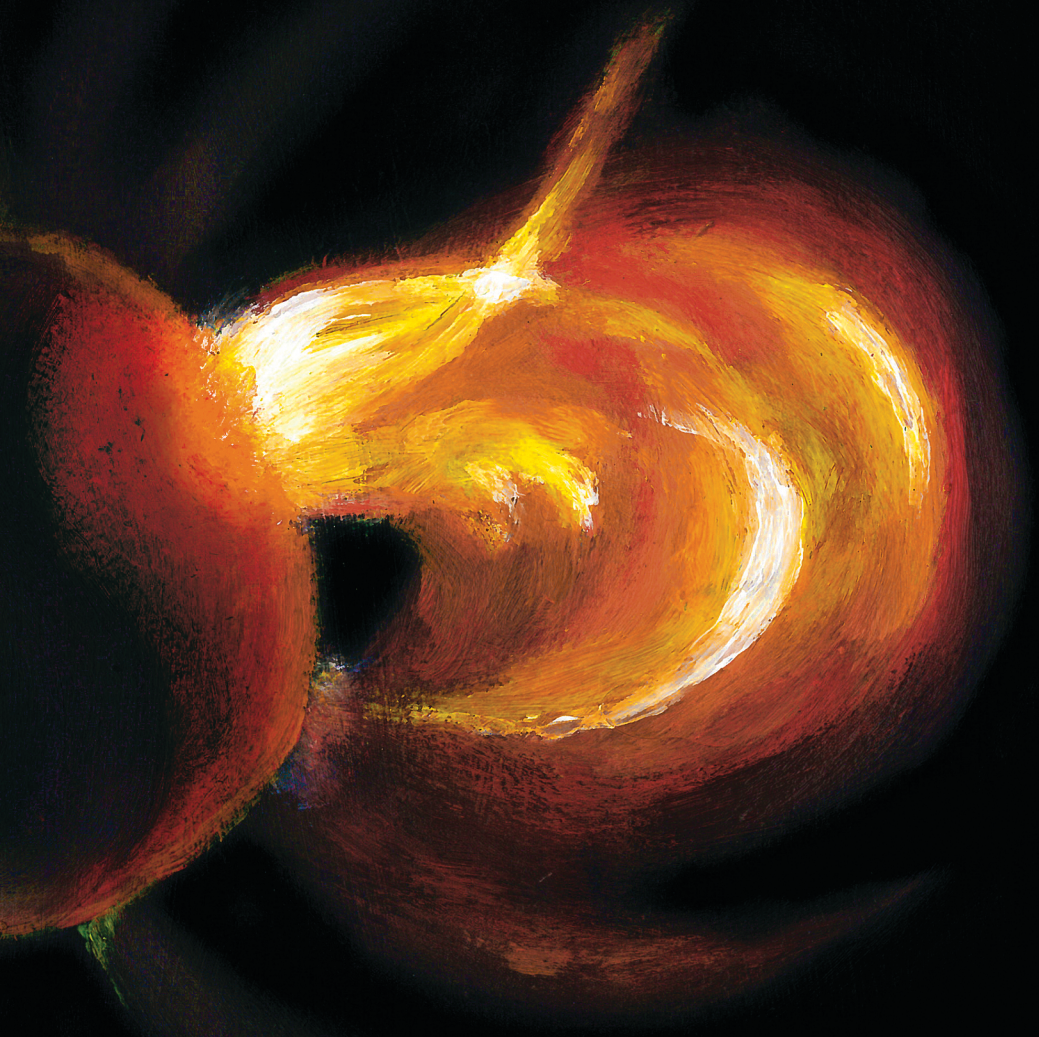
Hoven, M.B. van

Citation
Hoven, M. B. van. (2012, February 15). *Seismology of magnetars*. Retrieved from https://hdl.handle.net/1887/18484

Version:	Corrected Publisher's Version
License:	Licence agreement concerning inclusion of doctoral thesis in the Institutional Repository of the University of Leiden
Downloaded from:	https://hdl.handle.net/1887/18484

Note: To cite this publication please use the final published version (if applicable).

Seismology of Magnetars



M.B. van Hoven

Seismology of Magnetars

M.B. van Hoven

ISBN 978-94-6191-176-6
Cover by Harry Allaart & Maarten van Hoven

Seismology of Magnetars

PROEFSCHRIFT

ter verkrijging van
de graad van Doctor aan de Universiteit Leiden,
op gezag van de Rector Magnificus prof. mr. P. F. van der Heijden,
volgens besluit van het College voor Promoties
te verdedigen op woensdag 15 februari 2012
klokke 11.15 uur

door

Maarten Benjamin van Hoven
geboren te Leiden
op 7 juni 1981

Promotiecommissie

Promotor:

Prof. dr. K.H. Kuijken

Co-promotor:

Dr. Y. Levin (Universiteit Leiden/Monash University)

Overige leden:

Prof. dr. A.M. Beloborodov (Columbia University)

Prof. dr. K.D. Kokkotas (Eberhard Karls Universität Tübingen)

Prof. dr. F.W.M. Verbunt (Universiteit Utrecht)

Dr. A.L. Watts (Universiteit van Amsterdam)

This is how the world works. All energy flows according to the whims of the Great Magnet. What a fool I was to defy him.

HUNTER S. THOMPSON

Contents

Introduction **1**

History 1
Neutron stars 3
Magnetars 5
SGR giant flares and QPOs 7
Seismology of magnetars 9
This thesis 13
Chapter 1 13
Chapter 2 14
Chapter 3 15
Chapter 4 16
Acknowledgements 17

1 Hydromagnetic waves in a superfluid neutron star with strong vortex pinning **19**

Abstract 20
1.1 Introduction 21
1.2 Dispersion relations 25
1.3 Hydromagnetic waves in magnetars 28
1.4 Precession of neutron stars 29
1.4.1 Glaberson instability criterion 30
1.4.2 The maximum misalignment angle for fast precession . 31
1.5 Discussion 33
Acknowledgements 34

Appendix 1.A: Dispersion relation for arbitrary drag 35
Appendix 1.B: Instability criterion for non-zero viscosity 36

2 Excitation of f-modes and torsional modes by giant flares 39
Abstract 40
2.1 Introduction 41
2.2 The general formalism 42
2.2.1 Excitation by the EM 42
2.3 f-modes and gravitational waves 46
2.4 Torsional modes 48
2.4.1 Magnetic modes 49
2.5 Discussion 49
Acknowledgements 50
Appendix 2.A: Alternative derivation of the mode excitation 51
Appendix 2.B: Stellar oscillations 52

3 The strongly coupled dynamics of crust and core 55
Abstract 56
3.1 Introduction 57
3.2 An oscillator coupled to a continuum: edge modes 60
3.2.1 Time-dependent behavior. 61
3.2.2 Finding eigenmodes 65
3.2.3 Late time behavior of the system 67
3.2.4 The effect of viscosity 69
3.3 Transient and drifting QPOs 71
3.4 More realistic magnetar models 74
3.4.1 The model 75
3.4.2 The continuum 76
3.4.3 Results 82
3.5 Tangled magnetic fields 84
3.5.1 simple model: “square” neutron star 86
3.6 Discussion 92
Acknowledgements 96
Appendix 3.A: Multimodal crust-core system 97

Appendix 3.B: Core continua with a mixed toroidal-poloidal field . . 98

4 A spectral method for magnetar oscillations 101

Abstract . . . 102
4.1 Introduction . . . 103
4.2 Relativistic MHD equations . . . 106
4.3 Modes of a magnetized crust in General Relativity . . . 110
4.3.1 Magnetic force density in the free crust . . . 114
4.3.2 Relativistic equations for elastic forces . . . 115
4.3.3 The neutron star model . . . 117
4.3.4 Results . . . 118
4.4 Core continuum and the coupling between crust and core . . . 122
4.4.1 The continuum . . . 122
4.4.2 Equations of motion for the coupled crust and core . . . 125
4.4.3 Results . . . 129
4.5 Discussion . . . 132
Acknowledgements . . . 133
Appendix 4.A: Damped modes . . . 134

Bibliography 137

Nederlandstalige samenvatting 143

Het heelal in een notendop . . . 144
Het leven en sterven van een ster . . . 148
Neutronensterren . . . 152
Magnetars . . . 155
Oscillaties van sterren . . . 157
Seismologie van magnetars . . . 159
Hoofdstuk 1: Golven in de kern van een neutronenster . . . 161
Hoofdstuk 2: Het ontstaan van 'magnetarbevingen' . . . 164
Hoofdstukken 3 en 4: Een dynamisch model van een magnetar 166

Curriculum Vitae 171

Nawoord 173

Introduction

This thesis contains the results of a PhD project carried out during the past four and a half years at the University of Leiden. The basis for this work are four journal papers on the subject of magnetar seismology. The chapters 1, 2, 3 and 4 are completely or partly based on these articles.

In this introduction, a brief historical overview is given on the subject of neutron stars and in particular a special type of these objects; magnetars. The recent discovery of quasi-periodic oscillations during the afterglows of energetic outbursts on magnetars is reviewed and their importance for our understanding of neutron star interiors discussed.

History

By the end of the 1920s it seemed to many physicists that the physical picture of the structure of atoms was complete or at least nearly correct. Since Rutherford's discovery of the proton in 1918, it was commonly presumed that atoms consist of positively charged nuclei composed of protons and nuclear electrons (the only known sub atomic particles known at the time), surrounded negatively charged electrons circling around the nuclei in tight orbits. The energy levels and spectral frequencies for the hydrogen atom had been successfully reproduced by Schrödinger's quantum mechanical analysis in 1926. However, with the advent of this new quantum theory, the exact composition of the nucleus had become subject of debate. The existence of electrons in the tiny atomic nuclei seemed inconsistent with Heisenberg's un-

certainty principle. Moreover, results of nuclear spin measurements of the nitrogen-14 isotope, performed at Caltech in 1929 (Rasetti, 1929), were contradicting predictions of the Rutherford model. To all debate came an end when a series of particle scattering experiments led to the discovery of the neutron in 1932 by James Chadwick. In earlier experiments, German physicists Bothe and Becker (1929) and the French Irène and Frédéric Joliot-Curie (1932) had bombarded beryllium atoms with alpha particles and found that the beryllium gave off 'strongly penetrating radiation' as a result. This radiation, which the Joliot-Curies interpreted as high energy gamma-photons, was shown to be able to eject protons from a paraffin substrate. James Chadwick, highly sceptic about this interpretation, repeated the experiments at his Cambridge laboratory with beryllium and a number of other elements as targets and showed that the outcoming radiation had to consist of electrically neutral particles with a mass more or less the same as protons. The discovery of the neutron, which earned Chadwick the 1935 Nobel Prize in physics, solved all experimental discrepancies that existed within the old Rutherford model and changed our view of the nucleus dramatically.

In 1933, barely a year after the discovery of the neutron, astronomers Walter Baade from Mount Wilson Observatory and Fritz Zwicky from Caltech, presented some extraordinary new ideas at a scientific meeting at Standford University. Zwicky had been working on cosmic rays for a while and had proposed that these highly energetic particles originated from catastrophically exploding stars, which he called supernovae. Together with Baade, who notably had an encyclopedic astronomical knowledge and was aware of historical accounts of new, bright stars that suddenly appeared at the sky before fading away, Zwicky started working on his supernova idea (deGrasse Tyson & Soter, 2001). At the Stanford meeting, the two put forward the hypothesis that these supernovae were in fact the violent transitions from normal stars into an exotic type of compact objects existing almost entirely of neutrons. The amount of gravitational binding energy released during the collapse of a star to nuclear densities, they reasoned, would be sufficient to power the supernova.[1] The

[1] The possibility of stellar cores at nuclear densities was tentatively suggested a year earlier (short before the discovery of the neutron) by soviet physicist Lev Landau, who contemplated the physical nature of stellar equillibrium: "... the density of matter becomes so great that atomic

idea was met with skepticism and, perhaps partly due to Zwicky's unpopular character[1], didn't gain much acceptance among contemporary astrophysicists. In the years to follow Zwicky, attempting to convince the scientific community of his ideas, would pursue his research on supernovae, unsuccessfully. At the end of the 30s however, the idea of neutron stars, or more correctly compact stellar cores comprised of neutrons, gained some attention from theorists as it was thought that they were potential sources of stellar energy (Landau, 1938). In this line of thought, Robert Oppenheimer and George Volkoff in 1939 investigated the stability of these neutron cores and published the first hydrostatic model of neutron stars.[2] During the late 30s however, nuclear fusion processes became gradually understood and eventually recognized as the fundamental source of power in stars. And so it happened that neutron stars went out of fashion for the next couple of decades.

Until the late 60s neutron stars received little attention, due to their small sizes they were expected to be too faint to be observed by contemporary telescopes (Shapiro & Teukolsky, 1983). However, everything changed when Jocelyn Bell and Antony Hewish from Cambridge University discovered the first radio pulsar in 1967. It was soon realized that the new pulsating source had to be a neutron star.

Neutron stars

A typical neutron star has a mass between 1.2 and 2.0 $M_\odot$ inside a sphere of radius ~ 10 km. It is generally thought that the neutron star core consists of

nuclei come in close contact, forming one gigantic nucleus". Landau however, did not associate the formation of such "gigantic nuclei" with a catastrophic gravitational collapse of cores, but considered steadily growing dense cores inside ordinary stars as the source of stellar energy. (Landau, 1932, 1938)

[1] Zwicky used to call astronomers at Mount Wilson Observatory "spherical bastards", because "they were bastards no matter how you looked at them" (Kirshner, 2002). Also, Zwicky's relation with his German collaborator Baade, which he falsely accused of being a Nazi, was problematic to say the least. According to Bryson (2003), Zwicky threatened to kill Baade on at least one occasion.

[2] Much to Zwicky's dismay, the authors didn't give any reference to his work, even though Oppenheimer was a direct colleague at Caltech.

mixture of two quantum fluids; superfluid neutrons, which comprise roughly 95% of the mass and superconducting protons (see e.g. Link, 2007). The outer $\sim$ 1 km of the star forms a solid crust consisting of a lattice of heavy nuclei, which become more neutron rich at greater depth. In the inner portion of the crust, beyond a point called 'neutron drip', the neutrons leak out of the nuclei, forming a superfluid which coexists with the crustal solid. Neutron stars are penetrated by strong magnetic fields (in the wide range between 10^8 and 10^{15} G), which act to slow down the rotation of the stars: As the star rotates around its axis, the field lines which are anchored to the crust, rotate along with the star. In effect, angular momentum is transported from the star through the rotation induced magnetic stresses (Spitkovsky, 2006).

Although this standard picture is thought to be true for most neutron stars, the different astrophysical sources which are today identified as neutron stars vary wildly in their observational properties. Most types of neutron stars radiate in different parts of the electromagnetic spectrum with rotation rates spanning over three orders of magnitude. Some neutron stars show violent activity in the form of energetic outbursts, while others appear to lead quiet lifes. The largest subclass of neutron stars are the radio pulsars (PSR), which are best observed at radio wavelengths but are also known to pulsate in other frequency bands. A sub-class of radio pulsars are the millisecond pulsars (MSP), which are characterized by their fast rotation, which in many cases seems to originate from accretion powered spin-up. This spin-up might occur during a phase where the neutron star forms a low mass X-ray binary (LMXB): The companion star transfers angular momentum through accretion to the neutron star, which can theoretically spin up to millisecond periods. The persistent radio emission from both PSRs and MSPs is thought to be powered by the rotational energy loss due to magnetic spin-down. Yet another class of radio pulsars are the recently discovered rotating radio transients (RRAT), which seem to switch on and off in an unpredictable manner.

With the rapid developments of X-ray astronomy in the past decade, new varieties of isolated objects have been added to the list of neutron stars. These include the X-ray bright compact central objects (CCO) directly associated

with supernova remnants (see e.g. Pavlov, Sanwal & Teter, 2004) and the anomalous X-ray pulsars (AXP) and soft gamma repeaters (SGR) (see e.g. Woods & Thompson, 2004). As can be seen in the P-$\dot{P}$ diagram of figure 1, the AXPs and SGRs having long rotation periods and fast spin-down, form a distinct group of objects relative to the bulk of pulsars. Their extreme spin properties can be explained by tremendously strong (dipole) magnetic field strengths ($B = 10^{14} - 10^{15}$ G). Moreover, their quiescent X-ray luminosities exceed the energy loss due to spin-down by orders of magnitude, implying that instead they might be powered by the decay of a very strong magnetic field. Hence AXPs and SGRs are often referred to as 'magnetar candidates'.

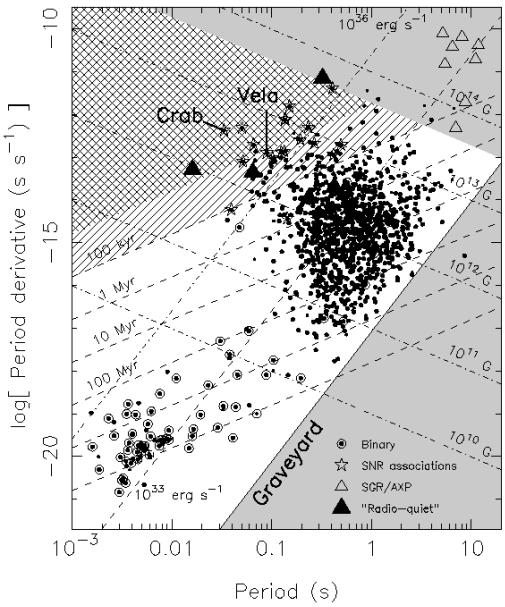


Figure 1: *P-$\dot{P}$ diagram for pulsars. The straight lines in the plot indicate the lines of constant age, the dipolar magnetic field strength and the spin-down luminosity. The grey region indicates areas where radio pulsars are not expected. Magnetar candidates, i.e. AXPs and SGRs are indicated with transparant triangles and are clearly separated from the main distribution of pulsars. (Reproduced with permission from "Handbook of Pulsar Astronomy" by Lorimer & Kramer, 2004.)*

Magnetars

The existence of magnetars was first hypothesized in the early 90s by Duncan & Thompson (1992), who studied dynamo mechanisms in newly born neutron stars. In their famous 1992 paper, they argued that during the first few moments after gravitational collapse, under the right circumstances, a

neutron star might be subject to very efficient dynamo action. The first 30 seconds after its formation, strong temperature gradients in the neutron star will drive a strong convection driven by the large neutrino flux. The strong convection, in combination with a very rapid spin ($P \sim 1$ ms) will lead to a very efficient $\alpha - \Omega$ dynamo which could easily amplify the magnetic field to values $B > 10^{15}$ G, at least 3 orders of magnitude stronger than the field strength of an ordinary pulsar. Another possible formation scenario for magnetars, is that they form during the collapse of a strongly magnetized massive star (Thompson & Duncan, 1993) or during the accretion induced collapse of a strongly magnetized white dwarf (Usov, 1992). In these cases, 10^{15} G magnetic fields could be established as a result of conservation of magnetic flux.

Since the early 1990s, it is thought that SGRs and AXPs are neutron stars powered by the decay of very strong magnetic fields. In contrast to radio pulsars, which are powered by the loss of rotational energy, SGRs and AXPs have quiescent luminosities exceeding their spin-down power, indicating that some other source of energy must be at work. Moreover, the SGRs in particular are known to be highly active, showing irregularly recurring short (0.1 s), energetic ($\sim 10^{41}$ erg s^{-1}) outbursts of X-rays and gamma-rays. As Thompson and Duncan (1995) pointed out, several independent arguments support the idea that SGRs are neutron stars with ultra-strong magnetic fields ($10^{14} - 10^{15}$ G); magnetars.[1] Ultra-strong magnetic fields would explain the spin properties and quiescent X-ray luminosities of SGRs. Other arguments in favor of ultra-strong magnetic fields are based on the properties of an extremely energetic outburst (*Giant Flare*) from the source SGR 0526-66, measured on March 5th 1979. This outburst was in fact so energetic, that if it was powered by the decay of a magnetic field, the field has to be $> 10^{15}$ G. On the other hand, similarly strong magnetic fields are required to confine the amount of energy in the tail of the burst and to reduce Compton scattering cross-sections, ex-

[1] Compelling observational evidence for this hypothesis was found by Kouveliotou et al. (1998), who observed X-ray pulsations with a period of 7.5 s for the soft gamma repeater SGR 1806-20. This discovery provided a 'missing link' between SGRs and the persistently pulsating AXPs. It is now generally accepted that both types of sources are magnetars.

plaining the measured hyper-Eddington fluxes (Paczyński, 1992; Thompson & Duncan, 1995). Another interesting observation is that all known magnetar candidates known to date[1] are isolated sources. In their 1992 paper on the formation of magnetars, Duncan and Thompson argued that during the formation several magnetically induced mechanisms could generate large recoil velocities ($\sim$ 1000 km s^{-2}), easily sufficient to unbind the magnetar from a possible companion star.

SGR giant flares and QPOs

On January 7th 1979 the first soft gamma repeater (SGR) was observed with gamma-ray sensors aboard the Soviet Venera 11 space craft, which detected a short, intense burst of soft gamma-rays coming from a source that was identified as a gamma ray burst (then named GB 790107, but now known as SGR 1806-20) (Mazets & Golenetskii, 1981). The January 7th event was followed by an extremely energetic flare on March the 5th that same year from another source. This event, had a peak luminosity roughly three orders of magnitude brighter than the one on January 7th and was followed by 3 minute exponentially decaying afterglow. In the months following the flare, the position of the source (SGR 0526-66) was accurately determined to be near the edge of a young supernova remnant located in the Large Magellanic Cloud (Evans et al., 1980), the distance to the source implying a peak luminosity of 10^{44} erg s^{-1}. Initially, both the January 7th and March 5th events were classified as Gamma Ray Bursts (GRB), but when in late 1983 more bursts occurred from SGR 1806-20, it became clear that this source had to belong to an independent class of objects; Soft Gamma Repeaters (SGR)[2] (Laros et al, 1987).

[1] To date a total of 16 magnetars are known. 7 Candidate sources are awaiting confirmation: 11 SGRs (7 confirmed, 4 candidates) and 12 AXPs (9 confirmed, 3 candidates). See http://www.physics.mcgill.ca/∼pulsar/magnetar/main.html

[2] The distinction between SGRs and GRBs was made due to the repetitive nature of flares: GRBs have never been found to repeat. Also, SGRs flares are characterized by their short duration ($0.1 - 0.2$ s) and relatively soft gamma-ray spectrum, with respect to GRBs.

Giant flares, such as the March 5th 1979 event on SGR 0526-66, are the

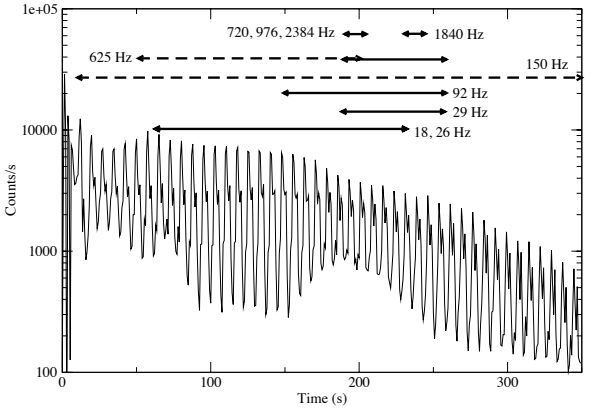


Figure 2: *Light curve showing the X-ray intensity during the afterglow of the December 2004 event from SGR 1806-20. At different time intervals during the afterglow, QPOs at various frequencies are measured as indicated by the arrows. The steady periodic modulations of the curve are due to the* 7.5 s *spin period of the star. (Reproduced with permission from Strohmayer & Watts, 2006.)*

most energetic bursts occurring on soft gamma repeaters. They are characterized by the sudden release of $> 10^{44}$ erg in hard X-rays during an initial spike of a few tenths of a second, followed by a spectrally softer, decaying, pulsating afterglow, lasting for several minutes. To date, only three such energetic events have been observed, of which the flare on December 27th 2004 from SGR 1806-20 was by far the most powerful, with a peak luminosity of $> 10^{47}$ erg s^{-1}. These events are thought to be powered by a catastrophic global reconfiguration of the magnetic field. Two possible mechanisms that could trigger such a reconfiguration are: (1) An internal mechanism: The strongly wound up internal magnetic field stresses the crust until an instability develops and the crust cracks (Thompson & Duncan, 1995, 2001). (2) An external mechanism: Due to a slow shearing motion of the magnetic footpoints, stresses build up in the magnetospheric field, eventually leading to a

fast reconnection event (Lyutikov, 2006; Gill & Heyl, 2010).[1]

Since the magnetic field is frozen into the solid magnetar crust, it is reasonable to believe that a fast global reconfiguration of the magnetic field triggers strong crustal vibrations. We explore the excitation of magnetar oscillations in chapter 2 of this thesis.

A remarkable discovery was made in 2005, when the analysis of the December 2004 giant flare on SGR 1806-20, revealed the presence of quasi periodic oscillations (QPOs) in the 3 minute afterglow following the event (Israel et al., 2005; Watts & Strohmayer, 2006; Strohmayer & Watts, 2006)[2]. Clear QPOs were found at several frequencies, ranging from 18 Hz to 1800 Hz, showing up at different time intervals during the afterglow (see figure 2). Following this discovery, QPOs at similar frequencies were also found in the 1998 giant flare from SGR 1900+14 (Strohmayer & Watts, 2005). Interestingly, the QPOs in both events appear at specific rotational phases of the stellar rotation, implying an association of the QPOs with specific areas of the neutron star surface or magnetosphere (Watts & Strohmayer, 2006). The physical origin of QPOs is generally believed to be torsional oscillations of the magnetar, which are relatively easy to excite (Duncan, 1998; Levin & van Hoven, 2011; chapter 2 of this thesis). Clearly, a proper explanation of the observed QPOs may give a unique insight in the interior structure of neutron stars.

Seismology of magnetars

In the past decades, the study of stellar oscillations has been a major force driving the advance of knowledge of the interior structures of stars. For example, the extraordinary wealth of oscillation data that exists for the Sun, has provided detailed information about its internal structure and rotation,

[1] The fast rise time (few microseconds) of the 2004 flare, gives reason to believe that the external mechanism is at play, as the internal mechanism works on the much longer Alfvén crossing time ($\sim$ 0.1 s).

[2] A pulsating component in the light curve of the March 1979 event on SGR 1806-20 was reported in Barat et al., 1983

as well as its chemical composition. Despite the relative scarcity of detected oscillation modes in stars other than our Sun, the study pulsating stars, e.g. RR-Lyrae variables, Delta Scuti stars and Cepheids, has led to considerable understanding of their internal structures and physical processes.

Our current understanding of neutron star interiors however, is much more uncertain. Observed oscillation modes of a neutron star, would greatly help to constrain basic properties like the equation of state, or crustal composition. In the past decades, oscillations of neutron stars have been subject of extensive theoretical study (see e.g. a review by Kokkotas & Schmidt, 1999) and it has become clear that general relativistic effects play an important role in oscillating neutron stars. Some types of modes couple strongly to the space-time continuum and damp on relatively short time scales by emitting gravitational waves. Andersson & Kokkotas (1998) showed that a single observed f-mode and its damping time would be sufficient to determine the mass and radius of the neutron star with errors of only a few percent. Other modes, in particular the r-modes, might be subject to the CFS (Chandrasekhar-Friedman-Schutz) mechanism, which causes a gravitational wave-driven instability (Chandrasekhar, 1970; Friedman & Schutz, 1978; Andersson & Kokkotas, 2001). Clearly, the strong coupling of neutron star oscillations to gravitational waves opens the interesting possibility to perform asteroseismological studies of neutron stars with future gravitational wave detectors. However, the recent observations of magnetar QPOs already enables us to perform asteroseismological analysis of magnetars, provided that we find a correct interpretation of their origin and of the physical nature of the oscillations.

Since the discovery of quasi periodic oscillations in the light curves of SGR giant flares (Barat et al., 1983; Israel et al., 2005; Strohmayer & Watts, 2005; Watts & Strohmayer, 2006), there has been extensive theoretical research of magnetar oscillations. One of the appealing explanations is that the QPOs are driven by torsional oscillations of the neutron star, i.e. nearly incompressible, horizontal oscillations. These modes are free of compressional stresses and do no work against the strong gravitational field of the star and are hence relatively easy to excite (Duncan, 1998). Initially it was thought that the observed

oscillations were due to torsional modes that are confined to the elastic neutron star crust (Piro, 2005; Watts & Stromayer, 2006). If this were true, the QPO frequencies would strongly constrain physical parameters in the crust. However, it was realized by Levin (2006) that the presence of an ultra-strong magnetic field ($\sim 10^{15}$ G) would complicate the analysis of the oscillations. Effectively the frozen-in magnetic field couples the motion of the crust to the magnetized core, by launching Alfvén waves (waves with magnetic tension as the restoring force) along the field lines into the stellar interior. In this way the crustal energy is drained on time-scales of < 1 s. Since the magnetar QPOs are observed for hundreds of seconds after the flare, one has to consider the hydro-magnetically coupled crust-core system as a whole. In the past few years several research groups have studied the coupled crust-core dynamics (Glampedakis et al., 2006; Levin, 2007; Gruzinov, 2008; Lee, 2008; van Hoven & Levin, 2011a and b (chapters 3 and 4 in this thesis); Gabler et al., 2011a and b; Colaiuda & Kokkotas, 2011). As pointed out by Levin (2006 & 2007), the dynamics of the crust-core system is further complicated as follows: In a star with an axisymmetric poloidal magnetic field, the Alfvén waves travelling along the field lines of different flux surfaces[1] in the fluid core are decoupled from each other, giving rise to a continuum of Alfvén frequencies[2]. The presence of a continuum in the magnetar core has some important implications for the oscillations: (1) Global modes with frequencies inside the continuum are damped exponentially. This phenomenon is well known in magnetohydrodynamic (MHD) studies (see Goedbloed & Poedts, 2004) and is called *resonant absorption*. It is thought that if the neutrons in the core form a superfluid and the protons a superconductor, the neutron component (~ 95 % of the mass) is dynamically decoupled from the Alfvén motion in the core (see chapter 1). In this case, the fundamental Alfvén frequencies are of the order of ~ 20 Hz for a $B \sim 10^{15}$ G magnetic field. Since the fundamental crustal frequencies are of the same order, resonant absorption is likely to occur for many of the crustal

[1] The flux surfaces that we consider here, are the axisymmetric surfaces that one obtains by rotating a single fieldline around the polar axis.

[2] Due to the dynamical decoupling of the different flux surfaces, one can view the magnetic field as an infinite collection of strings (field lines), each with unique length and tension. The eigenfrequencies vary in a continuous manner if one moves from flux surface to flux surface

modes. (2) After an initial period of exponential damping, the system settles in a steady state in which it oscillates at frequencies near the edges of the continuum; *edge modes* (Levin, 2007; Gruzinov, 2008; van Hoven & Levin, 2011a (see chapter 3), Gabler et al., 2011a; Colaiuda & Kokkotas, 2011). (3) For simple magnetic field geometries, one may expect the continuum to be piecewise. Gaps in the continuum occur at relatively low frequencies (< 200 Hz) and give rise to undamped motion due to edge-modes, or undamped crustal modes residing in the gaps (van Hoven & Levin, 2011a and b (see chapters 3 and 4); Colaiuda & Kokkotas, 2011).

In recent years the problem of magnetar oscillations has been approached with two distinct computational strategies:

(1) Several groups employed general relativistic *grid based MHD simulations* of magnetars. Sotani et al. (2009); Colaiuda et al., (2009) and Cerdá-Durán et al., (2009) produced continuum Alfvén modes in fluid neutron stars with axi-symmetric magnetic fields. Although these authors did not include a solid crust in their models, their simulations provided important benchmark tests for the ability of their codes to handle complex MHD simulations. Gabler et al. (2011a), (2011b) and Colaiuda & Kokkotas (2011) studied the coupled dynamics of the magnetar crust and core using their relativistic grid-based MHD codes. Colaiuda and Kokkotas (2011) in their study confirmed the existence of undamped motion in a gap between two contiguous continua.

(2) In the approach of Levin (2007), Lee (2008) and van Hoven & Levin (2011a and 2011b: chapters 3 and 4), the authors decomposed the motion of the magnetar into a set of basis functions and studied the dynamics of the coefficients of this series expansion; we refer to this as a *spectral method*. In particular, Levin (2007) and van Hoven & Levin (chapters 3 and 4) decompose the motion of the magnetar into eigenmodes of the'free crust' (a crust with no external stresses acting on it) and Alfvén eigenmodes on a dense grid (approaching continuum) of magnetic flux surfaces. Knowing the frequencies and eigenfunctions of the crust and the core flux surfaces, one can recast the problem of magnetar oscillations as a problem of coupled harmonic oscillators. One advantage of this approach is that one can run long and fast simulations of

the oscillating magnetar, without numerical dissipation. Another advantage is that one can sample the neutron star structure with great spatial detail.

To date the results of both the grid-based simulations and the spectral methods seem to be qualitatively in agreement. Simulations show that most oscillatory power resides at relatively low frequencies (< 200 Hz) in gaps or below the lowest fundamental Alfvén frequency. Although the exact results are sensitively dependent on the details of the model (location of gaps, crustal frequencies, etc.), the simulations consistently show no or very low power at higher frequencies. This poses a serious challenge for the interpretation of high frequency QPOs in the tails of SGR giant flares, in particular the strong QPO at 625 Hz. A correct explanation might eventually require one to investigate alternative QPO production mechanisms, or perhaps a somewhat radical revision of the magnetar model. An interesting alternative might be to consider poloidal MHD oscillations as studied by Sotani & Kokkotas (2009). These modes have frequencies in the order of several hundreds of Hz and may be interesting candidates for the high frequency QPOs if their coupling to the other Alfvén modes turns out to be weak.

This thesis

Chapter 1

In chapter 1, we explore some of the implications of the possible coexistence of a neutron superfluid and a type II superconductivity in the cores of neutron stars. If the protons form a type II superconductor, then there should be a strong hydromagnetic coupling between the proton flux tubes and the superfluid vortices. This coupling arises from the fact that not only the flux tubes, but also the superfluid vortices are strongly magnetized due to proton entrainment in the neutron super current. As a result, the vortices are pinned to the charged component (protons, electrons) of the star (Alpar, Langer & Sauls, 1984). We study the effect of strong pinning on the propagation of hydromagnetic waves in the core and derive the corresponding dispersion relations. We

discuss two astrophysical implications.

(1) We study Alfvén waves in magnetars, thought to be responsible for quasi-periodic oscillations (QPOs) observed in the light curves of SGR giant flares and show that strong vortex pinning does not lead to significant neutron mass loading of these waves. The resulting Alfvén frequencies are in fact in remarkable agreement with the observed QPO frequencies for a typical magnetar field strength of 10^{15} G, only if the neutrons are dynamically decoupled. However, in rapidly spinning neutron stars with orders of magnitude lower magnetic field strengths, neutron mass loading will play an important role in the Alfvén dynamics.

(2) We show that magnetic stresses in the fluid core tend to suppress the Donnelly-Glaberson instability, a potential source of superfluid turbulence in neutron stars that could act to prevent fast stellar precession. Although this instability is strongly suppressed, we show that fast precession at precession angles greater then ~ 1 degree is unlikely to occur, when the large mutual torques between the superfluid and superconductor can no longer be supported by magnetic tension.

Chapter 2

In chapter 2, we discuss the excitation of two types of magnetar oscillations during SGR giant flares, i.e. torsional modes of the crust and global f-modes. Both types of oscillations are of interest; torsional modes are generally associated with observed magnetar QPOs, whereas f-modes are gravitational wave emitters, potentially detectable by future instruments like Advanced LIGO and VIRGO. In recent years two distinct excitation mechanisms have been proposed that may be at play during giant flares. An internal mechanism (IM): increased magnetic stresses might lead to a global rearrangement of the internal field, culminating in a major rupture of the crust. Or an external mechanism (EM): a large-scale rearrangement of the magnetosphere accompanied by a fast reconnection event.

We argue that, due to the relatively long timescale on which the IM acts (Alfvén crossing time), the excitation of f-modes in the IM is strongly sup-

pressed with respect to their excitation in the EM. We show that even in the EM, only a small fraction of the flare energy is converted to the f-mode. This leads us to the conclusion, that the f-mode is unlikely to be detected by near future gravitational wave detectors like LIGO. Our calculation shows that in contrast to f-modes, torsional modes are strongly excited in both the IM and the EM.

Chapter 3

In chapter 3, we study torsional oscillations of magnetars which are thought to be the origin of QPOs observed during the afterglows of SGR giant flares. The oscillatory dynamics is largely determined by a strong hydro-magnetic coupling between discrete modes of the crust and a continuum of Alfvén modes in the fluid core. Using a simplified model that encompasses the basic characteristics of the system, we numerically simulate the dynamics that follows an initial perturbation of the crust. We find that the motion of the crust can be schematically decomposed into three stages: (1) An initial phase of exponential decay of the crustal motion. The crust transfers a large fraction of its energy to continuum through a mechanism called 'resonant absorption'. (2) The initial stage of exponential decay stops abruptly and the system enters a stage of slow algebraic decay[1]. (3) After some time the motion of the crust stabilizes and keeps oscillating at a constant amplitude. Fourier analysis of this stage reveals QPOs at frequencies close to the edges of the continuum. We examine these 'edge modes' analytically and show that they are a generic, long lived feature of the system.

We set up a realistic magnetar model, consisting of realistic core density profiles and axisymmetric poloidal magnetic field configurations, but with a simplified (infinitely thin) crust. The Alfvén continuum one obtains may, for some field configurations, contain gaps at low frequencies. These gaps give rise to two types of undamped motion: 'Edge modes' near the edges of

[1] For algebraic decay, the damping $\propto t^{-n}$, where n depends on properties of the continuum edges (see Levin, 2007). E.g. turning-point-generated oscillations decay as $t^{-1/2}$.

the continuum bands and crustal modes belonging to the gaps are somewhat shifted in frequency but remain undamped. We show that if the neutrons are decoupled from the Alfvén motion in the core, continuum gaps exist at frequencies below ~ 150 Hz and one may expect QPOs in this regime. If however, the core Alfvén motion *is* mass-loaded by neutrons, the crustal motion should be strongly damped, resulting in negligeble power at QPO frequencies. We thus argue, that the observed QPOs provide evidence for the dynamical decoupling of protons and neutrons. Although our model might account for the observed low frequency QPOs, the general absence of gaps above ~ 150 Hz in our models poses difficulties for the interpretation of some high frequency QPOs, notably the strong 625 Hz QPO. A satisfactory explanation may require either a magnetospheric production mechanism, or possibly a somewhat radical revision of the magnetar model.

We discuss the important issue of magnetic field tangling. We argue that if the field is tangled, the role of the Alfvén continuum will be limited to small scale flux tubes and the tangling will create a dense grid of large scale discrete modes with frequency separations depending on the degree of tangling. We show that this discrete grid of frequencies is in fact so dense (~ 20 Hz), that for high frequency crustal motion it would effectively act as a continuum.

Chapter 4

In chapter 4, we improve the magnetar model from chapter 3 in two ways: First, we replace the infinitely thin elastic crust by a magnetized crust of finite thickness and realistic equation of state. Second, we substitute the Newtonian equations of motion for the crust and the core by general relativistic ones.

As in chapter 3, we set up a spectral computational framework in which the magnetar's motion is decomposed into a series of basis functions which are associated with the crust and core vibrational eigenmodes. We derive general relativistic equations of motion for the magnetized, elastic crust and for the magnetic core. By coupling the crustal modes to the Alfvén modes of the core we obtain a fully relativistic dynamical model of a magnetar which

allows long and fast simulations of the magnetar motion without numerical dissipation, while using a very fine sampling of the stellar structure.

We show that in the presence of strong magnetic fields, the crustal modes with one ore more radial nodes become confined to a narrow region near the equator. In this region the horizontal magnetic field creates a magnetic tension-free cavity for modes with radial nodes, which are reflected back to the equator at higher lattitudes, where the field becomes more radial. Due to this confinement, the hydro-magnetic coupling to the Alfvén continuum is reduced, however, their energy is still drained on very small time-scales. Qualitatively, the results of our simulations are similar to the ones in chapter 3. In the appendix of chapter 4 we derive an analytical expression for the damping rate of a crustal mode that is resonantly absorbed by the continuum.

Acknowledgements

I thank Duncan Lorimer, Michael Kramer and Anna Watts for providing the figures printed in this introduction.

Chapter 1

Hydromagnetic waves in a superfluid neutron star with strong vortex pinning

Based on:
Hydromagnetic waves in a superfluid neutron star with strong vortex pinning
Maarten van Hoven & Yuri Levin, 2008, published in MNRAS

Abstract

Neutron-star cores may be hosts of a unique mixture of a neutron superfluid and a proton superconductor. Compelling theoretical arguments have been presented over the years that if the proton superconductor is of type II, than the superconductor fluxtubes and superfluid vortices should be strongly coupled and hence the vortices should be pinned to the proton-electron plasma in the core. We explore the effect of this pinning on the hydromagnetic waves in the core and discuss two astrophysical applications of our results: (1) We show that even in the case of strong pinning, the core Alfvén waves thought to be responsible for the low-frequency magnetar quasi-periodic oscillations (QPO) are not significantly mass-loaded by the neutrons. The decoupling of ~ 0.95 of the core mass from the Alfvén waves is in fact required in order to explain the QPO frequencies, for simple magnetic geometries and for magnetic fields not greater than 10^{15} Gauss. (2) We show that in the case of strong vortex pinning, hydromagnetic stresses exert stabilizing influence on the Glaberson instability, which has recently been proposed as a potential source of superfluid turbulence in neutron stars.

1.1 Introduction

Since the late 1950's, it has been realized that neutron-star interior may consist of a number of quantum fluids (see Shapiro & Teukolsky 1983 for a review). Currently, it is thought that both neutron superfluid and proton superconductor are likely to coexist in the neutron-star cores (see, e.g., Link 2007 for a discussion). Several researchers have argued that if the proton superconductivity were of the type II, then the superconductor fluxtubes would couple strongly to the neutron superfluid vortices. This line of reasoning is based on the fact that nuclear forces contain velocity-dependent terms, which results in the entrainment of protons in the neutron super current (Alpar, Langer & Sauls, 1984). Therefore, the vortices are sheathed by charged currents entrained in the superfluid flow and are strongly magnetized. Magnetic fluxtubes interact strongly with the magnetized vortices, similar to the way in which the fluxtubes interact between each other (Ruderman, Zhu, & Chen 1998 and references therein). As a result of this coupling, the vortices get strongly pinned to the proton-electron plasma in the core. Such pinning would have important implications for the neutron-star phenomenology. Ruderman, Zhu, & Chen (1998) have argued that the vortex-pinning in the core may be responsible for the observed glitches in the pulsar rotation rates. Link (2003) has considered the effect of the vortex-fluxtube interaction on the dynamics of the precessing pulsar PSR 1828-11 (observed by Stairs, Lyne, & Shemar 2000). Building on the theoretical work by Shaham (1977) and Sedrakian, Wasserman, & Cordes (1999), he has concluded that the interaction, if present, would ultimately lead to the fast precession. Since PSR 1828-11 is precessing slowly and persistently, Link (2003) has argued that the core vortex pinning is excluded by the observations and hence that either the proton superconductor might be of type I, or that both proton and neutron condensates do not coexist inside that pulsar. While Link's argument is suggestive, we believe it is premature to rule out strong vortex pinning in the cores of all neutron stars.

In this chapter we consider hydromagnetic waves in the case when the neutron vortices are strongly pinned to the proton-electron plasma in the core. We have two main astrophysical motivations for studying this problem. The first

one is due to the fairly recent observations of the quasi-periodic oscillations (QPOs) of the x-ray luminosity in the tails of giant magnetar flares (Israel et al. 2005, Strohmayer & Watts 2005, 2006, see also earlier but lower signal-to-noise measurements of Barat et al. 1983). Israel et al. 2005 has argued that the lowest-frequency and the longest-lived QPO of ~ 18 Hz is likely to represent an Alfvén-type oscillation in the magnetar core (this frequency is too low to be associated with the torsional modes of the crust). Levin (2006) has shown that for a magnetar-strength field the crustal motion [which is thought to be either powering the flare (Thompson & Duncan 1995) or responding to a global reconnection event in the magnetosphere (Lyutikov 2003)] would excite the core Alfvén waves on the timescale of several oscillation periods. Since then, a significant body of theoretical work has been devoted to a study of global magnetar vibrations, which would involve both hydromagnetic waves in the core and elasto-magnetic shear waves in the crust [Glampedakis, Samuelsson, & Andersson 2006, Levin 2007 (from here on L07), Sotani, Kokkotas, & Stergioulas 2007, Lee 2007]. In particular, L07 has argued that the long-lived low-frequency QPOs are associated with the special spectral points of the Afven continuum in the magnetar core. For simple B-field configurations these special points can be found analytically, and do not depend on the details of the crust. For example, for a uniform internal B-field, the lowest QPO is expected at the frequency

$$\nu_{\rm Alfven} \sim \frac{B_{\rm eff}}{2R\sqrt{4\pi\rho_c}} \tag{1.1}$$

where R is the radius of the fluid part of the star, ρ_c is the density of the the part of the fluid which is coupled to the Alfvén waves and $B_{\rm eff}$ is the effective magnetic field which is given by[1]

$$B_{\rm eff} = \sqrt{BB_{\rm cr}}. \tag{1.2}$$

[1]The occurence of $B_{\rm eff}$ in Eq. (1.1) and (1.2) can be understood as follows: the magnetic tension force acting on surface Σ perpendicular to the fluxtubes containing N fluxtubes is given by $N\Delta\Sigma\cdot B_{\rm cr}^2/4\pi = \Sigma\cdot T_{\rm eff}$, where $\Delta\Sigma$ is the cross section of a single fluxtube and $T_{\rm eff}$ is the effective tensile stress. The magnetic flux through Σ is $\Phi = \Sigma\cdot B = N\Delta\Sigma\cdot B_{\rm cr}$ and we find $T_{\rm eff} = BB_{\rm cr}/4\pi = B_{\rm eff}^2/4\pi$ (as opposed to $T = B^2/4\pi$, where T is the corresponding part of the Maxwell stress tensor). (A detailed derivation is given in Easson & Pethick, (1977)).

Here B is the average magnetic field, $B_{\rm cr} \simeq 10^{15}$ G is the value of the critical magnetic field confined to the fluxtubes. From Eq. (1.2) we see that the magnetar QPO frequencies could provide an interesting constraint on the magnetic-field strength and geometry. However, interaction between neutron and proton superfluids could affect core Alfvén waves, by effectively mass-loading them with neutrons. We shall consider the extreme case of such interaction—the strong vortex pinning on the fluxtubes, and show that it does not significantly alter the Alfvén-wave propagation in slowly-spinning magnetars (but is important for the Alfvén waves in the fast-spinning radio-pulsars). This simplifies the interpretation of the QPO frequencies and shows that it is valid to assume that ρ_c is just the density of protons, about 5% of the total fluid density.

Our second motivation is the recent theoretical discussion of the superfluid turbulence in the neutron-star cores. Superfluid turbulence has been discussed in the context of the laboratory Helium fluid for the last 30 years (see, e.g., Donnelly 1991 for a review). In a ground-breaking series Peralta, Melatos, Giacobello, & Ooi at the University of Melbourne (2005, 2006; hereafter PMGO5 and PMGO6) have applied the superfluid-helium ideas to neutron-star interiors. PMGO have developed from scratch a code which studies numerically the 2-component superfluid dynamics. The two components in PMGO are the neutron superfluid and the normal neutron fluid which are coupled via the mutual friction force at the superfluid vortices; this mixture is expected if the core temperature is a significant fraction of the critical temperature of the superfluid. The equations of motions used by PMGO were derived by Hall and Vinen (1956) and Bekharevich and Khalatnikov (1961). PMGO5 have studied, for the first time, the superfluid spherical Taylor-Couette flow and find that it becomes turbulent in 2 steps: (1) The normal component develops meridional circulation due to the Eckman pumping (see, e.g., Pedlosky 1987), and (2) the component of the meridional flow of the normal fluid which is directed *along* the superfluid vortices drives the vortex Kelvin waves unstable; this is known as the Glaberson (or sometimes Donnelly-Glaberson) instability (Glaberson, Johnson, Ostermeier 1974, Donnelly 1991). In PMGO5 simulations, the Glaberson instability leads to turbulence. Interestingly, PMGO6

and Melatos and Peralta (2007) demonstrate that the superfluid turbulence could affect the pulsar spin and could be behind the well-known pulsar timing noise and spin glitches.

More recently, Sidery, Andersson and Gomer (2007, hereafter SAG) and Glampedakis, Andersson and Jones (2007, hereafter GAJ1 and 2008, hereafter GAJ2) developed an analytical theory of the Glaberson instability in neutron stars. Their 2-component fluid consists of the neutron superfluid and the proton superconductor, which are, like in PMGO, coupled via the mutual-friction force. SAG have considered the limit of the weak mutual friction (see below) and infinitely heavy proton superfluid and found that it was the inertial waves in the neutron superfluid which were subject to the Glaberson instability. GAJ1 and GAJ2 have extended this analysis to include the regime of realistic proton-to-neutron mass ratio and of arbitrarily strong mutual friction. Notably, they found that the Glaberson instability operated even in the regime of strong pinning. But where would the initial relative flow between the protons and neutrons come from? GAJ have argued that if the pinned neutron vortices were misaligned with the angular velocity of the protons, then this would naturally lead to the relative proton-neutron flow which would potentially be strong enough to drive the turbulence in some parts of the star. Without turbulence, the star with misaligned pinned vortices would undergo fast precession (Shaham 1977) which, although probably hard to detect, has yet not been observed in any of the currently-timed radio pulsars or magnetars. In GAJ2 the authors argue that this Glaberson-instability-induced turbulence may generically prevent the star getting into a configuration with the fast precession. However, this conclusion is premature. One important piece of physics which is not considered in GAJ is the strong hydromagnetic stress inside the proton superfluid, which, as we show below, has a suppressing effect on the Glaberson instability and hence on the development of the superfluid turbulence. We will derive, however, a robust upper limit on the angle of fast precession, which is determined by the maximum possible mutual torque between the neutron superfluid and the proton superconductor. The maximal precession angle turns out to be much smaller than 1 degree and thus it is not surprising that the fast precession has never been observed in

real neutron stars.

The plan of the chapter is as follows. In the next section we derive the dispersion relation for the hydromagnetic waves when the superfluid vortices are rigidly attached to the core plasma. In sections 1.3 and 1.4, we consider applications to oscillating magnetars and precessing pulsars, respectively. We end with the general discussion in section 1.5.

1.2 Dispersion relations

As a starting point, we utilize the plane-wave analysis outlined in GAJ. We follow closely the notation of and reasoning behind GAJ1's basic equations (1)–(7) and our derived dispersion relation is identical to their Eq. (10) in the limit of zero hydromagnetic stress, but has important extra terms when the hydromagnetic stress is included. We begin with the two-fluid dynamical equations, cf. Eqs. (1) and (2) in GAJ1:

$$D_t^n \boldsymbol{v}_n + \boldsymbol{\nabla}\psi_n = 2\boldsymbol{v}_n \times \boldsymbol{\Omega} + \boldsymbol{f}_{\rm mf} \tag{1.3}$$

$$D_t^p \boldsymbol{v}_p + \boldsymbol{\nabla}\psi_p = 2\boldsymbol{v}_p \times \boldsymbol{\Omega} - \boldsymbol{f}_{\rm mf}/x_p + \nu_{\rm ee}\nabla^2\boldsymbol{v}_p + \boldsymbol{f}_{\rm hm} \tag{1.4}$$

Here $\boldsymbol{v}_n$ and $\boldsymbol{v}_p$ are the velocity vectors of the neutron and proton condensates respectively (throughout this thesis vectors are denoted by bold symbols), the full time derivatives D_t are defined in the usual way as $D_t^{n,p} = \partial/\partial t + \boldsymbol{v}_{n,p}\cdot\boldsymbol{\nabla}$, $\psi_{n,p}$ is the sum of specific chemical and gravitational potentials, $\boldsymbol{f}_{\rm mf}$ is the acceleration of the neutron superfluid due to the mutual friction between its vortices and the charged plasma, $x_p = \rho_p/\rho_n$ is the density ratio between the proton charged and neutral components of the interior ($\sim 5\%$), Ω is the angular velocity of the rotating frame in which all of the velocities are defined, $\nu_{\rm ee}$ is the kinetic viscosity of the plasma due to electron-electron scattering, and

$$\boldsymbol{f}_{\rm hm} = \boldsymbol{B}_{\rm eff}\cdot\boldsymbol{\nabla}\boldsymbol{B}_{\rm eff}/4\pi\rho_p \tag{1.5}$$

is the acceleration of the plasma due to the hydromagnetic stress. We note that because in a type-II superconductor the distance between the fluxtubes

is much larger than the fluxtube diameter, we ignore magnetic pressure. In writing down Eq. (1.3), we have followed GAJ and neglected explicitly the effect of superfluid entrainment (which we expect will not qualitatively change our results) and the individual tension force for the vortices (which can be neglected if the wavelength of the waves is much greater than the inter-vortex distance). We shall use the following conventional form (Hall & Vinen 1956, Bekharevich & Khalatnikov 1961, PMGO, SAG and GAJ) for the mutual-friction force:

$$\boldsymbol{f}_{\rm mf} = \frac{R}{1+R^2}\hat{\boldsymbol{\omega}}_n \times (\boldsymbol{\omega}_n \times \boldsymbol{w}_{\rm np}) + \frac{R^2}{1+R^2}\boldsymbol{\omega}_n \times \boldsymbol{w}_{\rm np}, \tag{1.6}$$

where $\boldsymbol{\omega}_n = \boldsymbol{\nabla}\times\boldsymbol{V}_n$ is the vorticity of the neutron fluid in a non-rotating frame (here $\boldsymbol{V}_n$ is the neutron velocity in the non-rotating frame)[1], $\hat{\boldsymbol{\omega}}_n = \boldsymbol{\omega}_n/|\boldsymbol{\omega_n}|$ is the associated unit vector, $\boldsymbol{w}_{\rm np} = \boldsymbol{v}_n - \boldsymbol{v}_p$ and R is the dimensionless number measuring the strength of the drag between the neutron vortices and the plasma. When $R \ll 1$ (the weak-drag limit), the first term on the right-hand side dominates. This entails that the neutron vortices mostly follow the motion of the neutron superfluid in the direction perpendicular to $\boldsymbol{\omega}_n$. When $R \gg 1$ (the strong-drag limit), the second term on the right-hand side dominates. This entails that the neutron vortices mostly follow the plasma motion. When $R = \infty$, which is the case on which this chapter focuses, the vortices get pinned to the plasma. In this limit, the plasma and the neutron superfluid interact exclusively via the Magnus force arising from the relative motion between the neutron vortices and neutron superfluid.

We choose the background state as follows: 1. the z-axis is directed along Ω; 2. the neutron vortices are aligned with $\boldsymbol{\Omega} = \Omega\boldsymbol{e}_z$, and are at rest in the rotating frame; 3. in the same frame, the plasma has a background velocity $\boldsymbol{w}_0 = w_0\boldsymbol{e}_z$, which is directed along the vortices; 4. the mean magnetic field is directed along the vortices, $\boldsymbol{B} = B\boldsymbol{e}_z$. We consider waves which are propagating along the z-axis. We are interested in the waves for which the restoring force is the combination of hydromagnetic stress, the Coriolis force and the Magnus force. This means that the wave must be nearly incompressible, which

[1] In GAJ1, $\boldsymbol{\omega}_n$ is erroneously defined as $\boldsymbol{\nabla}\times\boldsymbol{v}_n$. However, in their subsequent calculations they, most likely, use the correct expression.

implies

$$\boldsymbol{k} \cdot \delta \boldsymbol{v}_{n,p} = 0. \tag{1.7}$$

Here $\boldsymbol{k}$ is the wavevector, $\delta \boldsymbol{v}_{n,p}$ is the neutron/proton velocity perturbation due to the wave. Incompressibility and assumed homogeneity of the background state imply $\delta\psi_{n,p} = 0$.

Let us introduce the Lagrangian displacement vectors $\boldsymbol{\xi}_{n,p}$ of the neutron and proton fluids from their background positions, with $\delta \boldsymbol{v}_{n,p} = D_t^{n,p} \boldsymbol{\xi}_{n,p}$. We are looking for the solutions of the form

$$\boldsymbol{\xi}_{n,p}(z,t) = \left[\xi_{x0}^{n,p} \boldsymbol{e}_x + \xi_{y0}^{n,p} \boldsymbol{e}_y\right] e^{i(\sigma t + kz)}, \tag{1.8}$$

where σ is the angular frequency of the wave. We now perturb Equations (1.3), (1.4) and (1.6); we set $R = \infty$ in the latter. To the linear order in the velocity perturbation, we have:

$$\begin{aligned}
D_t^n \delta \boldsymbol{v}_n &= \partial^2 \boldsymbol{\xi}_n / \partial t^2 = -\sigma^2 \boldsymbol{\xi}_n, \\
D_t^p \delta \boldsymbol{v}_p &= -(\sigma + k w_0)^2 \boldsymbol{\xi}_p, \\
\delta \boldsymbol{f}_{\rm mf} &= 2\boldsymbol{\Omega} \times (\delta \boldsymbol{v}_n - \delta \boldsymbol{v}_p) - (\boldsymbol{\nabla} \times \delta \boldsymbol{v}_n) \times \boldsymbol{w}_0, \\
\nu_{\rm ee} \nabla^2 \delta \boldsymbol{v}_p &= -i \nu_{\rm ee} k^2 (\sigma + k w_0) \boldsymbol{\xi}_p, \\
\delta \boldsymbol{f}_{\rm hm} &= c_A^2 \partial^2 \boldsymbol{\xi}_p / \partial z^2 = -c_A^2 k^2 \boldsymbol{\xi}_p.
\end{aligned} \tag{1.9}$$

Here $c_A = \sqrt{B B_{\rm cr}/(4\pi\rho_p)}$ is the Alfvén velocity in the plasma. The expression for $\delta \boldsymbol{f}_{\rm hm}$ is obtained using the magnetic induction equation. Substituting these into Eqs. (1.3) and (1.4) and using $\boldsymbol{\nabla} \times \boldsymbol{\xi} = i\boldsymbol{k} \times \boldsymbol{\xi}$ together with $\delta \boldsymbol{v}_n = i\sigma \boldsymbol{\xi}_n$ and $\delta \boldsymbol{v}_p = i(\sigma + k w_0) \boldsymbol{\xi}_p$, we get two linear vector equations for $\boldsymbol{\xi}_n$ and $\boldsymbol{\xi}_p$. It is now convenient to proceed as follows: Let us represent a vector $\boldsymbol{\xi} = \xi_x \boldsymbol{e}_x + \xi_y \boldsymbol{e}_y$ by a complex number $\tilde{\xi} = \xi_x + i\xi_y$. Then a vector $\boldsymbol{e}_z \times \boldsymbol{\xi}$ is represented by $i\tilde{\xi}$. By using this, we can immediately rewrite the two real vector equations as two complex scalar equations:

$$\begin{aligned}
\sigma \tilde{\xi}_n + 2\Omega \tilde{\xi}_p &= 0, \\
\left[\bar{\sigma} + 2\Omega\left(1 - \frac{1}{x_p}\right) - \left(i\nu_{\rm ee} + c_A^2/\bar{\sigma}\right) k^2\right] \bar{\sigma} \tilde{\xi}_p + \frac{2\Omega - k w_0}{x_p} \sigma \tilde{\xi}_n &= 0,
\end{aligned} \tag{1.10}$$

where $\bar{\sigma} = \sigma + kw_0$. This pair of equation yields immediately the complex dispersion relation:

$$\bar{\sigma}^2 + \left[2\Omega\left(1 - \frac{1}{x_p}\right) - i\nu_{\rm ee}k^2\right]\bar{\sigma} - \frac{2\Omega(2\Omega - kw_0)}{x_p} - c_A^2k^2 = 0. \qquad (1.11)$$

The dispersion relation for arbitrary R is derived, for completeness, in Appendix 1.A. In the next two sections we consider two applications of the relation Eq. (1.11).

1.3 Hydromagnetic waves in magnetars

In this section we assume that there is no $\mathbf{\Omega}$-directed relative proton-neutron flow, i.e. we assume $w_0 = 0$. We also set $\nu_{\rm ee}$ to zero, since the ratio of the viscous to hydromagnetic stress is given by

$$\nu_{\rm ee}\sigma/c_A^2 \ll 1. \qquad (1.12)$$

With these simplifications, the dispersion relation (1.11) gives

$$\sigma = -\Omega\left(1 - \frac{1}{x_p}\right) \pm \sqrt{\Omega^2\left(1 + \frac{1}{x_p}\right)^2 + c_A^2k^2}. \qquad (1.13)$$

It is important to note that in this expression c_A is a function of only the proton density ρ_p ($c_A^2 \equiv BB_{\rm cr}/4\pi\rho_p$). All observed magnetars are slowly rotating, with $\Omega \sim 1$ rad s^{-1}. The observed lowest angular frequency for a magnetar QPO is 18 Hz, thus $\sigma \sim 113$ rad s^{-1}. The sum of Magnus and Coriolis forces, represented by the terms with Ω, contribute only a fraction $\delta\sigma/\sigma$ to the wave frequency, given by

$$\delta\sigma/\sigma \simeq \frac{\Omega}{x_p\sigma} = 0.18\left(\frac{\Omega}{1\text{ rad s}^{-1}}\right)\left(\frac{113\text{ rad s}^{-1}}{\sigma}\right)\left(\frac{0.05}{x_p}\right). \qquad (1.14)$$

We note that this does *not* depend on the assumption that σ represents some fundamental Alfvén mode. From the above equation, it is clear that for hydromagnetic waves associated with the magnetar QPO frequencies of 18Hz and

higher, the magnus forces from neutron superfluid introduce only a small correction to their propagation. Thus we conclude that the magnetar oscillations (as seen in the giant-flare QPOs) even in the case of strong pinning, do not couple significantly to the neutron superfluid.[1] Therefore, given the knowledge of the internal magnetic field, one should use $\rho_c \simeq x_p \rho_n$ in Eq. (1.1) to determine the frequency of the lowest QPO which, according to Levin (2007), corresponds to the turning point of the Alfvén continuum in the core. For Levin's the simplest computable magnetar model (uniform internal magnetic field and density), with the typical magnetar parameters, $B = 10^{15}$ G, $R = 10$ km, $\rho = 10^{15}$ g cm^{-3} and $x_p = 0.05$, Eq. (1.1) gives $\nu_a \simeq 22$ Hz, which is in qualitative agreement with the observed 18 Hz. If the whole neutron superfluid would mass-load the wave, this frequency would be reduced by a factor of ~ 4. While suggestive, the numbers above certainly should not be taken as evidence of neutron superfluidity, since the strength and geometry of magnetic fields inside the magnetar are highly uncertain.

1.4 Precession of neutron stars

Consider now a precessing neutron star where the neutron angular velocity and the crust+proton angular velocity[2] are equal in magnitude Ω but are misaligned by an angle θ. Suppose that this angle is fixed due to the strong vortex pinning. The relative velocity of the proton superfluid along the vortices is given by

$$w_0 = \Omega \sin\theta x_2, \tag{1.15}$$

[1] We note that we have used the plane-wave analysis for what is likely a non-plane-wave oscillation. This is clearly a limitation of our formalism. However, the plane-wave analysis illustrates the physics which is also valid for oscillatory mode of any geometry, namely that for high-frequency waves Alfvén restoring forces are much greater than the Magnus forces. This occurs essentially because the Magnus force is proportional to the velocity and thus scales as σ, while the total restoring force scales as σ^2. Thus, we believe that our analysis is qualitatively correct in the high-frequency regime, for non-plane-wave Alfvén-type oscillations.

[2] The crust and the core protons are co-precessing; this is enforced by the hydro-magnetic stresses (Levin & D'Angelo, 2004).

where x_2 is the coordinate measured along $\mathbf{\Omega}_n \times \mathbf{\Omega}_p$. Note that this expression agrees with Eq. (18) in GAJ1 when one notes that for small θ their wobble angle θ_w equals $I_p\theta/I_n$, where I_p and I_n are the moments of inertia of the proton and neutron components, respectively.

1.4.1 Glaberson instability criterion

It is convenient to express the general solution of Eq. (1.11) as follows:

$$\sigma = -kw_0 - \Omega\left(1 - \frac{1}{x_p}\right) + \frac{i\nu_{\rm ee}k^2}{2} \pm \sqrt{D},$$

where

$$D = \Omega^2\left(1 + \frac{1}{x_p}\right)^2 + c_A^2k^2 - \frac{2kw_0\Omega}{x_p} - \frac{\nu_{\rm ee}^2k^4}{4} - i\nu_{\rm ee}k^2\Omega\left(1 - \frac{1}{x_p}\right) \quad (1.16)$$

This is essentially the same as Eq. (10) of GAJ1 when $c_A = 0$.

First, let us consider the non-viscous case with $\nu_{\rm ee} = 0$. Then the minimum of D is attained for $k = \Omega w_0/(x_p c_A^2)$ and equals

$$D_{\rm min} = \Omega^2\left(1 + \frac{1}{x_p}\right)^2 - \frac{\Omega^2 w_0^2}{x_p^2 c_A^2}. \quad (1.17)$$

Thus the Glaberson instability appears only for

$$w_0 > c_A(1 + x_p) \simeq c_A. \quad (1.18)$$

We now allow for the viscous term in Eqs. (1.16) and (1.16). We find that a weak, viscosity-driven instability appears at a smaller velocity

$$w_0 > 2\sqrt{x_p}c_A = \sqrt{\frac{BB_{\rm cr}}{\pi\rho_n}}, \quad (1.19)$$

for the wave-vector range

$$k_- < k < k_+ \quad (1.20)$$

where

$$k_{\pm} = \frac{\Omega}{x_p c_A^2}\left[w_0 \pm \sqrt{w_0^2 - 4c_A^2 x_p}\right]; \tag{1.21}$$

see Appendix 1.B for the mathematical details.

Equation (1.19) expresses the lowest relative proton-neutron velocity which is required for the initiation of the Glaberson instability. Whether this velocity is achieved depends on the misalignment angle θ between the proton and neutron anglular velocity vectors. In the next subsection, we derive a simple but rigorous upper bound on θ.

1.4.2 The maximum misalignment angle for fast precession

The misalignment angle θ can be constrained, by requiring that the precessional torque τ_p of the proton component not exceed the maximum torque τ_m that the vortices can exert on the fluxtubes through magnetic stresses. The precessional torque is given by[1]

$$\tau_p = L_n \Omega_p \sin\theta \tag{1.22}$$

Here $L_n = I\Omega$ is the proton angular momentum, I is the total stellar moment of inertia and $\Omega_p = \Omega$. We find that for a typical neutron star with the mass of $M = 1.4\ M_\odot$ and radius of $R = 10^6$ cm, the precessional torque is given by

$$\tau_p \simeq 4 \cdot 10^{46} \sin\theta (P/1\ \mathrm{s})^{-2}\ \mathrm{g\ cm^2\ s^{-2}}. \tag{1.23}$$

Here P is the neutron-star rotational period. The maximal physically-admissible torque τ_m can be computed by assuming that the vortices have maximal contact with the fluxtubes, i.e. that the vortex is pushed/pulled with the stress

[1] Since the neutrons are pinned to the protons, the torque acting on the neutrons is given by the cross product of the instantaneous angular velocity of the protons and the neutrons angular momentum, and is therefore independent of x_p. In our derivation we assume that the angular velocities of the protons and the neutrons have the same magnitude Ω.

of $B_{\rm cr}^2/(8\pi)$ accross its whole side surface. The maximal torque exerted on a single vortex is given by

$$\tau_v = \frac{B_{\rm cr}^2}{8\pi} l^2 d, \tag{1.24}$$

where $d \sim 2 \cdot 10^{-12}$ cm is the vortex diameter and l is the vortex half-length. The total number of vortices is given by

$$N = \pi R^2 n_v \sim 3 \cdot 10^{16} (R/10^6 \text{ cm})^2 (P/1 \text{ s})^{-1}, \tag{1.25}$$

where n_v is the per-area vortex density (Shapiro and Teukolsky 1983, Link 2003). For a spherical star with a dense grid of the linear vortices, the average value of l^2 is $R^2/2$. Thus, by combining Eqs. (1.24) and (1.25), we arrive to the following expression:

$$\tau_m = \frac{B_{\rm cr}^2}{16} R^4 d n_v \simeq 1.3 \cdot 10^{45} (P/1 \text{ s})^{-1} \text{ g cm}^2 \text{ s}^{-2}. \tag{1.26}$$

From Eqs. (1.26) and (1.23), we see that our requirement $\tau_m > \tau_p$ implies that

$$\theta < 2^o (P/1 \text{ s}), \tag{1.27}$$

and therefore

$$w_0 \sim \Omega \theta R < 2 \cdot 10^5 \text{ cm s}^{-1}. \tag{1.28}$$

This upper limit on w_0 is spin-independent.

So, is this velocity sufficient to drive the Glaberson instability? Equation (1.19) tells us that for $x_p = 0.05$, $B = 10^{12}$ G and $\rho_n = 10^{15}$ g cm^{-3}, the critical relative velocity is $w_0 \sim 6 \cdot 10^5$ cm s^{-1}. Thus we conclude that in the presence of strong vortex pinning and magnetic fields $B > 10^{11}$ G the misalignment between the proton- and neutron angular velocities is unlikely to become large enough to provide wind velocities w_0 that are sufficient to drive the Glaberson instability.

1.5 Discussion

The calculations of this chapter have two main astrophysical implications. First, we have shown that the Alfvén waves which are associated with magnetar QPOs are not significantly mass-loaded by a neutron superfluid, even if the superfluid vortices are strongly pinned to the proton-electron plasma. For $B = 10^{15}$ G and the simplest B-field geometry, the expected frequency of lowest magnetar QPO is in remarkable agreement with observations, *if* only the protons, i.e. about 0.05 of the core mass, are mass-loading the Alfvén waves. Strong vortex pinning will, however, have a strong effect on the Alfvén waves in rapidly spinning and relatively non-magnetic neutron stars, i.e. those ones in the Low-Mass X-ray Binaries. In these stars the Alfvén waves may play an important role in damping of the r-mode instability, as discussed by Mendell (2001) and Kinney and Mendell (2003) for the cases of non-superfluid and superfluid core, respectively. Kinney and Mendell (2003) had not considered the vortex pinning (see also Mendell 1991); however from Eq. (1.14) and from the fact that $\sigma \sim \Omega$ for an r-mode, it is clear that the strong vortex pinning would have a huge (of order $1/x_p$) effect on the Alfvén waves with the r-mode frequency.

Second, we have shown that the hydromagnetic stresses generally suppress the Glaberson instability in the proton-neutron superfluid mixture, in the case of strongly pinned vortices[1]. We have also provided a robust upper bound Eq. (1.27) on the angle between proton and neutron angular velocities in the fast-precessing neutron stars. Even for slowly-spinning magnetars, the misalignment angle cannot exceed 20 degrees, which implies a wobble angle no greater than 1 degree. Thus a detection of neutron-star fast precession is difficult, if not impossible, observationally. An inspection of the XMM timing data on known anomalous x-ray pulsars produces no statistically-significant periodic signal which could be interpreted as fast precession [van Kerkwijk 2008, private communications].

[1] We have not considered here the PMGO case when some normal neutron component is present and is driving the instability.

Acknowledgements

We thank Andrew Melatos and Kostas Glampedakis for useful discussions, the anonymous referee for valuable suggestions. We thank Maarten van Kerkwijk for a search of fast magnetar precession in the XMM data.

Appendix 1.A: Dispersion relation for arbitrary drag

In this Appendix we perform a plane-wave analysis of the two-fluid dynamical equations defined in Eq's (1.3) and (1.4) and derive a dispersion relation for arbitrary drag strength R. Using the plane wave solutions from Eq. (1.8), we can perturb Eq's (1.3) and (1.4). Retaining linear terms we get:

$$D_t^n \delta \boldsymbol{v}_n = -\sigma^2 \boldsymbol{\xi}_n \tag{1.29}$$

$$D_t^p \delta \boldsymbol{v}_p = -\bar{\sigma}^2 \boldsymbol{\xi}_p \tag{1.30}$$

$$2\delta \boldsymbol{v}_n \times \boldsymbol{\Omega} = 2i\Omega\sigma \boldsymbol{\xi}_n \times \boldsymbol{e}_z \tag{1.31}$$

$$2\delta \boldsymbol{v}_p \times \boldsymbol{\Omega} = 2i\Omega\bar{\sigma} \boldsymbol{\xi}_p \times \boldsymbol{e}_z \tag{1.32}$$

$$\begin{aligned} \delta \boldsymbol{f}_{\mathrm{mf}} = \frac{R}{1+R^2} \big[& 2i\Omega \boldsymbol{e}_z \times \left(\boldsymbol{e}_z \times \left(\sigma \boldsymbol{\xi}_n - \bar{\sigma} \boldsymbol{\xi}_p \right) \right) \\ & + k w_0 \sigma \boldsymbol{e}_z \times \left(\left(\boldsymbol{e}_z \times \boldsymbol{\xi}_n \right) \times \boldsymbol{e}_z \right) \big] \\ + \frac{R^2}{1+R^2} \big[& 2i\Omega \boldsymbol{e}_z \times \left(\sigma \boldsymbol{\xi}_n - \bar{\sigma} \boldsymbol{\xi}_p \right) - w_0 k \sigma \boldsymbol{e}_z \times \left(\boldsymbol{e}_z \times \boldsymbol{\xi}_n \right) \big] \end{aligned} \tag{1.33}$$

$$\nu_{\mathrm{ee}} \nabla^2 \delta \boldsymbol{v}_p = -\nu_{\mathrm{ee}} k^2 \bar{\sigma} \boldsymbol{\xi}_p \tag{1.34}$$

$$\delta \boldsymbol{f}_{\mathrm{hm}} = -c_A^2 k^2 \boldsymbol{\xi}_p \tag{1.35}$$

Here $\bar{\sigma} \equiv \sigma + w_0 k$ and $c_A = \sqrt{B B_{\mathrm{cr}} / 4\pi \rho_c}$ is the Alfvén velocity in the plasma. We can simplify these expressions by using the same trick as in Section 1.2: Let us represent the vector $\boldsymbol{\xi} = \xi_x \boldsymbol{e}_x + \xi_y \boldsymbol{e}_y$ by a complex number $\tilde{\xi} = \xi_x + i\xi_y$. The cross product $\boldsymbol{e}_z \times \boldsymbol{\xi}$ corresponding to a simple rotation in the xy-plane, can then be represented by $i\tilde{\xi}$. Using this, we convert the two real vector equations (1.3) and (1.4) into two complex scalar equations:

$$-2\Omega C \bar{\sigma} \tilde{\xi}_p = \left[\bar{\sigma} + (C-1) \left(w_0 k - 2\Omega \right) \right] \sigma \tilde{\xi}_n \tag{1.36}$$

$$\left[\bar{\sigma}+\left(2\Omega\left(1-\frac{C}{x_p}\right)-i\nu_{\rm ee}k^2\right)-\frac{c_A^2}{\bar{\sigma}}k^2\right]\bar{\sigma}\tilde{\xi}_p=\frac{C}{x_p}\left(w_0k-2\Omega\right)\sigma\tilde{\xi}_n \quad (1.37)$$

where $C\equiv\frac{R(i+R)}{1+R^2}$. This pair of equations yields the following complex dispersion relation:

$$\begin{aligned}\bar{\sigma}^3+\bar{\sigma}^2\left[(C-1)\left(w_0k-2\Omega\right)+2\Omega\left(1-\frac{C}{x_p}\right)-i\nu_{\rm ee}k^2\right]\\ +\bar{\sigma}\left[\left(w_0k-2\Omega\right)\left((C-1)\left(2\Omega-i\nu_{\rm ee}k^2\right)+\frac{2\Omega C}{x_p}\right)-c_A^2k^2\right]\\ -c_A^2k^2\left(C-1\right)\left(w_0k-2\Omega\right)=0\end{aligned} \quad (1.38)$$

In the strong drag limit $R\to\infty$ ($C=1$) this cubic equation simplifies significantly:

$$\bar{\sigma}^2+\bar{\sigma}\left[2\Omega\left(1-\frac{1}{x_p}\right)-i\nu_{\rm ee}k^2\right]-\left[\frac{2\Omega\left(2\Omega-w_0k\right)}{x_p}+c_A^2k^2\right]=0, \quad (1.39)$$

which is Eq. (1.11) in the text.

Appendix 1.B: Instability criterion for non-zero viscosity

In this Appendix we derive a criterion for instability in the case of non-negligible viscosity, i.e. Eq. (1.19). We rewrite Eq. (1.16) as follows:

$$\sigma=A+iB\pm\sqrt{C+iD} \quad (1.40)$$

where

$$A=-w_0k-\Omega\left(1-\frac{1}{x_p}\right)$$

$$B=\frac{\nu_{\rm ee}k^2}{2}$$

$$C=\Omega^2\left(1+\frac{1}{x_p}\right)^2+c_A^2k^2-\frac{2w_0k\Omega}{x_p}-B^2 \quad (1.41)$$

$$D = -2\Omega\left(1 - \frac{1}{x_p}\right)B$$

The state of marginal stability is given by

$$Im\left(\sigma\right) = B \pm Im\left(\sqrt{C + iD}\right) = 0. \tag{1.42}$$

In order to find a convenient expression for $Im\left(\sqrt{C+iD}\right)$ we write $\sqrt{C+iD}$ in polar form. The imaginary part is then given by

$$Im\left(\sqrt{C + iD}\right) = \left(C^2 + D^2\right)^{\frac{1}{4}} \sin\left(\frac{1}{2}\arccos\left(\frac{C}{\sqrt{C^2 + D^2}}\right)\right) \tag{1.43}$$

Combining this with Eq. 1.42), we find

$$B^2 = \frac{1}{2}\sqrt{C^2 + D^2} - \frac{1}{2}C \tag{1.44}$$

Taking the square of this expression and using Eqs (4.46) we arrive at

$$\frac{2\Omega\left(2\Omega - w_0 k\right)}{x_p} + c_A^2 k^2 = 0 \tag{1.45}$$

And therefore,

$$k_\pm = \frac{\Omega}{x_p c_A^2}\left[w_0 \pm \sqrt{w_0^2 - 4c_A^2 x_p}\right] \tag{1.46}$$

The unstable waves have wave-vectors in the interval $k_- < k < k_+$, provided that k_- and k_+ are real. Thus the criterion for the instability is

$$w_0 > 2c_A\sqrt{x_p}, \tag{1.47}$$

this is Eq. (1.19) of the main text. We now make an estimate of the growth rate in this instability window. For a realistic neutron star, we take $\nu_{\rm ee} \approx 10^9$ cm^2 s^{-1} at $T \approx 10^7$ K (Flowers & Itoh 1979, Cutler & Lindblom 1987, Andersson, Comer & Glampedakis, 2005), $\Omega \approx 2\pi$ rad/s, $c_A \approx 10^6$ cm s^{-1} and therefore for $w_0 \sim c_A$, the wave-vector of an unstable wave is $k \sim 10^{-4}$ cm^{-1}. We now note that $\nu_{\rm ee}k^2/2 << \Omega/x_p$. Therefore the terms B from Eq. (3.69) and B^2 from Eq. (4.46) have a negligible contribution to $Im\left(\sigma\right)$ and can be ignored.

Consider first the case where $C < 0$. We note that $Im(\sigma)$ is completely dominated by C so that we arrive at the criterion of Eq. (1.18) again. With a growth rate of

$$-Im(\sigma) = \sqrt{C} \tag{1.48}$$

Next consider $C > 0$, i.e. $w_0 < (1 + x_p)\, c_A$. By means of a simple analysis in the complex plane one can show that

$$\frac{\sqrt{D}}{2} < -Im(\sigma) < \sqrt{\frac{D}{2}} \tag{1.49}$$

For $w_0 > 2\sqrt{x_p} c_A$, there is a range of k where the instability occurs; see Eq. (1.20). Substituting $k = k_+$ into Eq. (1.49) for the maximum k in this range, we find the growth rate of the instability

$$-Im(\sigma) \approx \sqrt{\frac{\nu_{\rm ee}\Omega^3}{2x_p^3 c_A^4}} \left[w_0 + \sqrt{w_0^2 - 4c_A^2 x_p} \right] \tag{1.50}$$

We note that because the viscosity is small, this growth rate is much smaller than the one in Eq. (1.48).

Chapter 2

Excitation of f-modes and torsional modes by giant flares

Partially based on:
On the excitation of f-modes and torsional modes by giant flares
Yuri Levin & Maarten van Hoven, 2011, published in MNRAS

Abstract

Magnetar giant flares may excite vibrational modes of neutron stars. Here we compute an estimate of initial post-flare amplitudes of both the torsional modes in the magnetar's crust and of the global f-modes. We show that while the torsional crustal modes can be strongly excited, only a small fraction of the flare's energy is converted directly into the lowest-order f-modes. For a conventional model of a magnetar, with the external magnetic field of $\sim 10^{15}$ G, the gravitational-wave detection of these f-modes with advanced LIGO is unlikely.

2.1 Introduction

The gamma- and x-ray flares from Soft Gamma Repeaters (SGRs; Mazetz et al. 1979, Hurley et al. 1998, 2004) are believed to be powered by a sudden release of magnetic energy stored in their host magnetars (Thompson & Duncan 1995). An SGR flare may excite vibrational modes of a magnetar (Duncan 1998). Indeed, torsional oscillations of a magnetar provide an attractive explanation for some of the quasi-periodic oscillations (QPOs) observed in the tails of giant flares (Barat et al. 1983, Israel et al. 2005, Strohmayer & Watts 2005, van Hoven & Levin 2011 (see chapter 3), Gabler et al. 2011, Colaiuda & Kokkotas 2011).

Excitation of low-order f-modes is also of considerable interest, because of the f-modes' strong coupling to potentially detectable gravitational radiation. The sensitivity of the ground-based gravitational-wave interferometers has dramatically improved over the last 5 years (Abott et al. 2009a, Acernese et al. 2008) and interesting upper limits on the f-mode gravitational- wave emission from the 2004 SGR 1806-20 giant flare, a possible 2009 SGR 1550–5418 giant flare and several less energetic bursts have recently been obtained (Abott et al. 2008, Abott et al. 2009b, Abadie et al. 2010, see also Kalmus et al. 2009). Advanced LIGO and VIRGO are expected to become operational in the next 5-7 years and it is of interest to predict the strength of expected gravitational-wave signal from future giant flares.

In this chapter, we compute a theoretical estimate for the amplitude of the torsional and f-modes expected to be excited in a giant flare. We show that only a small fraction of the flare energy is expected to be pumped into the low-order f-modes and estimate the signal-to-noise ratio for the future giant flare detection with advanced LIGO. By contrast, the torsional modes can be strongly excited and may well be responsible for some of the observed QPO's in magnetar flares.

2.2 The general formalism

The giant flares release a significant fraction of the free magnetic energy stored in their host magnetars. Two distinct mechanisms for this have been proposed: (1) Large-scale rearrangement of the internal field, facilitated by a major rupture of the crust (Thompson & Duncan 1995, 2001; we shall refer to it as the internal mechanism, IM) and (2) a large-scale rearrangement of the magnetospheric field, facilitated by fast reconnection (Lyutikov 2006, Gill & Heyl 2010; we shall refer to it as the external mechanism, EM). Both processes may well be at play: the IM would likely serve as a trigger for the EM (however, as was argued in Lyutikov 2003, EM may also be triggered by slow motion of the footpoints of a magnetospheric flux tube, leading to a sudden loss of magnetostatic equilibrium). Observationally, the extremely short, a few microseconds rise time of the 2004 giant flare in SGR 1806-20 (Hurley et al. 2004) gives reason to believe that EM was at play in that source: the IM operates on a much longer Alfvén crossing timescale of $0.05 - 0.1$ seconds. The long timescale for the IM implies that it would not be efficient in exciting the f-modes which have frequencies of over a kHz; this was recently independently emphasized by Kashiyama & Ioka (2011).

2.2.1 Excitation by the EM

During the large-scale EM event, the magnetic stresses at the stellar surface change rapidly by, at most[1], order 1. The magnetosphere comes to a new equilibrium, on the very short timescale of several Alfvén (light)-crossing times and the stresses change to new constant values. We shall characterize the change of the magnetic stress by the 3 components

$$\Delta T_{rr} = \frac{B^2}{4\pi} f_r(\theta, \phi),$$

[1]There is some observational evidence for the substantial magnetic-field reconfiguration in the magnetosphere, as seen from the difference between the persistent pre-flare and post-flare pulse profiles (Palmer et al. 2005). The global change of the magnetospheric twist would result in the comparable change in the tangential magnetic field at the surface, as is evident from e.g. the twisted-magnetosphere solution by Thompson, Lyutikov, & Kulkarni 2002.

$$\Delta T_{r\theta} = \frac{B^2}{4\pi} f_\theta(\theta, \phi), \tag{2.1}$$
$$\Delta T_{r\phi} = \frac{B^2}{4\pi} f_\phi(\theta, \phi),$$

where B is some characteristic value of the surface magnetic field and f_r, f_θ and f_ϕ are functions are of order 1 in the strongest possible flares and are smaller for the weaker flares. Consider now a normal mode of the star with an eigenfrequency ω_n and a displacement wavefunction $\boldsymbol{\xi}_n(r, \theta, \phi)$. We treat the changing surface magnetic stress as an external perturbation acting on the mode. We derive the mode excitation using the Lagrangian formalism; in Appendix 2.A we sketch the derivation directly from the equations of motion. The Lagrangian of the free (pre-perturbation) mode is given by

$$L_{\text{free}}(a_n, \dot{a}_n) = \frac{1}{2} m_n \dot{a}_n^2 - \frac{1}{2} m_n \omega_n^2 a_n^2, \tag{2.2}$$

where a_n is the generalized coordinate corresponding to the normal mode, m_n is the effective mass given by

$$m_n = \int d^3 r \rho(\boldsymbol{r}) \boldsymbol{\xi}_n^2(\boldsymbol{r}), \tag{2.3}$$

and $\rho(\boldsymbol{r})$ is the density. The Lagrangian term characterising the mode's interaction with external stress is given by (cf. section 2 of Levin 1998)

$$L_{\text{int}} = a_n \int R^2 \boldsymbol{\xi}_n \cdot \boldsymbol{F} \sin\theta d\theta d\phi, \tag{2.4}$$

where

$$\boldsymbol{F} = \Delta T_{rr} \boldsymbol{e}_r + \Delta T_{r\theta} \boldsymbol{e}_\theta + \Delta T_{r\phi} \boldsymbol{e}_\phi, \tag{2.5}$$

and the displacement $\boldsymbol{\xi}$ is evaluated at the radius of the star R. The full Lagrangian for the nth mode is given by[1]

$$L(a_n, \dot{a}_n) = L_{\text{free}} + E_{\text{mag}} \alpha_n \frac{a_n}{R}, \tag{2.6}$$

[1] We work in the linear regime and don't take into account the non-linear coupling between the modes. The mode amplitudes $\ll 1$ found at the end of our calculation indicate that this is a good approximation.

where

$$E_{\rm mag} = \frac{B^2 R^3}{4\pi} \tag{2.7}$$

is the characteristic energy stored in the star's magnetic field and and α_n is the coupling coefficient given by

$$\alpha_n = \int \boldsymbol{\xi}_n(R,\theta,\phi)\cdot\boldsymbol{f}(\theta,\phi)\sin\theta d\theta d\phi, \tag{2.8}$$

where

$$\boldsymbol{f} = f_r(\theta,\phi)\boldsymbol{e}_r + f_\theta(\theta,\phi)\boldsymbol{e}_\theta + f_\phi(\theta,\phi)\boldsymbol{e}_\phi \tag{2.9}$$

It is now trivial to find the motion resulting from the sudden introduction of the external stress at moment $t = 0$. The coordinate a_n oscillates as follows:

$$a_n(t) = \bar{a}_n\left[1 - \cos\left(\omega_n t\right)\right], \tag{2.10}$$

where the amplitude is given by

$$\bar{a}_n = \frac{\alpha_n E_{\rm mag}}{m_n \omega_n^2 R}. \tag{2.11}$$

The energy in the excited mode is given by

$$E_n = \frac{\alpha_n^2 E_{\rm mag}^2}{2 m_n \omega_n^2 R^2} \tag{2.12}$$

We now briefly revisit the mode excitation by the IM. In this case, the interaction Lagrangian of a mode with the magnetic field is described by the following volume integral:

$$L_{\rm int} = a_n \int d^3 r \boldsymbol{f}_L(\boldsymbol{r})\cdot\boldsymbol{\xi}_n(\boldsymbol{r}), \tag{2.13}$$

where $\boldsymbol{f}_L = [\nabla\times\boldsymbol{B}]\times\boldsymbol{B}$ is the lorentz force per unit volume. Since $f_L \sim B^2/R$, one can see that the coupling of the internal field variation to the mode is of the same order of magnitude as that of the external field variation, provided that the external and internal fields are of the same order of magnitude.

However, the IM mechanism acts on a much longer timescale[1] $\tau_{\rm Alfven} \sim 0.1$s than the typical f-mode period of $\tau_f \sim 0.0005$ s, so the f-mode oscillator would be adiabatically displaced without excitation of the periodic oscillations. One can show that the typical suppression factor of the IM relative to the EM excitation is *at least* of order $2\pi\tau_{\rm Alfven}/\tau_f$ in the mode amplitude[2]. This factor is so large that even if internal field was stronger than the external field by an order of magnitude, the IM excitation would still be suppresed relative to the EM one.

Is there a way around this suppression factor? Potentially, IM could feature a collection of many localized MHD excitations, with the timescale for each one being determined by the Alfvén-crossing time of each of the excitation domain. If the domains were small enough, their timescales could be more closely matched with the f-mode period (Melatos, private communications). However, in this case the magnitude of the overlap integral in Eq. (2.13) would be reduced by a factor $\sim (R/\Delta R)^3$, where ΔR is the characteristic size of the excited domain. The domains would contribute incoherently to the amplitude of the excited mode, thus the contribution of an individual domain would have to be multiplied by $(R/\Delta R)^{3/2}$ in the (somewhat unlikely) limit where the active domains occupy the whole star. Thus, while the timescale of the mini-flares could be well-matched with the f-mode period, their overall contribution to the overlap integral in Eq. (2.13) would be suppressed by $\sim (R/\Delta R)^{3/2}$. In the optimal case that the mini-flares have the same timescale as the f-mode period, $R/\Delta R \sim \tau_{\rm Alfven}/\tau_f$. Therefore, the collection of mini-flares would not give us any gain in the mode excitation amplitude, as compared to the IM estimate given in the previous paragraph. Two applications of the formalism

[1] This timescale could be shorter by a factor of $\sqrt{x_p} \sim 0.2$ (where x_p is the proton fraction) if the superfluid neutrons are decoupled from the MHD (Easson & Pethick 1979, van Hoven & Levin 2008 (see also chapter 1), Andersson, Glampedakis, & Samuelsson 2009). However, even in this case the timescale $\tau_{\rm Alfven}$ on which the IM acts is still a factor of ∼40 larger than the f-mode period τ_f.

[2] This can be formalized by the following argument: consider a harmonic oscillator of proper frequency ω_0, initially at rest, which is externally driven by force $f(t)$. The amplitude of the induced oscillation at the proper frequency is proportional to $\tilde{f}(\omega_0)$, the Fourier transform of $f(t)$ evaluated at ω_0. For a step function, representing the rapid transition (several light crossing times) to the new magnetospheric equillibrium in the EM, $\tilde{f}(\omega) \propto 1/\omega$. On the other hand, for a smooth pulse of duration τ, as expected in IM, the Fourier transform is suppressed and scales at most as $\tilde{f}(\omega) \propto (\omega\tau)^{-1} 1/\omega$ when $\omega\tau \gg 1$.

for the mode excitation by the EM mechanism developed above are presented in the next two sections.

2.3 f-modes and gravitational waves

In order to estimate an effective f-mode mass, we have computed the $l = 2$ f-mode displacement functions for a neutron star[1] in the Cowling approximation (see Appendix 2.B). Convenient scalings are

$$\begin{aligned} m_n &= q_M M, \\ \omega_n^2 &= q_\omega \frac{GM}{R^3}, \\ \xi_r(R,\theta,\phi) &= a_n Y_{2m}(\theta,\phi). \end{aligned} \tag{2.14}$$

In our fiducial model $q_M = 0.046$, where we have normalised the mode wavefunction so that $\boldsymbol{e}_r \cdot \boldsymbol{\xi}_{2m}(R,\theta,\phi) = Y_{2m}(\theta,\phi)$. Our reference number $q_\omega = 1.35$ was obtained using a fitting formula for fully relativistic f-mode frequencies[2] from Andersson & Kokkotas (1996). The amplitude of the f-mode is given by

$$\frac{\bar{a}_{2m}}{R} = \frac{\alpha_{2m}}{q_m q_\omega} \frac{E_{\rm mag}}{E_{\rm grav}}, \tag{2.15}$$

where

$$E_{\rm grav} = \frac{GM^2}{R} \tag{2.16}$$

[1] We constructed our neutron star model using the equation of state from Douchin & Haensel (2001) and Haensel & Pichon (1994). In calculating the f-mode we treated the whole star as a fluid, neglecting the effects of bulk- and shear moduli.

[2] We are not being consistent in, on the one hand, using the Cowling approximation for a Newtonian star to determine the effective mode mass, but on the other hand using the published relativistic calculations for the mode frequencies. Normally, Newtonian calculations would be sufficient, given the many unknown details of the flare and the many poorly constrained parameters we'd already introduced into the model and the formalism we developed in the previous section is manifestly Newtonian (but can be generalized to relativistic regime if the need arises). However, as we show below, the signal-to-noise ratio for the gravitational-wave detection is very sensitive to the mode frequency and therefore we try to be accurate in characterizing these frequencies.

is of the same order as the gravitational binding energy of the neutron star. We get

$$\frac{\bar{a}_{2m}}{R} \sim 3 \times 10^{-6} \alpha_{2m} \left(\frac{B}{10^{15}\mathrm{G}}\right)^2 \left(\frac{R}{10\mathrm{km}}\right)^4 \left(\frac{1.4M_\odot}{M}\right)^2 . \tag{2.17}$$

The energy in the f-mode is

$$E_f = \frac{\alpha_{2m}^2}{2q_m q_\omega} \frac{E_{\mathrm{mag}}^2}{E_{\mathrm{grav}}} \sim 1.5 \times 10^{-6} \alpha_{2m}^2 E_{\mathrm{mag}} \tag{2.18}$$

for our fiducial parameters. This energy is drained from the star primarily through emission of gravitational waves. The total amount of energy carried by gravitational waves is therefore

$$E_{\mathrm{GW}} = E_f = \frac{2\pi^2 d^2 f^2 c^3}{G} \int_{-\infty}^{\infty} \langle h^2 \rangle dt \tag{2.19}$$

where $f = \omega_n/2\pi$ is the f-mode frequency in Hz, $\langle h^2 \rangle$ is the direction and polarisation averaged value of the square of the gravitational-wave strain h as measured by observers at distance d from the source. This expression allows us to estimate the expected signal-to-noise ratio for ground based gravitational wave interferometers (cf. Abadie et al 2010). One can use the fact that nearly all the gravitational-wave signal is expected to arrive in a narrow-band around the f-mode frequency and that the signal form (the exponentially-decaying sinusoid) is known. The Wiener-filter expression for the signal-to-noise can be written as

$$\frac{S}{N} \approx \left[\frac{1}{S_h(f)} \int_{-\infty}^{\infty} |\tilde{h}^2(f')| df'\right]^{1/2} \tag{2.20}$$

$$\sim \left[\frac{G}{2\pi^2 c^3} \frac{E_f}{S_h(f) f^2 d^2}\right]^{1/2} \tag{2.21}$$

where $\tilde{h}(f)$ is the Fourier transform of the time-dependent gravitational wave strain $h(t)$. As is standard for narrow-band signal, we have used Parseval's theorem to convert the integral over f to the integral over t from Eq. (2.19), and, following Abadie et al. 2010, we have approximated h^2 with the average $\langle h^2 \rangle$. At frequencies of a few kHz the spectral density, $S_h(f)$, of the ground based detectors like Advanced LIGO and Virgo is dominated by shot-noise

and is proportional to f^2. This makes the signal-to-noise ratio for observations of magnetar f-modes excited in giant flares particularly sensitive to frequency ($\propto f^{-3}$). For Advanced LIGO we find

$$\frac{S}{N} \approx 0.07\ \alpha_{2m} \left(\frac{2\ \mathrm{kHz}}{f}\right)^3 \left(\frac{B}{10^{15}\ \mathrm{G}}\right)^2 \times \left(\frac{1\ \mathrm{kpc}}{d}\right) \left(\frac{R}{10\ \mathrm{km}}\right)^2 \left(\frac{0.07\ M_\odot}{m_n}\right)^{1/2} \tag{2.22}$$

Here we used tabulated[1] $S_h(f)$ from the LIGO document LIGO-T0900288, which gives $S_h(f) = 8.4 \cdot 10^{-47} \mathrm{Hz}^{-1}\,(f/2000\ \mathrm{Hz})^2$ for the shot-noise dominated part of the curve.

2.4 Torsional modes

Intuitively, one expects torsional modes to be strongly excited during the magnetar flares (Duncan 1998), since it is the free energy of the twisted magnetic field that is being released. These have much lower proper frequencies than the f-modes (with the fundamental believed to be in the range $10 - 40$ Hz, see Steiner & Watts 2009 and references therein), which can be well-matched to the Alfvén frequencies inside the star. Thus both EM and IM are likely to play a role in the torsional mode excitation. Here, we consider the EM explicitly but keep in mind that IM would give a similar answer.

For the torsional modes in the crust, the displacement is given by

$$\boldsymbol{\xi}_{nlm}(r,\theta,\phi) = g_n(r)\boldsymbol{r} \times \boldsymbol{\nabla} Y_{lm}(\theta,\phi), \tag{2.23}$$

and it is convenient to normalize the wavefunctions so that $g_n(R) = 1$. Here $n = 0, 1, ...$ is the number of radial nodes. With this normalization, the effective mode mass $m_{nlm} \sim m_{\mathrm{crust}} \sim 0.01M$ and from Eq. (2.11) one gets for the mode amplitude normalized by the star radius:

$$\frac{a_{nlm}}{R} \sim 0.01\alpha_{nlm} \left(\frac{B}{10^{15}\mathrm{G}}\right)^2 \frac{R}{10\mathrm{km}} \frac{0.014 M_\odot}{m_{nlm}} \left(\frac{100\mathrm{Hz}}{f}\right)^2. \tag{2.24}$$

[1] These sensitivity curves represent the incoherent sum of principal sources of noise as they are currently understood.

Thus we see that for a reasonable range of parameters it is feasible that the crustal torsional modes would be strongly excited by a giant flare.

2.4.1 Magnetic modes

Recently, Kashiyama & Ioka (KI, 2011) suggested that certain types of MHD modes that may be strongly excited during a giant flare, are coupled to gravitational radiation and may therefore become an interesting source for advanced LIGO. KI focus on the polar modes of Sotani & Kokkotas (2009); the MHD modes found by Lander & Jones (2011a,b) also satisfy some of the KI's criteria. While interesting, this idea has potential caveats that need further investigation. KI assume that the oscillations are long-lived, $\sim 10^7$ oscillation periods. However, MHD modes are notoriously capricious. While the idealized modes of Sotani & Kokkotas (2009) and Lander & Jones (2011a,b) are protected by symmetry, the global magnetic modes in more realistic configurations may couple to a variety of localized Alfvén-type modes and may thus be quickly damped via phase mixing and resonant absorption (Goedbloed & Poedts 2004, van Hoven & Levin 2011 (see chapter 3)). Thus, in our view, there is currently no compelling reason to believe that the magnetic modes can be substantially longer lived than the observed magnetar QPOs.

2.5 Discussion

In this chapter, we have computed the excitation of the f-modes and crustal tosional neutron-star modes by a giant flare. Corsi & Owen (2011) recently computed the magnetic energy that can be released during the flare[1] and found values comparable to $E_{\rm mag}$. However, in this work we showed that only a small fraction of the released flare energy is converted into the f-modes and that the associated gravitational-wave emission is correspondingly weaker

[1] These analytical calculations necessarily make simplifying assumptions about the structure of an equilibrium magnetic field inside the magnetar, but they are likely to give correct order-of-magnitude values.

than has been previously hoped (cf. Abadie et al. 2010 and Corsi & Owen 2011). From Eq. (2.22), our fiducial model does not look promising for future advanced LIGO detection of a giant flare, even if $\alpha_{2m} \sim 1$, i.e. if the flare comprises a global reconfiguration of the magnetospheric field so that the released electro-magnetic energy is of order of the total magnetic energy of the star, $\sim 10^{47}$ erg (the most energetic of the 3 observed giant flares released few$\times 10^{46}$ erg). However, if the surface field is significantly larger than 10^{15} G and/or the star is greater than 10 km in radius (which would reduce the f-mode frequency and increase the contact surface area), then one can become more hopeful about the potential detection. On the other hand, we have seen that there is no difficulty in exciting the crustal torsional modes to a large amplitude. Whether or not this leads to the observed quasi-periodic oscillations in the flare's tail (Israel et al. 2005, Strohmayer & Watts 2005, Watts & Strohmayer 2006) depends crucially on the dynamics of hydromagnetic coupling between the crustal modes and the Alfvén modes of the magnetar core (Levin 2006, 2007, van Hoven & Levin 2011 (see chapter 3), Gabler et al. 2011, Colaiuda & Kokkotas 2011).

Acknowledgements

We thank Ben Owen for useful discussions, Andrew Melatos and Peter Kamus for helpful comments on the initial draft of Levin & van Hoven (2011), which formed the basis for this chapter. And we thank the anonymous referee for useful comments and suggestions. This research was supported, in part, by Leiden Observatory and Lorentz Institute through internal grants. MvH thanks Monash School of Physics for hospitality during his extensive visit.

Appendix 2.A: Alternative derivation of the mode excitation

In this Appendix we derive, for completeness, the formalism for mode excitation directly from the equations of motion; cf. Unno et al (1989). Let $\xi(\boldsymbol{r}, t)$ be the small displacement of the star from its equilibrium position. The equations of motion are given by

$$\rho\ddot{\boldsymbol{\xi}} = \boldsymbol{F}(\boldsymbol{\xi}) + \boldsymbol{f}_{\rm ext}(\boldsymbol{r}, t), \tag{2.25}$$

where ρ is the density, $\boldsymbol{F}(\boldsymbol{\xi})$ is the restoring force linear in $\boldsymbol{\xi}$ and $\boldsymbol{f}_{\rm ext}$ is the external force per unit volume. For a normal-mode eigenfunction $\boldsymbol{\xi}_n$ with the angular frequency ω_n, one has $\boldsymbol{F}_n = -\rho\omega_n^2\xi_n$. We now decompose the star displacement into its eigenmodes

$$\boldsymbol{\xi}(\boldsymbol{r}, t) = \Sigma_n a_n(t)\boldsymbol{\xi}_n(\boldsymbol{r}) \tag{2.26}$$

and suibstitute this series into Eq. (2.25) to obtain

$$\Sigma_n[\ddot{a}_n + \omega_n^2 a_n]\boldsymbol{\xi}_n(\boldsymbol{r}) = \boldsymbol{f}_{\rm ext}(\boldsymbol{r}, t). \tag{2.27}$$

Taking a dot product of the above equation with $\boldsymbol{\xi}_k(\boldsymbol{r})$, integrating over the volume of the star and using the orthogonality relation

$$\int d^3r\rho\boldsymbol{\xi}_n \cdot \boldsymbol{\xi}_k \propto \delta_{mk}, \tag{2.28}$$

we obtain the equation of motion for a_k:

$$\ddot{a}_k + \omega_k^2 a_k = \frac{\alpha_k(t)}{m_k}, \tag{2.29}$$

where

$$\alpha_k = \int d^3r\boldsymbol{f}_{\rm ext} \cdot \boldsymbol{\xi}_k(\boldsymbol{r}) \tag{2.30}$$

and

$$m_k = \int d^3r\rho(\boldsymbol{r})\boldsymbol{\xi}_k^2(\boldsymbol{r}). \tag{2.31}$$

These equations of motion are identical to those derived from the Lagrangian in Eqs (2.2) and (2.13). For the case when the external force is applied at the surface, one recovers equations of motion derived from Eqs (2.2) and (2.4).

Appendix 2.B: Stellar oscillations

In this appendix we give the non-relativistic equations that govern adiabatic fluid motion in non-rotating, spherical stars. We derive linearized equations of motion for small fluid displacements $\boldsymbol{\xi}$ in the Cowling approximation. That is, we ignore perturbations of the gravitational potential resulting from the small fluid displacement $\boldsymbol{\xi}$. In non-rotating stars, the fluid flow obeys the continuity- and Euler equations,

$$\frac{\partial \rho}{\partial t} = -\boldsymbol{\nabla}\cdot(\rho \boldsymbol{v}) \tag{2.32}$$

$$\rho \frac{d\boldsymbol{v}}{dt} = -\boldsymbol{\nabla} P - \rho \boldsymbol{\nabla}\Phi, \tag{2.33}$$

where ρ is the mass-density, $\boldsymbol{v}$ is the velocity vector and P is the pressure. The gravitational potential Φ satisfies Poisson's equation

$$\nabla^2 \Phi = 4\pi G \rho. \tag{2.34}$$

Together with an equation for adiabatic motion,

$$\frac{dP}{dt} = \frac{\Gamma_1 P}{\rho}\frac{d\rho}{dt}, \tag{2.35}$$

where Γ_1 is the adiabatic constant, the above equations provide a complete dynamical description of the star. In order to find eigenmodes of the star, we proceed as follows:

(1) We construct an equillibrium stellar model. We assume that our star is non-rotating and neglect deformations due to magnetic pressure, which are expected to be small. Therefore, we adopt a spherically symmetric background stellar model that is a solution of the Tolman-Oppenheimer-Volkoff equation (TOV equation). We calculate the hydrostatic equillibrium using a SLy equation of state (Douchin & Haensel, 2001; Haensel & Potekhin, 2004; Haensel, Potekhin & Yakovlev, 2007). The model that we use here has a mass of $M_* = 1.4\ M_\odot$, a radius $R_* = 1.16 \cdot 10^6$ cm, a central density $\rho_c = 9.83 \cdot 10^{14}$ g cm^{-3} and cental pressure $P_c = 1.36 \cdot 10^{35}$ dyn cm^{-2}. As a further simplification, we treat the whole star as a fluid, neglecting effects due to non-zero bulk- and shear moduli in the crust.

(2) We introduce a small fluid displacement $\boldsymbol{\xi}(\boldsymbol{x}, t)$ and assume for this displacement a harmonic time dependence, i.e. $\boldsymbol{\xi}(\boldsymbol{x}, t) \propto \boldsymbol{\xi}(\boldsymbol{x}) e^{i\omega t}$. Using the perturbation $\boldsymbol{\xi}$, we linearize the fluid equations (2.33) - (2.35) around the static equillibrium model. This yields the following pair of ordinary differential equations (see e.g. Cox, 1980; Unno et al., 1989; Christensen-Dalsgaard, 2003):

$$\frac{d\xi_r}{dr} = -\left[\frac{2}{r} + \frac{1}{\Gamma_1 P}\frac{dP}{dr}\right]\xi_r + \frac{r\omega^2}{c^2}\left[\frac{l(l+1)c^2}{r^2\omega^2} - 1\right]\xi_h \tag{2.36}$$

$$\frac{d\xi_h}{dr} = \frac{1}{r\omega^2}\left[\omega^2 - N^2\right]\xi_r + \left[\frac{N^2}{g} - \frac{1}{r}\right]\xi_h \tag{2.37}$$

where ξ_r and ξ_h are radial- and horizontal components of the fluid displacement. The integer l enters the equation due to an expansion of the perturbed quantities into spherical harmonics $Y_l^m(\theta, \phi)$. In terms of ξ_r and ξ_h, the displacement field $\boldsymbol{\xi}_{lm}(\boldsymbol{x})$ corresponding to a spherical harmonic degree l and order m, can be expressed as

$$\boldsymbol{\xi}_{lm}(\boldsymbol{x}) = \mathrm{Re}[\xi_r(r)\, Y_l^m \hat{\boldsymbol{r}} + \xi_h(r) r \boldsymbol{\nabla} Y_l^m], \tag{2.38}$$

where $\hat{\boldsymbol{r}}$ is the unit vector in the radial direction. Further, in Eq. (2.37), g is the gravitational acceleration and N^2 is the square of the buoyancy frequency (Brunt-Väisälä frequency) is given by:

$$N^2 = g\left(\frac{1}{\Gamma_1 P}\frac{dP}{dr} - \frac{1}{\rho}\frac{d\rho}{dr}\right) \tag{2.39}$$

(3) We supplement the equations (2.36) and (2.37) with boundary conditions at $r = 0$ and $r = R_*$. The boundary condition in the center of the star is obtained by requiring the solutions to be regular functions at $r = 0$. One may show (see e.g. Unno, 1989) that this leads to the condition

$$\xi_r = l\xi_h \qquad \text{at} \quad r = 0. \tag{2.40}$$

At the stellar surface, we enforce a zero-stress boundary condition, i.e. the Lagrangian perturbation of the pressure $\delta P = 0$. This gives

$$\xi_h = -\frac{1}{r\rho\omega^2}\frac{dP}{dr}\xi_r \qquad \text{at} \quad r = R_*. \tag{2.41}$$

Equations (2.36) and (2.37) augmented with the boundary conditions of equations (2.40) and (2.41), constitutes a boundary value problem, which yields, for each index l, a unique series of solutions (eigenmodes) $\xi_{r,ln}(r)$ and $\xi_{h,ln}(r)$ corresponding to eigenfrequencies $\omega = \omega_{ln}$. Here the index n denotes the number nodes along the radial axis. Since there are two separate classes of solutions for a given number of radial nodes, i.e. the low frequency g-modes and the high frequency p-modes, we label the g-modes with negative integer n and the p-modes with positive integer n. These two branches of modes are separated by the nodeless ($n = 0$) f-mode.

(4) We obtain solutions of the above boundary value problem by means of a shooting method. For a fixed value of ω, we integrate Eq's (2.36) and (2.37) from $r = 0$, where Eq. (2.40) is satisfied, to the surface at $r = R_*$, using the 4-th order Runge-Kutta scheme. Eigenvalues ω_{ln} and eigenfunctions $\xi_{r,ln}, \xi_{h,ln}$ are obtained by repeating this procedure for different values of ω, until the boundary condition Eq. (2.41) is satisfied at R_*.

Chapter 3

The strongly coupled dynamics of crust and core

Based on:
Magnetar oscillations I: the strongly coupled dynamics of the crust and the core
Maarten van Hoven & Yuri Levin, 2011, published in MNRAS

Abstract

Quasi-Periodic Oscillations (QPOs) observed at the tail end of Soft Gamma Repeaters giant flares are commonly interpreted as the torsional oscillations of magnetars. From a theoretical perspective, the oscillatory motion is influenced by the strong interaction between the shear modes of the crust and magnetohydrodynamic Alfvén-like modes in the core. We study the dynamics which arises through this interaction and present several new results: (1) We show that discrete *edge modes* frequently reside near the edges of the core Alfvén continuum, and explain using simple models why these are generic and long-lived. (2) We compute the magnetar's oscillatory motion for realistic axisymmetric magnetic field configurations and core density profiles, but with a simplified model of the elastic crust. We show that one may generically get multiple gaps in the Alfvén continuum. One obtains strong discrete *gap modes* if the crustal frequencies belong to the gaps; the resulting frequencies do not coincide with, but are in some cases close to the crustal frequencies. (3) We deal with the issue of tangled magnetic fields in the core by developing a phenomenological model to quantify the tangling. We show that field tangling enhances the role of the core discrete Alfvén modes and reduces the role of the core Alfvén continuum in the overall oscillatory dynamics of the magnetar. (4) We demonstrate that the system displays transient QPOs when parts of the spectrum of the core Alfvén modes contain discrete modes which are densely and regularly spaced in frequency. The transient QPOs are the strongest when they are located near the frequencies of the crustal modes. (5) We show that if the neutrons are coupled into the core Alfvén motion, then the post-flare crustal motion is strongly damped and has a very weak amplitude. We thus argue that magnetar QPOs give evidence that the proton and neutron components in the core are dynamically decoupled and that at least one of them is a quantum fluid. (6) We show that it is difficult to identify the high-frequency 625 Hz QPO as being due to the physical oscillatory mode of the magnetar, if the latter's fluid core consists of the standard proton-neutron-electron mixture and is magnetised to the same extent as the crust.

3.1 Introduction

Since the discovery of quasi periodic oscillations (QPOs) in the lightcurves of giant flares from soft gamma repeaters (SGR) (Israel et al., 2005; Strohmayer & Watts, 2005; Watts & Strohmayer, 2006; Barat et al., 1983) there has been considerable interest in their physical origin. One of the appealing explanations is that the QPOs are driven by torsional oscillations[1] of the neutron stars whose magnetic energy powers the flares (Duncan 1998). This opens a unique possibility to perform an asteroseismological analysis of neutron stars and possibly obtain a new observational window to study the neutron-star interiors. Many authors have considered torsional modes to be confined to the magnetar crust and have shown that seismological information about such modes would strongly constrain the physics of the crust (Piro 2005, Watts & Strohmayer 2006, Watts & Reddy 2007, Samuelsson & Andersson 2007, Steiner & Watts 2009). However, it was quickly understood that the theoretical analysis of magnetar oscillations is complicated by the presence of an ultra-strong magnetic field ($B \sim 10^{14} - 10^{15}$ G) that is frozen into the neutron star and penetrates both the crust and the core. The field provides a channel for an intense hydro-magnetic interaction between the motion of the crust and the core, which becomes effective on the timescale of $\ll 1$ second (Levin 2006). Since the QPOs are observed for hundreds of seconds after the flare, it is clear that the coupled motion of the crust and the core must be considered. In recent years, significant theoretical effort has gone into the study of this problem (e.g., Glampedakis et al. 2006, Levin 2007, Gruzinov 2008b, Lee 2008). This chapter's analysis is based, in part, on an approach of Levin (2007, L07).

To make progress in computing the coupled crust-core motion, L07 has studied the time evolution of an axisymmetric toroidal displacement of a star with axisymmetric poloidal magnetic field. In that case the Alfvén-type motions on different flux surfaces decouple from each other, a well-known fact from previous MHD studies (for a review see Goedbloed & Poedts 2004, here-

[1] By torsional oscillations we mean those which are nearly incompressible. Modes with compression have strong restoring forces and feature much higher frequencies than most of the observed QPOs.

after GP). One can then formulate the full dynamics of the system in terms of discrete modes of the crust which are coupled to a continuum of Alfvén modes in the core. L07 demonstrated that (1) the global modes with frequencies inside the continuum are strongly damped via a phenomenon known in MHD as *resonant absorption* (see GP) and (2) in many cases, asymptotically the system tends to oscillate with the frequencies close to the continuum edges. This result was later confirmed by Gruzinov 2008b, who has used a powerful analytical technique to solve the L07's normal-mode problem (Gruzinov noted that the resonant absorption is mathematically equivalent to Landau damping). Oscillations near the continuum edge frequencies were also observed in a number of numerical general-relativistic MHD simulations of purely fluid stars (Sotani et al. 2008, Colaiuda et al. 2009, Cerdá-Durán et al. 2009). Apart from finding QPOs near the continuum edges, L07's dynamical simulations identified transient QPOs with drifting frequencies; these were transiently amplified near the crustal frequencies. No explanation for the origin of the drifts was given.

In this chapter, we extend the previous analyses of the hydro-magnetic crust-core coupling in an essential way. In section 3.2, we re-analyse L07's toy model of a single oscillator coupled to a continuum and we show that this system generically contains the *edge normal modes* with frequencies near the continuum edges. We show that these modes dominate the late-time dynamics of the system, and develop a formalism which allows one to predict analytically the edge mode's amplitude from the initial data. We then explore the effect of viscosity on the system (introduced as a friction between the neighboring continuum oscillators) and show that the edge mode is longer lived than all other motions of the system. We also provide a non-trivial analytical formula for the time dependence of the overall energy dissipation.

In section 3.3, we describe how transient QPOs, not associated with the normal modes of the system, are obtained when parts of the core spectrum consist of densely and regularly spaced discrete modes (and in section 3.5 we show that such an array of discrete modes is expected when the magnetic field in the core is not perfectly axisymmetric but has some degree of tangling).

As a by-product of our analysis, we explain the origin of the QPO frequency drifts seen in L07 simulations. We provide simple analytical fits to the drifts, and show that when the regularity of the continuum sampling is removed (e.g, when the frequencies are sampled as random numbers picked from the continuum range), the drifts disappear.

In section 3.4, we set up models with a more realistic hydro-magnetic structure of the neutron-star core. We show how to find the continuum modes and their coupling to the crust for an arbitrary axisymmetric poloidal field, with an arbitrary density profile on the core (L07s calculations, for simplicity and concreteness, were restricted to constant-density core and homogeneous magnetic field). We treat a more complicated case of a mixed axisymmetric toroidal-poloidal field, with radial stratification, in Appendix 3.B. We demonstrate that for realistic field configurations, the Alfvén continuum of modes coupled to the crust may show a number of gaps. If a crustal mode frequency belongs to one of these gaps, a strong global discrete mode arises which dominates the late-time dynamics and whose frequency also belongs to the gap. The frequency of the gap global mode does not generally coincide with, but is often close to that of the crust. We suggest that it was these gap modes that appeared in Lee's (2008) calculations as well-defined discrete global modes.

So far, only axisymmetric magnetic fields have been considered in the magnetar-QPO literature, with the Alfvén continuum modes occupying the flux surfaces of the field. In section 3.5 we argue that if the field is not axisymmetric but instead is highly tangled, then the Alfvén continuum modes become localized within small regions of individual field lines and therefore become dynamically unimportant. Instead, a set of discrete Alfvén modes appears, with the spacing between the modes strongly dependent on the degree of field tangling. We devise a phenomenological prescription which allows us to parametrize the field tangling for computing the dynamically important modes and introduce an easily solvable "square box" model suitable for exploring the parameter range.

Finally, in section 3.6, we use the suite of models built in the previous sections to explore their connection to the QPO phenomenology. We find that (a) within the standard magnetar model, it is possible to produce strong

long-lived or transient QPOs with frequencies in the range of around 20-150 Hz, but only if the neutrons are decoupled from the Alfvén-like motion of the core; this implies that at least one of the baryonic components of the core is a quantum fluid. (b) Our models could not produce the high-frequency 625 Hz QPO within the standard paradigm of a magnetar core composition.

3.2 An oscillator coupled to a continuum: edge modes

In this section, we study the motion of a harmonic oscillator (which we hereafter call the large oscillator) which is coupled to a continuum of modes.[1]. This model was introduced in L07 and it provides a qualitative insight into the behaviour of crustal modes (represented by the large oscillator) coupled to a continuum of Alfvén modes in the core of a magnetar. L07 found that if the large oscillator's proper frequency was within the range of the continuum frequencies, then the late-time behaviour of the system was dominated by oscillatory motion near the edges of the continuum interval. Here, we give an explanation of this phenomenon in terms of the *edge modes*. Our analysis allows us to use initial data and predict the displacement amplitudes and frequencies of the system at late times.

The model consists of the large mechanical oscillator with mass M and proper frequency ω_0, representing a crustal elastic shear mode. Attached to the large oscillator is a set of N smaller oscillators of mass m_n and proper frequency ω_n constituting a quasi-continuum of frequencies ω_n (where $n = 1, 2, ..., N$). The continuum is achieved when $N \to \infty$ while the total small-oscillator mass Σm_n remains finite. The convenient pictorial representation is through suspended pendulae, as shown in Fig. 4.2 (see also Fig. 2 of L07). The equations of motion are obtained as follows. Each small oscillator is driven by the motion

[1] In many areas of physics similar models have been studied, notably in quantum optics and plasma physics. By contrast with the case studied here, in these models the range of the continuum frequencies is not limited.

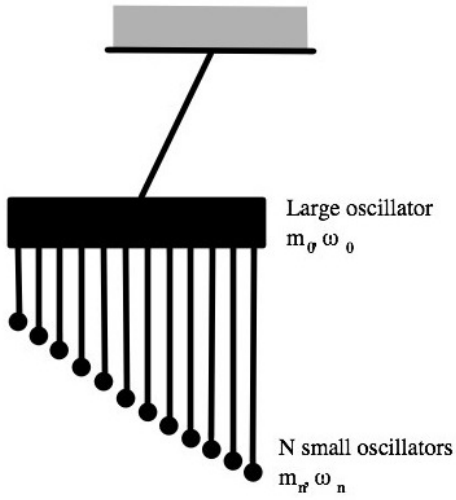


Figure 3.1: *Schematic picture of the toy-model. A large number N of small pendulae, representing the (quasi-) continuum, are coupled to one large pendulum, representing the crust.*

of the large oscillator:

$$\ddot{x}_n + \omega_n^2 x_n = -\ddot{x}_0 \tag{3.1}$$

where x_n is the displacement of the $n'th$ small oscillator in the frame of reference of the large oscillator, x_0 is the displacement of the large oscillator in the inertial frame of reference and the right-hand side represents the non-inertial force acting on the small oscillator due to the acceleration of the large one. The large oscillator experiences the combined pull of the small ones:

$$M\ddot{x}_0 + M\tilde{\omega}_0^2 x_0 = \sum_i m_i \omega_i^2 x_i \tag{3.2}$$

Here $\tilde{\omega}_0$ is the frequency of the big pendulum corrected for the mass loading by the small pendulae, i.e. $\tilde{\omega}_0^2 = \omega_0^2 \left(M + \sum_i m_i\right)/M$.

3.2.1 Time-dependent behavior.

In this subsection we explore the behavior of this system by direct numerical simulations. We found this to be helpful in the building of our intuition. We defer a semi-analytical normal-mode analysis to the next subsection.

We follow L07 and for concreteness concentrate on a specific example; it will be clear that the conclusions we reach are general. We choose $\omega_0 = 1$ rad s^{-1} and mass $M = 1$. We choose a total number of 1000 small pendulae with frequencies $\omega_n = (0.5 + n/1000)$ rad s^{-1} and masses $m_n = m = 10^{-4}$, to mimic the continuum frequency range between 0.5 rad s^{-1} and 1.5 rad s^{-1}. The simulation is initiated by displacing the large oscillator while keeping the small pendulae relaxed (this mimics the stresses in the crust) and then releasing. The subsequent motion of the system is then followed numerically by using a second order leapfrog integration scheme which conserves the energy with high precision. The resulting motion of the large pendulum can be decomposed into three stages (see Fig. 3.2 and Fig. 3.3): (1) During the

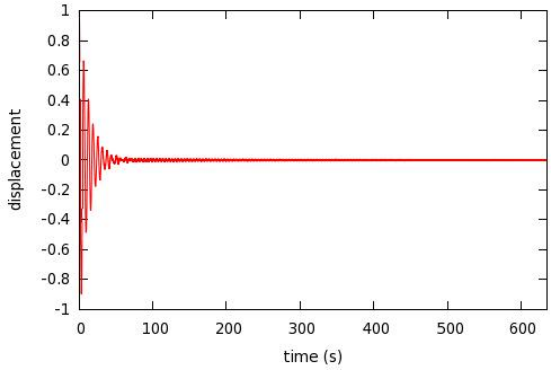


Figure 3.2: *Displacement of the big oscillator as a function of time.*

first 50-60 seconds, there is a rapid exponential decay of the large oscillator's motion, during which most of the energy is transferred to the multitude (i.e., the 'continuum') of small oscillators. This is the so-called phenomenon of "resonant absorption", which has been studied for decades in the MHD and plasma physics community (e.g., Ionson 1978, Hollweg 1987, Goedbloed & Poedts 2004, L07, Gruzinov 2008b). In this first stage, the amplitude of the big pendulum motions drops by a factor of ~ 100. (2) After ~ 60 seconds, the exponential decay stops abruptly as the large oscillator now reacts to the collective pull of the small ones. This second stage is characterized by a slow algebraic decay of the amplitude of the big pendulum displacement. Gruzi-

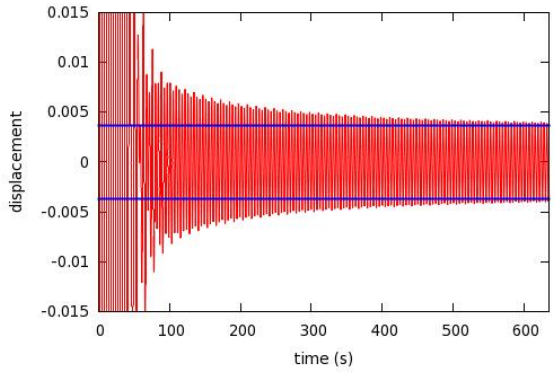


Figure 3.3: *A zoomed-in version of Fig. 3.2. The blue horizontal lines denote the theoretically predicted amplitude of the dominating upper edge-mode (see section 3.2.3).*

nov (2008b) explains this as being due to the branch cut in the oscillator's response function. (3) The motion of the large oscillator stabilizes at a constant level (L07 missed this stage in his simulations, which he stopped too early). Fourier transform reveals two QPOs at the frequencies close to the continuum edges, $\omega = 0.5$ and $\omega = 1.5$; the same QPO frequencies can be observed in the previous stage (2) as well.

What is the origin of the QPOs and how is this eventual stability established? In Fig. 3.4 and 3.5, we show how the amplitude of the small oscillators evolves with time. After the initial resonant absorption phase, the amplitude is distributed as a Lorentzian centered on the frequency around $\omega = 1$; this is because the small oscillators in resonance with the large one are the ones which gain the most energy. However, in subsequent times we see that the energy exchange occurs between the small oscillators[1] and that the net result of this exchange is the energy flow towards the oscillators whose frequencies are near the edges. By the time the third stage begins, the amplitudes of the oscillators near the edge stabilize and their phases become locked. They are

[1] This is much akin to the well-known phenomenon of resonant energy exchange between two equal-frequency pendulae hanging on the same supporting wall.

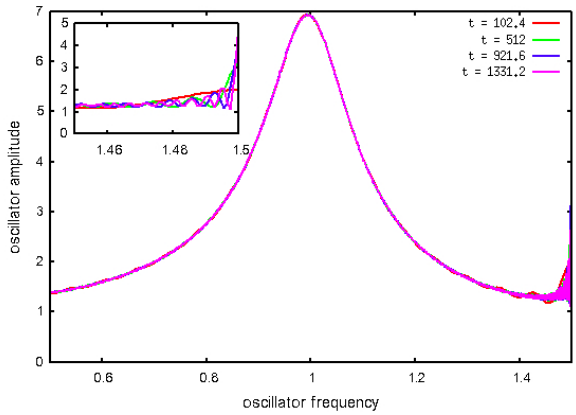


Figure 3.4: *The colored curves show the amplitudes of the small oscillators during the numerical simulation, at different times t.*

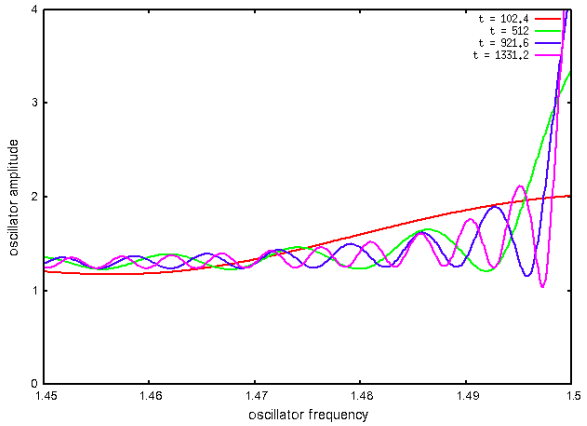


Figure 3.5: *A zoomed-in version of Fig. 3.4. At later times energy is transferred to the oscillators near the edge of the continuum.*

pulling and pushing the large oscillator in unison. In the next subsection, we show that this behavior is due to the presence of the *edge normal modes*, and we shall derive their frequencies and amplitudes.

3.2.2 Finding eigenmodes

In this section we deal with the system of coupled harmonic oscillators and one should be able to find its normal modes using the standard techniques (Landau and Lifshitz mechanics, §23). However, the fact that all small oscillators are attached to the large one and there is no direct coupling between the small oscillators, allows us a significant shortcut (in Appendix 3.A, we treat a more general problem of *several* large oscillators coupled to a multitude of the core modes). We proceed as follows: Suppose that we impose on the large oscillator a periodic motion with angular frequency Ω, by driving it externally with the force $F_{\text{ext}} = F_0(\Omega)\exp(i\Omega t)$. This motion in turn drives the small oscillators according to Eq. (3.1):

$$\ddot{x}_n + \omega_n^2 x_n = \Omega^2 x_0, \tag{3.3}$$

which has the steady state solution:

$$x_n = \frac{\Omega^2}{\omega_n^2 - \Omega^2} x_0 \tag{3.4}$$

where we have omitted the time dependent factor $\exp(i\Omega t)$ on both sides. The combined force f_{cont} of the small oscillators acting back on the large one (see Eq. (3.2)) is given by

$$f_{\text{cont}}(\Omega) = \sum_n m_n \omega_n^2 \frac{\Omega^2}{\omega_n^2 - \Omega^2} x_0. \tag{3.5}$$

According to Newton's second law,

$$F_0(\Omega) + f_{\text{cont}}(\Omega) = -M(\Omega^2 - \omega_0^2)x_0. \tag{3.6}$$

If Ω corresponds to the normal-mode frequency, then $F_0(\Omega) = 0$. Hence by substituting Eq. (3.5) into Eq. (3.6) we get the following eigenvalue equation

for Ω:

$$G(\Omega) = M\left(\omega_0^2 - \Omega^2\right) - \sum_n m_n \omega_n^2 \frac{\Omega^2}{\omega_n^2 - \Omega^2} = 0. \tag{3.7}$$

In the continuum limit $N \to \infty$, the above equation becomes

$$G(\Omega) = M\left(\omega_0^2 - \Omega^2\right) - \int_{\omega_{\min}}^{\omega_{\max}} d\omega \rho(\omega) \omega^2 \frac{\Omega^2}{\omega^2 - \Omega^2} = 0, \tag{3.8}$$

where $\rho(\omega) = dm/d\omega$ is the mass per unit frequency of the continuum modes. In the discrete case, the solutions of Eq. (3.7) are $N-1$ frequencies Ω_i that are within the quasi-continuum ($\omega_i < \Omega_{i+1} < \omega_{i+1}$, for $i = 1, 2, ...N-1$; 'quasi-continuum modes') and 2 modes with frequencies $\Omega_{\rm low}$ and $\Omega_{\rm high}$ that are near the edges, but outside, of the continuum (we will refer to these modes as 'edge-modes' from now on). In other words; $\Omega_{\rm low}$ is in general slightly smaller than the lowest frequency in the continuum, i.e. $\Omega_{\rm low} \lesssim \omega_1$ and $\Omega_{\rm high}$ is slightly larger than the highest frequency in the continuum, i.e. $\Omega_{\rm high} \gtrsim \omega_N$. It can be shown from Eq. (3.7) that in the limit $N \gg 1$ and $m_n \ll M$, the contribution of the small oscillator to the i-th quasi-continuum mode is completely dominated by the pendulae that are in close resonance with the mode. More precisely, one can show that as the number of oscillators N increases and m_n decreases, the number of small oscillators contributing to the mode energy remains constant. However, for the two edge modes there is no such singular behavior in the limit of large N and consequently they play a special role in the dynamics of the system. This last point is clearly seen in the continuum case represented by Eq. (3.8). The eigenvalue equation has no real solutions in the range of small-oscillator continuum $\omega_{\min} < \Omega < \omega_{\max}$, since the response function $G(\Omega)$ is ill-defined in this interval[1]. However, the edge modes on both sides of the continuum interval remain and their frequencies can be found by numerically evaluating the zero points of $G(\Omega)$ in Eq. (3.8). For the numerical calculation of the previous subsection, one finds $\Omega_{\rm low} = 0.5 - 8.2 \cdot 10^{-6}$ and $\Omega_{\rm high} = 1.5 + 8.6 \cdot 10^{-4}$. Analytically, one can find

[1] There is a complex solution if the integration in the expression for $G(\Omega)$ is performed along the contour chosen according to the Landau rule. One then obtains a "resonantly absorbed" or "Landau-damped" mode (Gruzinov 2008b, L07), which exactly represents the exponential decay of stage (1) in our numerical experiment of the previous subsection.

the following scaling for the distance $\delta\omega_{\rm edge}$ between the mode frequency and the nearest edge $\omega_{\rm edge}$ of the continuum range:

$$\frac{\delta\omega_{\rm edge}}{\omega_{\rm edge}} = C\exp\left\{-\frac{M|\Omega_0^2-\omega_{\rm edge}^2|}{\rho(\omega_{\rm edge})\omega_{\rm edge}^3}\right\}, \tag{3.9}$$

where C is a constant of order unity. The larger is the density of continuum modes at the edge $\rho(\omega_{\rm edge})$, the further is the edge mode pushed away from the continuum range. It is particularly interesting to consider the case when the continuum interval is limited by a turning point (L07) with the divergent density of states near the edge, $\rho(\omega) = A/\sqrt{|\omega-\omega_{\rm edge}|}$, where A is a constant. In this case the distance from the edge-mode frequency to the nearest continuum edge is given by

$$\frac{\delta\omega_{\rm edge}}{\omega_{\rm edge}} = C\left\{\frac{A\omega_{\rm edge}^{7/2}}{M|\Omega_0^2-\omega_{\rm edge}^2|}\right\}^2. \tag{3.10}$$

The quadratic dependence in Eq. (3.10) vs. the exponential dependence in Eq. (3.9) implies that the continua with turning points typically feature much more pronounced edge modes and stronger QPOs than the ones with linear edges. In the next section, we show how to calculate the edge-mode amplitudes and QPO strengths from the initial data.

3.2.3 Late time behavior of the system

In the continuum limit, the only modes with real oscillatory frequency are the edge modes. Thus, as we demonstrate explicitly below, they dominate the late-time dynamics of the system when the number N of small oscillators becomes large. Our analysis proceeds as follows: Let us define a new set of variables, expressed as a vector $\boldsymbol{X}$ with components $X_0 = \sqrt{M}x_0$ and $X_n = \sqrt{m_n}\,(x_0+x_n)$ for $n = 1, ..., N$. With these new variables, the kinetic energy of the system is a trivial quadratic expression

$$K = \frac{1}{2}\dot{\boldsymbol{X}}\cdot\dot{\boldsymbol{X}}, \tag{3.11}$$

where the inner product of two vectors $\boldsymbol{A}$ and $\boldsymbol{B}$ is defined as $\boldsymbol{A} \cdot \boldsymbol{B} = \Sigma_{j=0}^{N} A_j B_j$. The potential energy is a positive-definite quadratic form, whose exact form is unimportant here. The mutually orthogonal eigenmodes $\boldsymbol{X}^i$ can be found via a procedure outlined in the previous section[1]. Their eigenfreguencies Ω_i are identified by finding zeros of $G(\Omega)$ in Eq. (3.7) and the corresponding eigenvector components are given by

$$\begin{aligned} X_0^i &= 1 \\ X_n^i &= \frac{\omega_n^2}{\Omega_i^2 - \omega_n^2}. \end{aligned} \tag{3.12}$$

Let's assume that we initiate our simulation by displacing the large oscillator by an amount $x_0\,(0)$ while keeping the small oscillators relaxed $x_n\,(0) = 0$ and all initial velocities at zero. In the new variables, the initial state of the system is given by the vector $\boldsymbol{X}(0)$, where $\boldsymbol{X}_0 = \sqrt{M} x_0(0)$ and $\boldsymbol{X}_n = \sqrt{m_n} x_0(0)$. The time evolution of the system is given by:

$$\boldsymbol{X}(t) = \Sigma_{\Omega_i} \cos(\Omega_i t) \left(\boldsymbol{X}^i \cdot \boldsymbol{X}^i\right)^{-1} \left(\boldsymbol{X}(0) \cdot \boldsymbol{X}^i\right) \boldsymbol{X}^i. \tag{3.13}$$

Substituting the initial conditions and the expression in Eq. (3.12) for the eigenvector components, we get

$$\boldsymbol{X}(t) = \sum_{\Omega_i} \cos(\Omega_i t) \frac{M + \sum_n \frac{m_n \omega_n^2}{\omega_n^2 - \Omega_i^2}}{M + \sum_n \frac{m_n \omega_n^4}{(\omega_n^2 - \Omega_i^2)^2}} \boldsymbol{X}^i. \tag{3.14}$$

The coordinate of the large oscillator is simply given by $x_0(t) = \boldsymbol{X}_0(t)/\sqrt{M}$. For the continuum of small modes, the above expansion breaks down, since the eigenvalue equation has no real solutions inside the continuum range. However, the edge modes are well defined and they determine the dynamics at late times. Therefore, for the continuum case we can still write down the analogous expression which is valid only at late times:

$$\boldsymbol{X}(t) = \Sigma_{\Omega_{\text{edge}}} \cos(\Omega_{\text{edge}} t) \frac{\boldsymbol{X}(0) \cdot \boldsymbol{X}_{\text{edge}}}{\boldsymbol{X}_{\text{edge}} \cdot \boldsymbol{X}_{\text{edge}}} \boldsymbol{X}_{\text{edge}} \tag{3.15}$$

The sums of Eq. (3.14) are replaced with the corresponding integrals, and we have the following expression for the displacement of the large oscillator at

[1] Alternatively, they can be found by diagonalizing the potential-energy quadratic form.

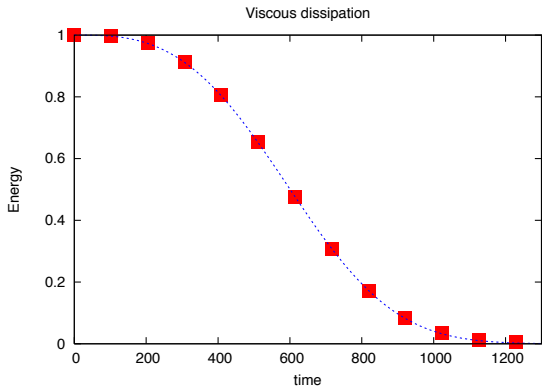


Figure 3.6: *The red squares show the viscous dissipation of the total energy during the numerical simulation. The dotted blue curve shows the analytical solution from Eq. (3.23).*

late times:

$$x_0(t) = x_0(0) \sum_{\Omega_{\rm edge}} \cos(\Omega_{\rm edge} t) \frac{M + \int d\omega \rho(\omega) \frac{\omega_n^2}{\omega_n^2 - \Omega_{\rm edge}^2}}{M + \int d\omega \rho(\omega) \frac{\omega_n^4}{(\omega_n^2 - \Omega_{\rm edge}^2)^2}} \tag{3.16}$$

This expression is in excellent agreement with the numerical simulations. In the numerical example of subsection 3.2.1, the upper edge mode dominates the late-time behavior of the system and its calculated contribution is plotted in Fig. 3.3, together with the numerically simulated motion.

3.2.4 The effect of viscosity

We now add an extra degree of realism by introducing viscous friction into the system. In MHD, continuum modes are spatially localized and the effect of viscosity is to frictionally couple the neighboring modes (see, e.g., Hollweg 1987). In our simple model we introduce viscosity by adding frictional forces between the neighboring oscillators,

$$f_{n,n+1} = -f_{n+1,n} = \gamma(\dot{x}_n - \dot{x}_{n+1}), \tag{3.17}$$

where $f_{n,n+1}$ is the force from the n'th oscillator acting on the $(n+1)$'th. We now calculate how the system dissipates energy as a function of time. We will show that it occurs in two stages (see Fig. 3.6): (1) Initially, the small

oscillators are strongly and simultaneously excited by the "Landau-damped" large oscillator, then they become dephased, with the average relative motion between the neighboring oscillators growing linearly in time. This leads to a very rapid dissipation of the bulk of the initial energy. (2) The edge modes persist, since the participating small oscillators move in phase and the energy dissipation is small. The energy of the modes is damped exponentially on a timescale much longer than that of the first stage. The dissipated energy is given by

$$W_{\rm diss} = \Sigma_{n=1}^{N-1}\gamma(\dot{x}_{n+1} - \dot{x}_n)^2. \tag{3.18}$$

In the continuum limit, the small oscillators are labeled not by a discrete index n, but by a continuous variable λ. The expression for the dissipated energy is then

$$W_{\rm diss} = \int d\lambda\tilde{\gamma}\left(\frac{\partial^2 x_\lambda(t)}{\partial\lambda\partial t}\right)^2, \tag{3.19}$$

where $\tilde{\gamma}$ is the viscous coefficient. After the initial exponential damping of the large oscillator and the excitation of the small oscillators, the latter initially move independently, with

$$x_\lambda(t) \simeq \tilde{x}(\lambda)\cos[\omega_\lambda t], \tag{3.20}$$

where $\tilde{x}(\lambda)$ is the amplitude of the λ'th oscillator. From the above equation, we then obtain

$$\left\langle\left(\frac{\partial^2 x_\lambda(t)}{\partial\lambda\partial t}\right)^2\right\rangle = \frac{1}{2}\left\{[d(\tilde{x}_\lambda\omega_\lambda)/d\lambda]^2 + \omega_\lambda^2\tilde{x}_\lambda^2(d\omega_\lambda/d\lambda)^2t^2\right], \tag{3.21}$$

where the $\langle ...\rangle$ stands for time-averaging over many oscillation periods. For times $t \gg d\log x_\lambda/d\omega_\lambda$ the second term on the right-hand side of Eq. (3.21) dominates. For a simple model with $d\omega_\lambda/d\lambda = const$ and $\rho(\omega) = const$,

$$dE/dt \propto -At^2E, \tag{3.22}$$

where E is the total energy of the system and $A = (\tilde{\gamma}/\rho)(d\omega_\lambda/d\lambda)$. The analytical solution for the energy and dissipated power,

$$E = E_0\exp\left(-\frac{1}{3}At^3\right), \tag{3.23}$$

$$W_{\rm diss} = -\frac{dE}{dt} = At^2E_0\exp\left(-\frac{1}{3}At^3\right)$$

agrees very well with numerical simulations, see Fig. 3.6. While the equations above were derived for restrictive assumptions ($d\omega_\lambda/d\lambda = const$ and $\rho(\omega) = const$), we found that the analytical formulae in Eq. (3.23) provide a good fit for a large variety of simulations. This is because it is the small oscillators with the frequencies near that of the large oscillator which carry most of the energy and in that narrow band our approximations hold.

After the energy dissipation due to dephasing is over, only the edge modes remain. This is illustrated in Fig. 3.7, where we show how the energies of the small oscillators evolve with time. At late times, only the oscillators taking part in the edge modes move substantially; this is because they remain in phase and do not dissipate much. At this stage the energy is drained by slow exponential decay of the edge modes.

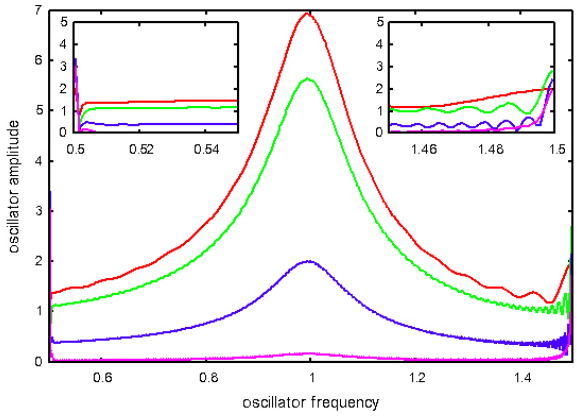


Figure 3.7: *As in Fig. (3.4), this figure shows the amplitudes of the small oscillators at different times t. The energy of most oscillators is drained due to viscous dissipation. At late times, only the oscillators near the edges of the continuum have substantial energy.*

3.3 Transient and drifting QPOs

Finite-size MHD systems feature a mix of continuum and discrete modes (see Poedts et al., 1985 and GP). For axisymmetric field configurations the con-

tinuum modes occupy the whole flux surfaces and play an important role in the oscillatory dynamics; this was the motivation for L07 and our study of the previous section. We argue in section 3.5 that if the core field is highly tangled, the continuum modes become localized in space and discrete core modes will play a more important role. Thus it is important to study the case when the crustal modes are coupled to a set of discrete core modes. In this section we show that if the frequencies of the discrete modes are regularly spaced in some frequency intervals, then the system displays *transient QPOs* that are entirely missed by its normal-mode analysis. This is interesting from the observational point of view, since many of the observed magnetar QPO features are transient.

Suppose that a set of discrete modes are located in the interval $\Delta\omega$ around frequency ω_0 and are separated by a regular frequency interval $\delta\omega$ and assume the following hierarchy:

$$\delta\omega \ll \Delta\omega \ll \omega_0. \tag{3.24}$$

After the modes are excited, they are initially in phase but will de-phase rapidly on the timescale $1/\Delta\omega$. However, at times $t_n = 2\pi n/\delta\omega$ the modes come into phase again and pull coherently on the large oscillator. Therefore, a transient QPO feature should appear around these times at a frequency close to ω_0. In Fig. 3.8 and Fig. 3.9 we show the dynamical spectrum from a simulation where the model was designed to produce QPOs at two specific frequencies. The transient QPOs agree well with the expectations. As is seen from the figures, the strongest transient QPOs are those whose frequencies are the closest to that of the large oscillator; this is because the response of the large oscillator is the strongest around its proper frequency. One can now easily understand the frequency drifts in Fig. 10 of L07 (Fig. 3.10 in this chapter) as an artefact of the discrete sampling of the continuum. In the simulations of that paper, the core continuum was sampled with a set of densely and regularly-placed Alfvén modes by slicing the field into finite-width flux shells. The spacing $\delta\omega$ between the modes was not constant but a function of the Alfvén frequency ω. In that case, the QPO drifts with the

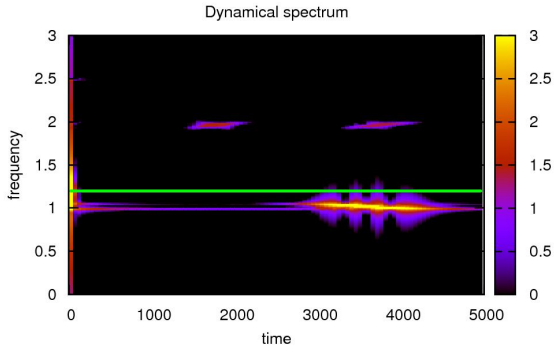


Figure 3.8: *Dynamical spectrum from a simulation where we have designed the continuum so as to produce transient QPO's at frequencies* $\omega = 1$ *and* $\omega = 2$ *(the colored scale denotes* $\log(\text{power})$*). The green horizontal line denotes the frequency of the large oscillator* ($\Omega = 1.2$).

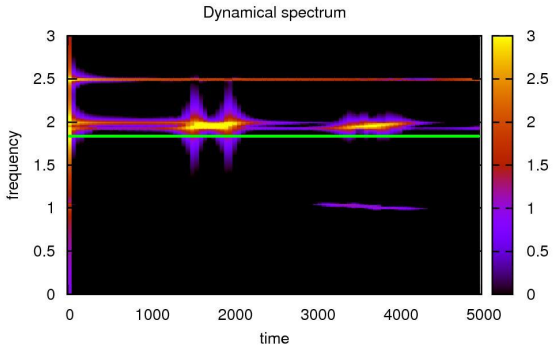


Figure 3.9: *We have shifted the frequency of the large oscillator (green horizontal line) to* $\Omega = 1.8$*. By comparison with Fig. 3.8, the drifting QPO's at* $\omega = 2$ *are now much stronger as they are closer to the large oscillator frequency. Note that the edge mode at* $\omega = 2.5$ *is clearly visible.*

QPO frequency $\omega(t)$ given by the inverse relation

$$t(\omega) = \frac{2\pi n}{\delta\omega(\omega)}. \tag{3.25}$$

With this relation we are able to fit all of L07 drifting QPOs, as shown in Fig. 3.10 and 3.11. Note that multiple QPOs correspond to different branches of the Alfvén continuum. As expected, the drifting QPOs are amplified near the crustal frequencies, since there the response of the crust to the core modes' pull is the strongest.

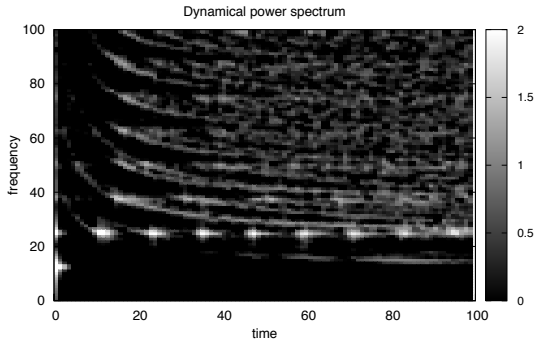


Figure 3.10: *Dynamical power spectrum of the spherical magnetar model from L07. The gray scale denotes* log(power).

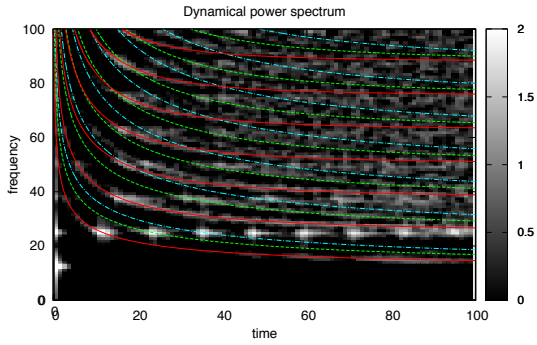


Figure 3.11: *We have used Eq. (3.25) to fit the drifting QPO's from figure 3.10. The red curves are $n = 1$ drifts, green curves are $n = 2$ and blue curves are $n = 3$. The higher frequency drifts originate from Alfvén overtones.*

3.4 More realistic magnetar models

In this section we extend the constant magnetic field and constant-density magnetar model from L07 to include more realistic pressure and density profiles and more general (but still axisymmetric) magnetic field configurations. Our aim is to use this model to: (1) calculate numerically Alfvén eigenmodes and their eigenfrequencies on different flux surfaces inside the star, in order to determine the continuous spectrum of the fluid core and (2) use these modes to simulate the dynamics of a realistic magnetar. In order to calculate the Alfvén eigenmodes and eigenfrequencies for a realistic magnetar model, we employ the linearized equations of motion for an axisymmetric magnetized,

self-gravitating plasma. The general equations, which are derived in detail in Poedts et al. (1985, hereafter P85) and given in their equations (53) and (54), constitute a fourth order system of coupled ordinary differential equations in the case of a mixed poloidal and toroidal magnetic field. The formalism of P85 is briefly summarized in Appendix 3.B. In the case of a purely poloidal magnetic field, the system simplifies to two uncoupled second order differential equations (P85, equations (70) and (71)).

3.4.1 The model

We assume our star is non-rotating and neglect its deformation due to the magnetic pressure, which is expected to be small. Therefore, we consider a spherically symmetric background model that is a solution of the Tolman-Oppenheimer-Volkoff equation (TOV equation)[1]. The hydrostatic equilibrium is calculated using a SLy equation of state (Douchin & Haensel 2001; Haensel & Potekhin, 2004; Haensel, Potekhin & Yakovlev 2007), see the website *http://www.ioffe.ru/astro/NSG/NSEOS/* for a tubulated version. The integration of the TOV equation is performed using a 4th order Runge-Kutta scheme, integrating from the center of the star outward until we reach a mass density $\rho = 1.3 \cdot 10^{14}$ g cm^3, which is consistent with the crust-core interface in the equation of state from Douchin & Haensel (2001). The resulting model has a central mass density $\rho_c = 10^{15}$ g cm^3, a total mass of 1.40 $M_\odot$ and a radius of $R_{\rm core} = 1.07 \cdot 10^6$ cm. To this spherical model we add a poloidal magnetic field, which we generate by placing a circular current loop of radius a and current I around the center of the star. The field is singular near the current loop, however all the field lines which connect to the crust (and thus are physically related to observable oscillations) carry finite field values. This particular field configuration is chosen as an example; there is an infinite number of ways to generate poloidal field configurations. In appendix 3.B we will add to this field a toroidal component and calculate the corresponding Alfvén continuum of the core.

[1] Note that although our background equillibrium model is based on the relativistic TOV equation, our equations of motion will be derived using classical MHD.

3.4.2 The continuum

In order to find the equations of motion for the magnetized material in the neutron star core, we would need to add self-gravity to the ideal magnetohydrodynamic equations. This problem has been solved by P85 in a tour the force mathematical approach. In that paper the authors assume a self-gravitating axisymmetric equilibrium with a field geometry consisting of mixed poloidal and toroidal field components and they derive linearized equations of motion. For this field geometry it is convenient to work with so-called flux-coordinates (ψ, χ, ϕ).[1] The basic concept behind this curvilinear coordinate system is the magnetic flux-surface, which is defined as the surface perpendicular to the Lorentz force $\boldsymbol{F}_L \propto \boldsymbol{j} \times \boldsymbol{B}$. From this definition it is clear that the magnetic field lines lie in flux surfaces. If one considers a closed loop on a flux surface which makes one revolution around the axis of symmetry, then the magnetic flux ψ through the loop depends on the flux surface only and is the same for all of the loops. Therefore ψ is chosen as the coordinate labeling the flux surfaces. In each flux-surface we can denote a position by its azimuthal angle ϕ and its 'poloidal' coordinate χ, which is defined as the length along $\phi = const$ line. In P85, it is shown that the equations of motion allow for a class of oscillatory solutions that are located on singular flux surfaces, constituting a continuum of eigenmodes and eigenfrequencies. In the case of a purely poloidal field ($B = B_\chi$), the continuum solutions are degenerate and polarized either parallel (ξ_χ) or perpendicular (ξ_ϕ) to the magnetic field lines. In the latter case the displacement is ϕ-independent. It is clear that in contrast to the χ-polarized modes, the ϕ-polarized modes are purely horizontal and are therefore unaffected by gravity. This latter case is considered here. The equation of motion is then simply the Alfvén wave equation:

$$\frac{\partial^2 \xi_\phi(\psi, \chi)}{\partial t^2} = F\left[\xi_\phi(\psi, \chi)\right], \tag{3.26}$$

[1] There exists a variaty of magnetic coordinate systems that can be used to study axisymmetric magnetohydrodynamic equilibria. A useful overview of systems used by plasma and MHD physicists is given in Alladio & Micozzi (1996). In Colaiuda et al. (2009), the authors employ an alternative relativistic system of coordinates for their study of torsional Alfvén oscillations of magnetars, which allows them to reduce the 1+2 dimensional evolution equation for magnetar oscillations to a 1+1 dimensional form.

where the operator F is given by

$$F\left[\xi_\phi(\psi,\chi)\right] = \frac{B}{4\pi x\rho}\frac{\partial}{\partial\chi}\left[x^2 B\frac{\partial}{\partial\chi}\left(\frac{\xi_\phi(\psi,\chi)}{x}\right)\right]. \tag{3.27}$$

Here x is the distance to the magnetic axis of symmetry. Although in the presence of a mixed poloidal and toroidal field the equations still give rise to a continuous set of solutions, the calculations are significantly complicated as the continuum modes are affected by the toroidal component of the field, by gravity and by compressibility. For the sake of simplicity we will ignore toroidal fields in our dynamic simulations. We will however, calculate the continuum frequencies for a mixed poloidal and toroidal field in Appendix 3.B.

For determining the spectrum of the core continuum, the appropriate boundary conditions are $\xi_\phi(\chi = \chi_c) = 0$, where $\chi_c(\phi)$ marks the location of the crust-core interface. The full significance of this boundary condition will become apparent in later in this section when we develop the analysis for the crust-core interaction. With this boundary condition, Equation (3.26) constitutes a Sturm-Liouville problem on each separate flux surface ψ. Using the stellar structure model and magnetic field configuration from section 3.4.1, we can calculate the eigenfunctions and eigenfrequencies for each flux surface ψ. The reflection symmetry of the stellar model and the magnetic field with respect to the equatorial plane assures that the eigenfunctions of Eq. (3.26) are either symmetric or anti-symmetric with respect to the equatorial plane. We can therefore determine the eigenfunctions by integrating Eq. (3.26) along the magnetic field lines from the equatorial plane $\chi = 0$ to the crust-core interface $\chi = \chi_c(\psi)$. Let us consider the odd modes here for which $\xi_\phi(0) = 0$ and solve Eq. (3.26) with the boundary condition $\xi_\phi(\chi_c) = 0$ at the crust-core interface; for even modes, the boundary condition is $d\xi_\phi(0)/d\chi = 0$. We find the eigenfunctions by means of a shooting method; using fourth order Runge-Kutta integration we integrate from $\chi = 0$ to $\chi = \chi_c$. The correct eigenvalues σ_n and eigenfunctions $\xi_n(\chi)$ are found by changing the value of σ until the boundary condition at ξ_n is satisfied. In this way we gradually increase the value of σ until the desired number of harmonics is obtained. In figure 3.12 we show a typical resulting core-continuum. According to Sturm-Liouville

theory the normalized eigenfunctions ξ_n of Eq. (3.26) form an orthonormal basis with respect to the following inner product:

$$\langle \xi_m, \xi_n \rangle = \int_0^{\chi_c} r(\chi)\, \xi_m(\chi)\, \xi_n(\chi)\, d\chi = \delta_{m,n} \tag{3.28}$$

Where $\delta_{m,n}$ is the Kronecker delta and $r = 4\pi\rho/B_\chi$ is the weight function. We have checked that the solutions we find satisfy the orthogonality relations.

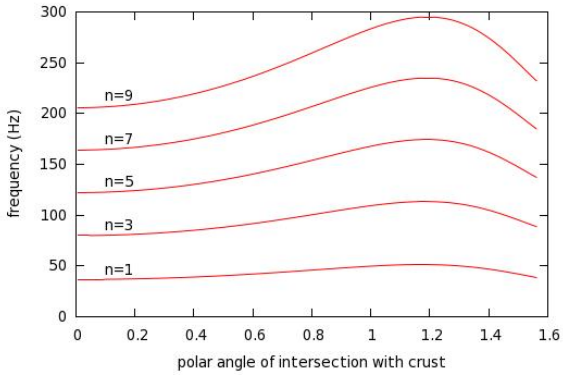


Figure 3.12: *The red curves show the Alfvén frequencies σ_n as a function of the angle $\theta(\psi)$, the polar angle at which the flux-surface ψ intersects the crust. Since we are only considering odd crustal modes, the only Alfvén modes that couple to the motion of the star are the ones with an odd harmonic number n. This particular continuum was calculated using a poloidal field with an average surface value $B_{\rm surface} \sim 6 \cdot 10^{14}$ G, generated by a circular ring current of radius $a = R_*/2$.*

We are now ready to compute the coupled crust-core motion. Here we follow L07 and assume that the crust is an infinitely thin elastic shell[1]. We label the lattitudinal location by the flux surface ψ intersecting the crust and consider the crustal axisymmetric displacements $\bar{\xi}_\phi(\psi)$. In the MHD approximation, the magnetic stresses enforce a no-slip boundary condition at the

[1]It is straightforward to relax this assumption and carry out the analysis of this section for the finite crustal thickness. However, from Section 3.2 it is clear that the interesting dynamics is dominated by the spectral structure of the core Alfvén waves; therefore in order to flesh out the physics we choose the simplified model of the crust.

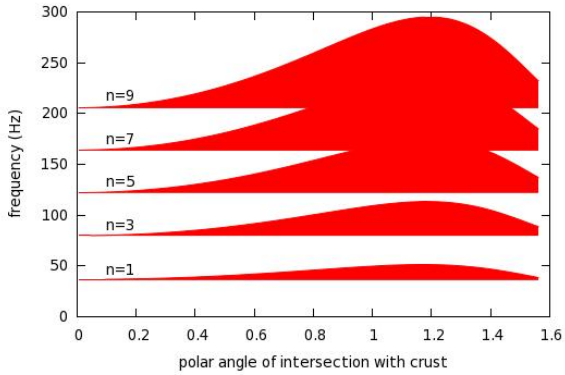


Figure 3.13: *After filling the curves from Fig. 3.12, 'gaps' in the continuum become visible around* $\sigma \sim 70$ Hz *and* $\sigma \sim 120$ Hz.

crust-core interface, such that $\xi_\phi(\psi, \chi_c) = \bar{\xi}_\phi(\psi, \chi_c)$ instead of $\xi_\phi(\psi, \chi_c) = 0$. It is useful to make the following substitution

$$\zeta(\psi, \chi) \equiv \xi_\phi(\psi, \chi) - \bar{\xi}_\phi(\psi)\, w(\psi, \chi) \tag{3.29}$$

where we choose the function $w(\psi, \chi)$ so that (a) it corresponds to the static displacement in the core and hence satisfies $F(w(\psi, \chi)) = 0$ and (2) $w(\psi, \chi_c) = 1$. Therefore the new quantity satisfies the boundary condition $\zeta(\psi, \chi_c) = 0$ and can be expanded into the Alfvén normal modes ξ_n which satisfy the same boundary conditions.

We proceed by substituting Eq. (3.29) into Eq. (3.26) thus obtaining a simple equation of motion for ζ

$$\frac{\partial^2 \zeta(\psi, \chi)}{\partial t^2} - F(\zeta(\psi, \chi)) = -w(\psi, \chi)\frac{\partial^2 \bar{\xi}_\phi(\psi)}{\partial t^2} \tag{3.30}$$

From the definition of the operator F it follows that for the odd modes

$$w(\psi, \chi) = x(\psi, \chi)\int_0^\chi \frac{K(\psi)}{x^2(\psi, \chi')\, B_\chi(\psi, \chi')} d\chi'. \tag{3.31}$$

Here the constant $K(\psi)$ is chosen such that $w(\psi, \chi_c) = 1$, in order that $\zeta = 0$ on both boundaries. We expand ζ and w into a series of ξ_n's:

$$\zeta(\psi, \chi, t) = \sum_n a_n(\psi, t)\, \xi_n(\psi, \chi) \tag{3.32}$$

$$w(\psi,\chi) = \sum_n b_n(\psi)\,\xi_n(\psi,\chi) \tag{3.33}$$

Eq. (3.30) reduces to the following equations of motion for the eigenmode amplitudes a_n

$$\frac{\partial^2 a_n(\psi)}{\partial t^2} + \sigma_n^2(\psi)\,a_n(\psi) = -b_n(\psi)\,\frac{\partial^2 \bar{\xi}_\phi}{\partial t^2} \tag{3.34}$$

These equations show how the core Alfvén modes are driven by the motion of the crust. To close the system, we must address the motion of the crust driven by the hydromagnetic pull from the core. The equation of motion for the crust is given by

$$\frac{\partial^2 \bar{\xi}_\phi}{\partial t^2} = L_{\rm el}\left(\bar{\xi}_\phi\right) + L_B \tag{3.35}$$

Where the acceleration due to elastic stresses $L_{\rm el}$ is

$$L_{\rm el}\left(\bar{\xi}_\phi\right) = \omega_{\rm el}^2\left[\frac{\partial^2 \bar{\xi}_\phi}{\partial\theta^2} + \cot(\theta)\frac{\partial \bar{\xi}_\phi}{\partial\theta} - \left(\cot(\theta)^2 - 1\right)\bar{\xi}_\phi\right] \tag{3.36}$$

where θ is the polar angle (cf. L07). The acceleration L_B due to the magnetic stresses between the crust and the core can be expressed as

$$L_B = -\frac{xB^2}{4\pi\Sigma}\cos\alpha\frac{\partial}{\partial\chi}\left(\frac{\xi_\phi}{x}\right)_{\chi=\chi_{\rm crust}} \tag{3.37}$$

where x is the distance to the axis of the star, Σ is column mass-density of the crust and α is the angle between the magnetic field line and the normal vector of the crust. It is convenient to express the crustal displacement $\bar{\xi}_\phi$ as a Fourier series, being a sum normal modes of the free-crust problem. Using Eq. (3.36) is straightforward to show analytically that the eigenfunctions f_l of the free-crust problem (Eq. (3.35) with $L_B = 0$) are

$$f_l(\theta) \propto \frac{dY_{l0}(\theta)}{d\theta} \tag{3.38}$$

with eigenfrequencies

$$\omega_l = \omega_{\rm el}\sqrt{(l-1)(l+2)} \tag{3.39}$$

Here Y_{l0} is the $m = 0$ spherical harmonic of degree l. The normalized functions f_l form an orthonormal basis, so that

$$\int_0^\infty f_l(\theta) f_m(\theta) \sin(\theta) d\theta = \delta_{l,m} \tag{3.40}$$

where $\delta_{l,m}$ is again the Kronecker delta. The crustal displacement can then be expressed in terms of f_l

$$\bar{\xi}_\phi(\theta, t) = \sum_l c_l(t) f_l(\theta) \tag{3.41}$$

Substituting Eq. (3.41) into Eq. (3.35) we obtain the equations of motion for the crustal mode amplitudes c_l

$$\frac{\partial^2 c_l}{\partial t^2} + \omega_l^2 c_l = \int_0^\pi L_B(\theta, t) f_l(\theta) \sin\theta d\theta \tag{3.42}$$

We can express L_B as

$$\begin{aligned} L_B(\psi, t) = -\frac{B_\chi^2(\psi)}{4\pi\Sigma} \cos(\alpha(\psi)) \Bigg[\sum_n a_n(t) \frac{\partial \xi_n(\psi)}{\partial \chi} \\ + \frac{K(\psi)}{x(\psi) B(\psi)} \sum_k c_k(t) f_k(\theta(\psi)) \Bigg]_{\chi=\chi_c} \end{aligned} \tag{3.43}$$

Up to this point the derived equations of motion for the crust and the fluid core are exact. We are now ready to discretize the continuum by converting the integral of Eq. (3.42) into a sum over N points θ_i. In order to avoid the effect of phase coherence (see section 3.3) which caused drifts in the results from L07, we sample the continuum randomly over the θ-interval $[0, \pi/2]$. In the following, functional dependence of the coordinate ψ or $\theta(\psi)$ is substituted by the discrete index i which denotes the i-th flux surface.

$$\begin{aligned} \frac{\partial^2 c_l}{\partial t^2} + \omega_l^2 c_l &= 2 \sum_i L_B(\theta_i, t) f_{il} \sin\theta_i \Delta\theta_i \\ &= -\sum_i \sin(\theta_i) \Delta\theta_i f_{il} \Bigg[\frac{B_{\chi,i}^2}{2\pi\Sigma} \cos(\alpha_i) \Bigg(\sum_n a_{in} \frac{\partial \xi_{in}}{\partial \chi} \\ &\qquad + \frac{K_i}{x_i B_{\chi,i}} \sum_k c_k f_{ik} \Bigg) \Bigg]_{\chi=\chi_c} \end{aligned} \tag{3.44}$$

$$\frac{\partial^2 a_{in}}{\partial t^2} + \sigma_{in}^2 a_{in} = -b_{in} \sum_l \frac{\partial^2 c_l}{\partial t^2} f_{il} \tag{3.45}$$

These are the equations that fully describe dynamics of our magnetar model. As with the toy model from section 3.2 we integrate them using a second order leap-frog scheme which conserves the total energy to high precision. As a test we keep track of the total energy of the system during the simulations. Further we have checked our results by integrating equations (44) and (45) with the fourth-order Runge-Kutta scheme and found good agreement with leap-frog integration.

3.4.3 Results

Based on our section 3.2 results, we have a good idea of what type of dynamical behavior should occur in our more realistic magnetar model. First, we expect that crustal modes with frequencies inside the Alfvén continuum will be damped quickly by resonant absorption ("Landau-damping" in the terminology of Gruzinov 2008b). Second, as with our previous model we expect the late time behavior of the system to show QPO's near the edges of the continuum, or edge modes. The third important feature of our model is that the continuum may possibly contain gaps, as is shown in Fig. 3.13. In this case there is the possibility that crustal frequencies fall inside the gaps and remain undamped. In all of our simulations these expectations have come true. We will now show the results from a simulation which illustrate the above mentioned effects.

The basic freedom of choice that we have for our model is the strength and geometry of the equilibrium magnetic field. We choose here a purely poloidal magnetic field with an average strength at the surface of $B_{\rm surf} = 10^{15}$ G, induced by a circular current loop of radius $a = 0.5R_*$. This field gives us a gap in the continuum at frequencies $53 < \omega < 78$ Hz. We consider the lowest degree odd crustal modes with frequencies $\omega_2 = 40$ Hz and $\omega_4 = 84.5$ Hz, which we couple to 5000 continuum oscillators (the Alfvén continuum). We sample the continuum at 1000 randomly chosen flux surfaces, and at each flux

surface we consider 5 Alfvén overtones. As with our toy model from section 3.2, we initiate the simulation by displacing the crust ($c_2 = c_4 = 1$) while keeping the continuum oscillators (the Alfvén modes) relaxed ($a_{in} = 0$).

In Figures 3.14 and 3.15 we show the resulting power spectrum for two different models. In the first one, the crustal frequencies are located inside the core continuum range and the peaks due to the edge modes appear. By contrast, in the second case one of the crustal frequencies belongs to the gap and a peak representing the global gap mode stands strongly above the background. We note that the gap-mode's frequency lies close to but does not coincide with the crustal-mode frequency; we found this to be a generic feature of our models, with the difference of 10% for the typical model parameters. The gap modes are particularly interesting because they have relatively large amplitudes, and are not as strongly damped by viscosity as the edge modes.

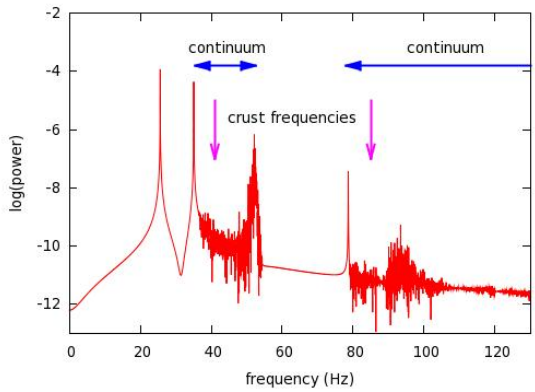


Figure 3.14: *Power spectrum of the crustal dynamics for a magnetar with a single 'gap' in the Alfvén continuum. In this case the crustal frequencies are within the continuum, causing the crust modes to be Landau-damped.*

It must be emphasized that for all persistent modes in the system, the position in the frequency space of the core Alfvén continuum plays the key role in setting the global-mode frequency and in determining its longevity. We note that Lee (2008) has used a different method to identify discrete modes in a magnetar with similar magnetic configuration to ours. These modes were not associated with crustal frequencies and we strongly suspect that they were located in the gaps of the continuum spectrum and could be identified with the edge or gap modes presented in this work.

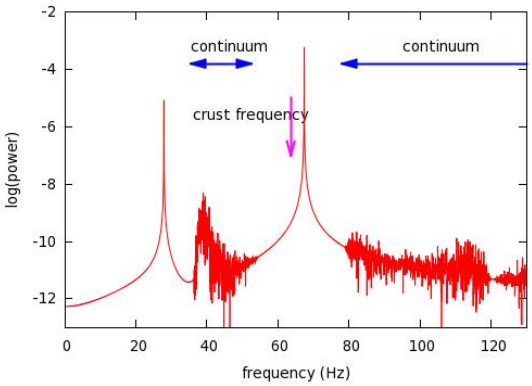


Figure 3.15: *Power spectrum of the crustal dynamics for a magnetar with a single 'gap' in the Alfvén continuum. The global mode within the gap is not damped and its frequency is similar, but not identical, to that of the crustal mode in the same gap.*

3.5 Tangled magnetic fields

Our preceding discussion of the continuum was predicated on the foliation of the axisymmetric magnetic field into the flux surfaces, with each of the singular continuum mode localized on the flux surfaces. These modes are "large"-they are coherent over the spacial extent comparable to the size of the system, and thus they play an important role in the overall dynamics-they are responsible for the resonant absorption of the crust oscillations and contribute to generating the edge and gap modes. But what happens if the field cannot be foliated into the flux surfaces, but is instead tangled in a complicated way? One can argue that the continuum part of the spectrum still persists, as follows: Consider an arbitrary field line anchored at the crust-core interface at both ends, and choose a tube of field lines of infinitesimal radius which is centered on the original field line (see Fig. 3.16). It is clear that a twisting Alfvén mode exists in the tube: it is obtained by the circular rotation of the fluid around the central field line, propagating along the central field line with the local Alfvén velocity. Since there is a continuum of the field-line lengths, there is also a continuum of Alfvén modes. However, the modes we constructed are highly localized in space and and have a small leverage in the overall dynamics. We conjecture that the more tangled the fields are, the less role do the singular continuum modes play in the overall dynamics. Whilst we cannot rigorously prove this conjecture, we can motivate it as follows: consider an area element δS of random orientation with the normal $\hat{\boldsymbol{n}}$ inside

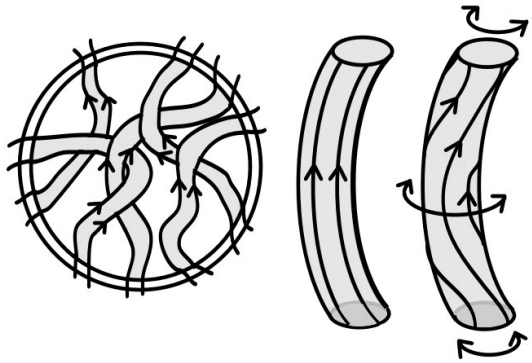


Figure 3.16: *Schematic illustration of tangled a magnetic field inside a magnetar. Locally, the field consists of flux tubes which contain a continuum of twisting Alfvén modes.*

the star and consider a shearing motion along the element. This shearing motion will be resisted by the $B_{\hat{\boldsymbol{n}}}$ component of the magnetic field, with the effective shear modulus of order

$$\mu_{\rm eff} \sim \frac{\langle B^2_{\hat{\boldsymbol{n}}} \rangle}{4\pi}, \tag{3.46}$$

where $\langle ... \rangle$ stands for averaging over the area element. For ordered field, it is possible to choose the orientation of the area element so that $\mu_{\rm eff} \simeq 0$; the presence of such an orientation makes a fundamental difference between MHD and elasticity theory and is responsible for the presence of continuous spectrum in MHD. However, if the linear size of the δS is greater than the characteristic length on which the field is tangled, then $\mu_{\rm eff}$ is non-zero for all orientations of $\hat{\boldsymbol{n}}$. Therefore, for highly-tangled fields there can be no large-scale singular continuum modes and their existence is restricted to the small scales. Hence our assertion that for strongly tangled fields continuum modes play a secondary dynamical role. One is then faced with the problem when crustal modes are coupled to a set of discrete core Alfvén modes. In Appendix 3.A we show how to find the eigen-solution of such a problem, provided that all of the coupling coefficients are known.

How does one quantify the degree to which the fields are tangled? Some insight comes from the numerical simulations of Braithwaite and colleagues, who have studied what type of fossil fields remain in a stratified star after an initial period of fast relaxation. Consider a stable fossil field field configuration, such as the one obtained in the simulations of Braithwaite and Spruit

(2004) and Braithwaite and Nordlund (2006) (see also Gruzinov (2008a) for analytical considerations). There, the final field is nearly, but not perfectly axisymmetric and has a small-scale random component. For a less-centrally concentrated initial field, Braithwaite (2008) shows that the final fossil field is in general non-axisymmetric and can have a complicated topology.[1]

As a starting point, we shall consider the nearly axisymmetric field with a small random component. The latter acts like a small extra shear modulus μ_{eff} and dynamically couples the flux surfaces of the axisymmetric component. We then quantify the degree of tangling by the relative value of μ_{eff} and $B^2/(4\pi)$.

3.5.1 simple model: "square" neutron star

To study this idea further, we specify a very simple model of a neutron star, motivated by the one considered in Levin (2006, hereafter L06) see Fig. 3.17 that never-the-less captures the essential physics. Consider a perfectly conducting homogeneous fluid of density ρ contained in a box with width L_x, length L_y and depth L_z. The magnetic field in this box is everywhere aligned with the y-axis and its strength is a function of x only. We assume that gravity is zero and consider a Lagrangian displacement $\xi(x, y, t)$ of the fluid along the z-direction; we specify periodic boundary conditions in this direction (one should think of the z direction as azimuthal). We now add to this model a small effective shear modulus μ_{eff} due to the field tangling. The fluid equation of motion is:

$$\frac{\partial^2 \xi}{\partial t^2} = c_A^2(x) \frac{\partial^2 \xi}{\partial y^2} + c_s^2 \nabla^2 \xi \tag{3.47}$$

Here $c_A(x)$ is the Alfvén velocity and $c_s = \sqrt{\mu_{\text{eff}}/\rho}$ is the μ_{eff}-generated shear velocity. If we assume a small shear speed, i.e. $c_s << c_A$, Eq. (3.47) reduces

[1] Gruzinov (2009) demonstrates that even this situation is not the most general. He finds that the relaxed field generally has multiple current sheets and argues that the global field relaxation is dominated by the dissipation within these singular layers. The details do not concern us for the purposes of this chapter.

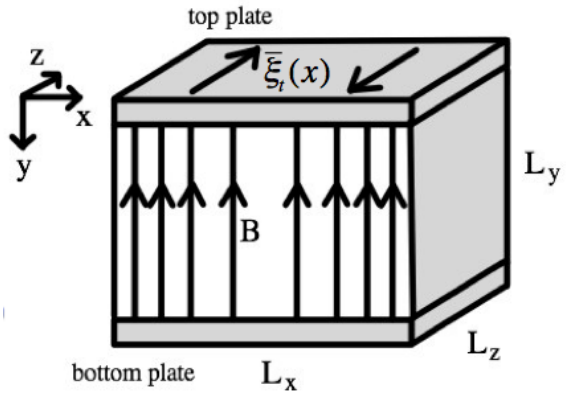


Figure 3.17: *Schematic illustration of the box model. Perfectly conducting incompressible fluid is sandwiched between perfectly conducting top and bottom plates. The box is periodic in z-direction and the displacements of the plates (crust) are in the z-direction. The magnetic field is directed along y-axis and its strength varies as a function of x.*

to the following:

$$\frac{\partial^2 \xi}{\partial t^2} = c_A^2(x)\frac{\partial^2 \xi}{\partial y^2} + c_s^2\frac{\partial^2 \xi}{\partial x^2}. \tag{3.48}$$

We now find the core Alfvén eigenmodes. After adapting the no-slip boundary conditions

$$\begin{aligned} \xi\left(-\frac{L_x}{2}, y, t\right) &= \xi\left(\frac{L_x}{2}, y, t\right) = 0, \\ \xi\left(x, -\frac{L_y}{2}, t\right) &= \xi\left(x, \frac{L_y}{2}, t\right) = 0, \end{aligned} \tag{3.49}$$

the problem can be easily solved by separation of variables $\xi(x,y,t) \propto e^{i\omega t} \times \sin\{\pi m[(y/L_y)+1/2]\} X(x)$, where $m = 1, 2, ...$ Plugging this in Eq. (3.48) we find for the the $x-$dependent part of the solution:

$$c_s^2\frac{\partial^2 X}{\partial x^2} = \left[\omega^2 - \omega_{A,m}^2(x)\right] X. \tag{3.50}$$

Here $\omega_{A,m}(x) = \pi m c_A(x)/L_y$ can be interpreted as the frequency of the m-th Alfvén overtone at x. From the above expression it is clear that in the limit of very small c_s, the solution for X must be close to zero everywhere except in a very small neighborhood of $\omega_{A,m}(x) = \omega$. It is in this limit that the

solutions are located on singular flux surfaces. However, in the presence of the non-vanishing shear velocity c_s, the eigenmodes spread out on neighboring field lines, effectively coupling the motion on different flux surfaces. The continuum of Alfvén frequencies $\omega_{A,m}(x)$ will in this case be no longer solutions of the system. Instead, the coupling term gives rise to a discrete set of solutions rather than a continuum. Eq. (3.50) is the mathematical equivalent of Schrödingers equation, which can in general cases be solved numerically. However, for many special cases exact solutions exist. Let us consider, for the sake of simplicity, a field configuration in our box such that:

$$c_A^2(x) = a_{c_A} x^2 + c_{A,0}^2 \tag{3.51}$$

We can rewrite Eq. (3.50) as follows:

$$c_s^2 \frac{\partial^2 X}{\partial x^2} = -\frac{\pi^2 m^2 a_{c_A}}{L_y} x^2 X + \left(\omega_m^2 - \frac{\pi^2 m^2 c_{A,0}^2}{L_y} \right) X \tag{3.52}$$

This differential equation is the mathematical equivalent of the quantum harmonic oscillator problem for which the exact solution is well known. The eigenfrequencies are given by

$$\omega_{mn}^2 = \pi (1+2n) m c_s \sqrt{a_{c_A}}/L_y + c_{A,0}^2 \pi^2 m^2 / L_y. \tag{3.53}$$

Here n $(= 0, 1, ...)$ is the 'quantum' number labeling the harmonic-oscillator wavefunctions. We see that instead of a continuum, we obtain a densely packed discrete set of frequencies with the frequency spacing $\omega_{m,n} - \omega_{m,n-1} \sim \pi m c_s \sqrt{a_{c_A}}/L_y \omega_{m,n}$.

With the no-slip boundary conditions on the left and right sides $x = \pm L_x/2$, the eigenvalue equation must be solved numerically. An example of such calculation is shown in Fig. 3.18. There, the spacing between the discrete Alfvén modes is shown to increase as one increases the effect of the field tangling characterized by the μ_{eff}. We now introduce the crustal modes into the problem by making the top and bottom of the box elastic and mobile. We allow their displacement $\bar{\xi}_{t,b}(x,t)$ in the z-direction and impose the boundary conditions on the sides:

$$\bar{\xi}_{t,b}(-L_x/2, t) = \bar{\xi}_{t,b}(L_x/2, t) = 0. \tag{3.54}$$

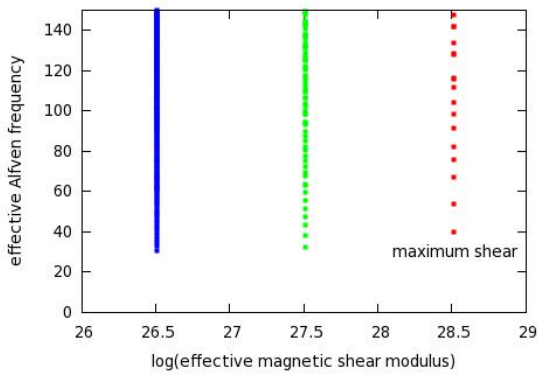


Figure 3.18: *Alfvén frequencies as a function of the effective magnetic shear modulus. As one decreases the shear, the spectrum tends to a continuum.*

Here the subscripts "t" and "b" stand for the top and bottom of the box, respectively. The top and bottom are assumed to be thin and have mass $M_{\rm cr}$ and surface density $\sigma = M_{\rm cr}/(L_x L_z)$. The crustal equation of motion is given by

$$\begin{aligned} \frac{\partial^2 \bar{\xi}_t}{\partial t^2} &= v_s^2 \frac{\partial^2 \bar{\xi}_t}{\partial x^2} - \frac{\{B_z B_x\}_t}{4\pi\sigma} \\ \frac{\partial^2 \bar{\xi}_b}{\partial t^2} &= v_s^2 \frac{\partial^2 \bar{\xi}_b}{\partial x^2} + \frac{\{B_z B_x\}_b}{4\pi\sigma}, \end{aligned} \tag{3.55}$$

where v_s is the shear velocity in the crust. The crustal angular frequencies are given by $\omega_j^{\rm cr} = j\pi v_s/L_y$ with the corresponding crustal mode eigenfunctions $\bar{\xi}_j = \sin\{j\pi[(x/L_x)+1/2]\}$, where $j = 1, 2, ...$ is roughly equivalent to l in the spherical case. The symmetry of the problem allows one to consider either symmetric $\bar{\xi}_t = \bar{\xi}_b$ or antisymmetric $\bar{\xi}_t = -\bar{\xi}_b$ crustal modes. This will couple to the symmetric ($m = 1, 3, 5, ...$) or antisymmetric ($m = 2, 4, 6, ...$) Alfvén modes of the core.

Just as in section 3.4, it is now convenient to define a new variable $\zeta(x, y, t)$ for the core displacement:

$$\zeta(x, y, t) = \xi(x, y, t) - \xi_0(x, y, t), \tag{3.56}$$

where

$$\xi_0(x, y, t) = \frac{1}{2}\left(\bar{\xi}_t(x, t) + \bar{\xi}_b(x, t)\right) + \left(\bar{\xi}_t(x, t) - \bar{\xi}_b(x, t)\right)\frac{y}{L_y}. \tag{3.57}$$

The new variable observes the regular boundary condition $\zeta = 0$ on all the box edge and satisfies the following inhomogeneous partial differential equation:

$$\left(\frac{\partial^2}{\partial t^2} - c_A^2(x)\frac{\partial^2}{\partial y^2} - c_s^2\frac{\partial^2}{\partial x^2}\right)\zeta(x,y,t) = g(x,y,t), \tag{3.58}$$

where

$$g(x,y,t) = -\left(\frac{\partial^2}{\partial t^2} - c_s^2\frac{\partial^2}{\partial x^2}\right)\xi_0(x,y,t). \tag{3.59}$$

The advantage of the new variable is that it satisfies the regular boundary condition $\zeta = 0$ on all the boundaries of the box. It can therefore be expanded as a series consisting of eigenfunctions ξ_{mn} of the right-hand side of Equation (3.48):

$$\zeta(x,y,t) = \Sigma_{mn} a_{mn}(t)\xi_{mn}(x,y). \tag{3.60}$$

The rest of the procedure is very similar to that in section 3.4. We expand the crustal displacement into a series consisting of the eigenmode wavefunctions $\bar{\xi}_j$:

$$\begin{aligned}\bar{\xi}_t(x,t) &= \Sigma_j p_j(t)\bar{\xi}_j(x)\\ \bar{\xi}_b(x,t) &= \Sigma_j q_j(t)\bar{\xi}_j(x),\end{aligned} \tag{3.61}$$

where $p_j(t)$ and $q_j(t)$ are real numbers. The magnetar deformation is now fully represented by a set of generalized coordinates $[p_j(t), q_j(t), a_{mn}(t)]$. The coupled equations of motion are derived by following the procedure specified in section 3.4. We obtain the following system of equations:

$$\begin{aligned}\ddot{a}_{mn} + \omega_{mn}^2 a_{mn} = &-\Sigma_j\left[\ddot{p}_j + c_s^2\left(\frac{j\pi}{L_x}\right)^2 p_j\right]\alpha^{(p)}_{(mn)j}\\ &-\Sigma_j\left[\ddot{q}_j + c_s^2\left(\frac{j\pi}{L_x}\right)^2 q_j\right]\alpha^{(q)}_{(mn)j},\end{aligned} \tag{3.62}$$

and

$$\begin{aligned}\ddot{p}_j + \omega_j^{\mathrm{cr}2} p_j &= -\frac{\rho c_A^2}{\sigma}\Sigma_{mn}\beta_{j(mn)}a_{mn}\\ \ddot{q}_j + \omega_j^{\mathrm{cr}2} q_j &= -\frac{\rho c_A^2}{\sigma}\Sigma_{mn}(-1)^{m+1}\beta_{j(mn)}a_{mn}\end{aligned} \tag{3.63}$$

where

$$\alpha^{(p)}_{(mn)j} = \frac{\int \left(\frac{1}{2} + \frac{y}{L_y}\right) \xi_{mn}(x,y)\bar{\xi}_j(x)dxdy}{\int [\xi_{mn}(x,y)]^2 dxdy}$$
$$\alpha^{(q)}_{(mn)j} = \frac{\int \left(\frac{1}{2} - \frac{y}{L_y}\right) \xi_{mn}(x,y)\bar{\xi}_j(x)dxdy}{\int [\xi_{mn}(x,y)]^2 dxdy} \tag{3.64}$$

and

$$\beta_{j(mn)} = \frac{\int \left(\frac{\partial \xi_{mn}(x,y)}{\partial y}\right)_{y=L_y/2} \bar{\xi}_j(x)dx}{\int [\bar{\xi}_j(x)]^2 dx}. \tag{3.65}$$

Thus we have obtained a system of linear second-order differential equations, which describes the time evolution of the square-box magnetar. These equations are solved by truncating all the series [i.e., restricting the range of indices (m, n, j)] and then by either solving the eigenvalue problem in order to find the normal modes, or by integrating the equations numerically[1]. One then checks that the series truncation does not introduce errors in the magnetar's motion within the frequency range of our interest.

So far we have worked in the approximation of the thin crust, i.e. we have effectively included the crustal modes which have no radial nodes in their wavefunction. However, several observed high-frequency QPOs, and in particular the strong QPO at 625 Hz (Watts & Strohmayer 2006) necessitate introduction of higher radial-order modes into our model. In the square-box model we do this phenomenologically, as follows. We assume that higher radial-order crustal modes have amplitudes $p_{sj}(t)$ and $q_{sj}(t)$ and natural eigenfrequencies $\omega^{\rm cr}_{sj}$, with s being the number of radial nodes and assume that they cause displacement at the crust-core interface given by $\bar{\xi}_j(x)$. This mirrors realistic spherically-symmetric case where the functional form of the crust-core displacement due to the torsional $\nabla \times Y_{lm}$ mode of the n'th radial order is a very weak function n. The amplitudes $p_{sj}(t)$ and $q_{sj}(t)$ are then introduced on into the equations of motions (3.62) and (3.63) in the same way as the other p_j and q_j amplitudes, with the same j-dependent coupling coefficients

[1] Our favored method here is again the energy-conserving second-order leapfrog. It is both fast and stable over long integration times.

but with $\omega_{sj}^{\rm cr}$ instead of $\omega_j^{\rm cr}$ on the left-hand side of Eq. (3.63).

We now have the basic ingredients of building a phenomenological modes with tangled fields. To sum up, (1) we quantify tangling using the effective shear modulus, (2) find discrete core eigenmodes and evaluate their coupling to the crustal model and (3) either find eigenfrequencies of the total star by diagonalizing the potential energy of the system, or simulate the time-dependent behavior directly. An example of a resulting power spectrum for the model described in this section is shown in Fig 3.19.

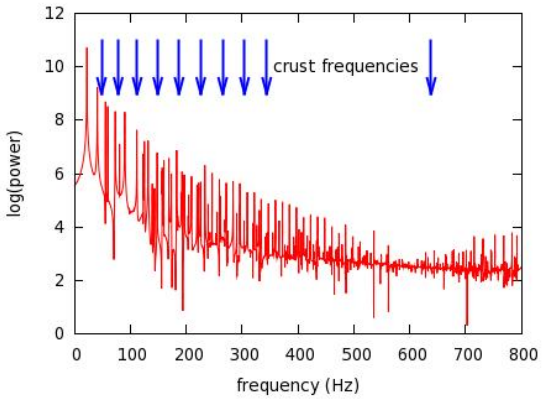


Figure 3.19: *Power spectrum for the dynamics of a magnetized box as described in the text. In this particular model we have used the maximum possible shear modulus, corresponding to a maximally tangled field. The Alfvén motion in the box is coupled to 9 of the lowest frequency 'crustal' modes, plus a high frequency crust mode at 630* Hz.

3.6 Discussion

In this chapter we have developed a formalism which allows one to build a magnetar model with a variety of the spectral features of the core Alfvén waves, including continua with gaps and edges and the large-scale discrete modes generated by the field tangling. We have constructed a number of magnetar models and explored the resulting QPOs, both for the case of axisymmetric magnetar with core Alfvén continuum and for the "square" magnetar models

with the tangled fields (see the previous section). The full range of model parameters and detailed comparison with the data will be the subject of a separate study. For now, we have restricted ourselves to the standard magnetar model, in which the core is a perfect conductor, the field of $\sim 10^{15}$ G penetrates both the core and the crust and the proton fraction in the star is the one tabulated in Haensel, Potekin and Yakovlev (2007). Our models give us the following robust conclusions, as compared against QPO observations:

(1) A number of strong QPOs have been observed in the 1998 and 2004 giant flares, with frequencies ranging between 18 Hz and 150 Hz (Israel et al. 2005, Strohmayer and Watts 2006, Watts and Strohmayer 2006). These QPOs can be qualitatively explained as gap and/or edge modes of sections 3.4 and 3.2, or even transient QPOs of section 3.3[1]. However, this was only possible if the neutrons were decoupled from the Alfvén waves in the core. If the neutrons took part in the Alfvén motion, then the effective mass of the Alfvén modes shifted up by a factor of $20-40$ and their frequencies shifted down by a factor $4-8$ (Easson & Pethick 1979, Alpar et al. 1984, van Hoven & Levin 2008 (see chapter 1), Andersson et al. 2009). As a result, all modes at frequencies above ~ 50 Hz were strongly damped (see Fig. 3.20). Increasing the magnetic-field tension by a factor of 3 did not affect this conclusion (Fig 3.21). For the spherical magnetar models of section 3.4 we obtain similar results if couple the neutrons to the Alfvén motion in the core. The key point that we would like the reader to appreciate is that Alfvén modes in the core are key to determining the frequency and strength of the observable QPOs and thus QPOs are very sensitive probe of the core interior.

(2) A number of the high-frequency QPOs have been measured in the 2004 giant flare by Watts and Strohmayer (2006), the strongest among them being the QPO at 625 Hz. This QPO is particularly strong and long-lived in the hard x-rays, reaching the amplitude of $\sim 25\%$ over the time interval of ~ 100 seconds (i.e., it persists for almost 10^5 oscillation periods!). Watts

[1] L07 and Gruzinov 2008b associated the long-lived 18-20 Hz QPO with the lower edge of the Alfvén continuum. However, recent calculations of Steiner and Watts (2009) have argued that the crustal frequencies can be as low as 10 Hz due to the uncertainty in our theoretical knowledge of the crustal shear modulus. It is therefore plausible that the fundamental crustal mode has the proper frequency below that lower edge of the core Alfvén continuum. In this case, the 18-20 Hz QPO could be the gap mode which is dominated by the fundamental crustal mode.

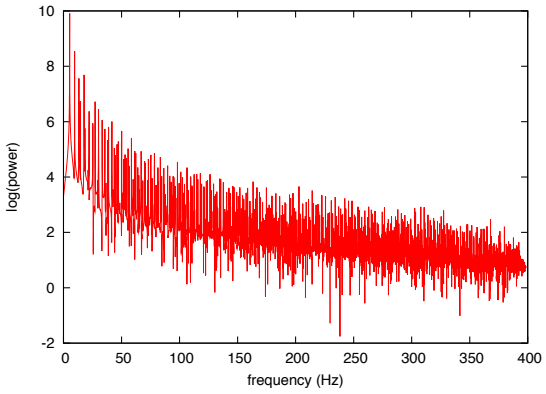


Figure 3.20: *This spectrum was generated using a box model similar to the one from figure 3.19 but with neutron mass-loading. Due to the mass-loading the frequencies have shifted down by a factor of* ~ 4*. Note that there is no significant power above the lower edge-mode frequency of* 5.3 Hz.

and Strohmayer (2006) argued that this frequency corresponds to the crustal shear mode with a single radial node (see also Piro 2005); this interpretation, if correct, would strongly constrain the thickness of the crust and rule out the fluid strange stars as magnetar candidates (Watts & Reddy, 2007). To investigate this suggestion, we have introduced several high-frequency low-j crustal modes into our square-box simulations. However, as is demonstrated in Figs. 3.14 and 3.15, the high-frequency modes are strongly damped and at no time during the simulations do we observe any significant power at those frequencies. This is to be expected. No natural axisymmetric model has gaps in the Alfvén continuum at such high frequencies, so global modes are strongly

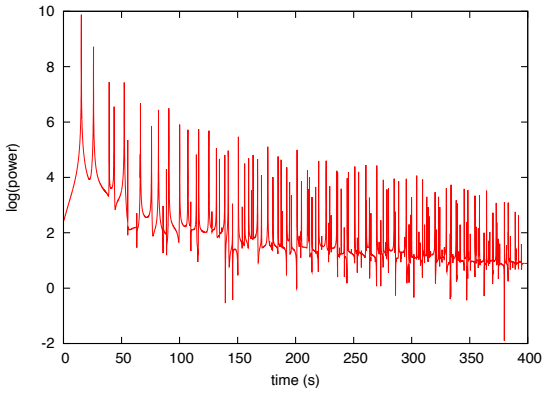


Figure 3.21: *This spectrum was generated with the same box model as in figures 3.20, but in addition to the neutron mass-loading, we have increased the magnetic field strength by a factor of 3. All frequencies above* ~ 16 Hz *are significantly damped.*

absorbed. We have argued that in realistic magnetic equillibria like the ones obtained by Braithwaite & Spruit (2004), field tangling will make continuum modes localized in small scale flux tubes. Moreover, the field tangling creates a dense array of large-scale discrete modes, with the frequency seperation between neighbouring modes being proportional to the degree of tangling. One could expect that if the Alfvén modes are discrete in the core due to field tangling, the absorption of high frequency crustal modes would not arise. However, even in the discrete case the frequency spacing between the modes is around 20 Hz, which is much smaller than 600 Hz. Thus the grid of Alfvén waves is so dense that it is effectively seen as the absorbing continuum by the modes around 600 Hz. Our detailed simulations, of the type shown in Figs. 3.14 and 3.15, fully confirm this qualitative picture.

The concern about the viability of high-frequency QPOs as being due to the physical oscillations of standard-model magnetars has been raised in the original L06 paper on the basis of rather simplistic calculations. As our work here shows, more detailed calculations partially alleviate the L06 concern for the frequencies below ~ 150 Hz, but only if the neutrons are decoupled from the Alfvén motion in the core, i.e. if at least one baryonic superfluid (protons or neutrons) are present in the neutron-star core. Our analysis sustains L06 concern for the high-frequency QPOs, in particular for the strong long-lived QPO at 625 Hz. Its explanation seems to require either QPO production in the magnetosphere, or a somewhat radical revision of the magnetar model. Just how radical this revision has to be will be explored in a separate study.

Our work presented here has several shortcomings. We have limited ourselves to the linear approximation, and a non-linear regime may bring surprises. Direct non-linear simulations of axisymmetric oscillations of a magnetised fluid star has been carried out recently by Cerdá-Durán, Stergioulas, & Font (2009). At this stage it is difficult to say whether non-linearities introduce significantly new QPO features to their model; their results have largely been in agreement with the linear simulations of Colaiuda, Beyer, & Kokkotas (2009). However, the computational techniques seem promising and we do not exclude that large-amplitude simulations of stars with the crust will show

qualitatively new features. Another limitation of our work is that we have assumed that once the flare sets the magnetar into motion, the magnetar's oscillations are not driven externally. This may not be the case in real flares: some energy stored in the pre-flare magnetar may be released gradually and this release could be extended in time into the flare's tail[1]. The latter consideration is straightforward to incorporate phenomenologically into our model and we plan to address it in our future work.

Acknowledgements

We thank Andrei Beloborodov, Anna Watts, Peter Goldreich, Chris Thompson and especially Andrei Gruzinov for useful discussions. This research has been supported by Leiden Observatory and Lorentz Institute for theoretical physics through internal grants.

[1] We thank Chris Thompson for pointing out this possibility.

Appendix 3.A: Multimodal crust-core system

In this Appendix we generalize the normal-mode treatment of Section 3.2.2, and write down the general prescription of how to find the eigenmodes when *several* "large" crustal shear modes are coupled to a multitude of small core Alfvén modes, provided the coupling coefficients are known. In this chapter, the coupling coefficients are worked out in simple models of sections 3.4 and 3.5; we postpone the discussion of how the coefficients are computed in a more general case in future work.

Let us denote the displacement of the crustal and core modes by X_n and x_i respectively. Since both the crustal and the core modes are not directly coupled to themselves (i.e., X's are only coupled to x's), most general equations of motion take the form

$$\begin{aligned} \ddot{X}_n + \Omega^2 X_n &= \Sigma_i \alpha_{ni} x_i \\ \ddot{x}_j + \omega_j^2 x_i &= \Sigma_m \beta_{jm} X_m, \end{aligned} \tag{3.66}$$

where Ω_n and ω_j are the proper frequencies of the crustal and core modes and α's and β's are the coupling coefficients. We look for an oscillatory solutions of the above equations with angular frequency Ω. One can trivially re-write these equation as a matrix eigen-equation with Ω^2 as an eigenvalue and solve it using standard methods. However, if the number of crustal modes is not too large, it is convenient to make a shortcut. Using the second of Eq. (3.66) to express x_i's through X_n's and substituting into the first one, we get the following equation:

$$\Sigma_n G_{mn}(\Omega) X_n = 0, \tag{3.67}$$

where the elements of the matrix G are given by

$$G_{mn}(\Omega) = (\Omega^2 - \Omega_n^2)\delta_{nm} + \Sigma_i \frac{\alpha_{ni}\beta_{im}}{\omega_i^2 - \Omega^2}. \tag{3.68}$$

One obtains the eigenfrequencies by finding numerically the zeros of $\det G_{mn}$.

Appendix 3.B: Core continua with a mixed toroidal-poloidal field

In this appendix we will calculate the continuum of Alfvén frequencies in a magnetar core in the case of a axisymmetric magnetic field with mixed toroidal and poloidal components. The general MHD equations of motion for spherically symmetric, self-gravitating equilibrium with an axisymmetric field, are derived in detail in P85. In contrast to the special case of a purely poloidal field (see section 3.4.2) which leads to two uncoupled differential equations, the continuum for a mixed toroidal-poloidal field is described by a system of fourth order coupled ODEs. Due to this coupling, the solutions are complicated as they are no longer polarized in the directions parallel (so-called "cusp solutions") and perpendicular (Alfvén solutions) to the magnetic field lines, but rather have a mixed character. Strictly speaking, one can only speak of an "Alfvén continuum" in the limit that the variations in ρ, P and B^2 are small in the magnetic flux-surfaces. The general equations of motion are given in Eqs. (53) and (54) of P85. We note however, that in magnetars the speed of sound $c >> c_A$ and therefore we consider Poedts et al.'s equations (53) and (54) in the incompressible limit (P85, Eqs. (73) and (74)). For completeness we give the equations here,

$$\rho\sigma^2\frac{B_\chi^2B^2}{B_\phi^2}Y = B^2F\frac{B_\chi^2}{B_\phi^2B^2}F\left(\rho c_A^2Y\right) + \frac{1}{\rho c_A^2}\left[\frac{\partial}{\partial\chi}\left(\rho c_A^2\right)\right]^2 Y + \rho B_\chi^2N_\chi^2\left(Y+Z\right) - \frac{\partial}{\partial\chi}\left(\rho c_A^2\right)FZ \qquad (3.69)$$

$$\rho\sigma^2B^2Z = iF\left[\frac{\partial}{\partial\chi}\left(\rho c_A^2\right)Y\right] + \rho B_\chi^2N_\chi^2\left(Y+Z\right) + F\left(\rho c_A^2FZ\right) \qquad (3.70)$$

The variables $Y \equiv i\left(B_\phi^2\xi_\chi - B_\phi B_\chi\xi_\phi\right)/B_\chi B^2$ and $Z \equiv i\left(B_\chi\xi_\chi + B_\phi\xi_\phi\right)/B^2$ are components of the fluid displacement perpendicular and parallel to the magnetic field lines, the operator $F \equiv i\partial/\partial\chi$ is a differential operator along the field lines, $N_\chi \equiv -\left(1/B_\chi\rho\right)\sqrt{\left(\partial\rho/\partial\chi\right)\left(\partial P/\partial\chi\right)}$ can be thought of as a Brunt-Väisälä frequency for displacements along the field lines. According to Gauss' law for magnetism, the toroidal component of the magnetic field is of

the form $B_\phi = f(\psi)/\varpi$, where ϖ is the distance to the polar axis and $f(\psi)$ is an arbitrary function of ψ. In the following calculation we adopt a toroidal field component of the form

$$B_\phi = \frac{B_{\mathrm{t},0} R_*}{\varpi\,(\chi)} \sin\left(\theta(\psi)\right), \tag{3.71}$$

Here $\theta(\psi)$ is the polar angle at which the flux surface ψ intersects the stellar crust. Clearly this choice for B_ϕ is completely arbitrary and one could in principle try many different toroidal geometries.

As with our calculation of the Alfvén continuum in the case of a purely poloidal field (section 3.4.2), we adopt the zero-displacement boundary conditions at the crust and use the fact that our equilibrium model is (point-) symmetric with respect to the equatorial plane. This enforces the existence of classes of symmetric and anti-symmetric eigenfunctions, $Y_n(\chi)$ and $Z_n(\chi)$. We consider only the odd modes and calculate the eigenfunctions by means of the shooting method; we use a fourth order Runge-Kutta scheme to integrate Eqs. (3.69) and (4.46). Starting with $Y(0) = 0$ and $Z(0) = 0$ at the equator, we integrate outward until we reach the crust at $\chi = \chi_c$. We find the eigenfrequencies by changing the value of σ until we match the boundary conditions at the crust. A resulting continuum is plotted in Figure 3.22.

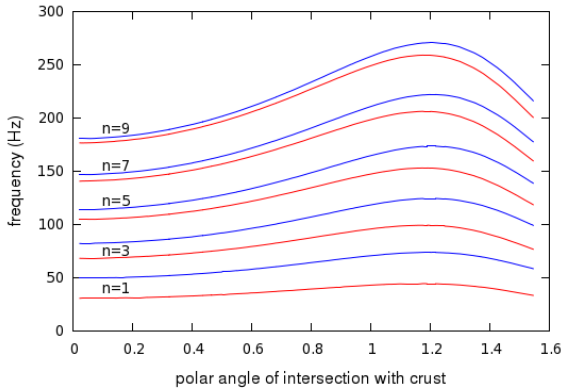


Figure 3.22: *The curves show the continuum frequencies σ_n as a function of the angle $\theta(\psi)$, the polar angle at which the flux-surface ψ intersects the crust. In the presence of a toroidal field, the degeneracy between the cusp-solutions and the Alfvén solutions is broken and we find two separate solutions for each wave number n; waves with primarily Alfvén character (red curves) and waves with primarily cusp character (blue curves). This particular continuum was calculated using a poloidal field with an average surface value $B_{\rm p,surface} \sim 6\cdot 10^{14}$ G (again generated by a circular ring current of radius $a = R_*/2$) and a toroidal field strength at the equator and the crust-core interface of $B_{\rm t,0} = 3\cdot 10^{14}$ G (see Eq. (3.71)).*

Chapter 4

A spectral method for magnetar oscillations

Based on:
Magnetar oscillations II: spectral method
Maarten van Hoven & Yuri Levin, 2011, accepted to MNRAS

Abstract

The seismological dynamics of magnetars is largely determined by a strong hydro-magnetic coupling between the solid crust and the fluid core. In this chapter we set up a "spectral" computational framework in which the magnetar's motion is decomposed into a series of basis functions which are associated with the crust and core vibrational eigenmodes. A general-relativistic formalism is presented for evaluation of the core Alfvén modes in the magnetic-flux coordinates, as well for eigenmode computation of a strongly magnetized crust of finite thickness. By considering coupling of the crustal modes to the continuum of Alfvén modes in the core, we construct a fully relativistic dynamical model of the magnetar which allows: (1) Fast and long simulations without numerical dissipation. (2) Very fine sampling of the stellar structure. We find that the presence of strong magnetic field in the crust results in localizing of some high-frequency crustal elasto-magnetic modes with the radial number $n \geq 1$ to the regions of the crust where the field is nearly horizontal. While the hydro-magnetic coupling of these localized modes to the Alfvén continuum in the core is reduced, their energy is drained on a time-scale of $\ll 1$ s. Therefore the puzzle of QPOs with frequencies larger than 600 Hz still stands.

4.1 Introduction

Magnetar oscillations have been subject of extensive theoretical research since the discovery of quasi-periodic oscillations (QPOs) in the light curves of giant flares from soft gamma repeaters (SGR) (Israel et al. 2005; Strohmayer & Watts 2005; Watts & Strohmayer 2006; see also Barat et al. 1983). The observed oscillations are measured with high signal-to-noise ratios during time intervals of typically few minutes in the frequency range between 18 and 1800 Hz. It has been proposed by many authors that the physical origin of the QPOs are seismic vibrations of the star; an idea which opens the possibility to perform asteroseismological analysis of neutron stars, giving a unique observational window into the stellar interior. Initially it was hypothesized that the observed oscillations originate from torsional shear modes which are confined in the magnetar crust (e.g. Duncan 1998, Piro 2005; Watts & Strohmayer 2006; Samuelsson & Andersson 2007; Watts & Reddy 2007; Steiner & Watts 2009). If this hypothesis were true, then the observed QPOs would strongly constrain physical parameters in the neutron star crust. However, it was soon realized that, due to the presence of ultra-strong magnetic fields ($B \sim 10^{14} - 10^{15}$ G; Kouveliotou et al., 1999) which are frozen both in the crust and the core of the star, the crustal motion is strongly coupled to the fluid core on timescales $\ll 1$ s Levin (2006, hereafter L06). Over the years several authors have studied the coupled crust-core problem (Glampedakis, Samuelsson & Andersson 2006; Levin 2007, hereafter L07; Gruzinov 2008; Lee 2008; van Hoven & Levin 2011a, hereafter vHL11 (see also chapter 3); Gabler et al. 2011a; Colaiuda & Kokkotas 2011; Gabler et al. 2011b). In particular L06 and L07 argued that for sufficiently simple magnetic field configurations (i.e. axisymmetric poloidal fields), the Alfvén-type motions on different flux surfaces are decoupled so that the Alfvén frequencies in the core feature a continuum. This result is well known from previous magnetohydrodynamic (MHD) studies and it applies to general axisymmetric poloidal-toroidal magnetic fields (Poedts et al. 1985). It allows one to describe the problem of magnetar dynamics in terms of discrete crustal modes that couple to a continuum of Alfvén modes in the core. With this approach, L07 and vHL11 demonstrated that the presence of an Alfvén continuum has some important

implications for magnetar oscillations: (1) Global modes of the star with frequencies that are located inside the continuum undergo strong exponential damping (this phenomenon is often called *resonant absorption* in the context of MHD (Goedbloed & Poedts 2004)). (2) After the initial period (< 1 s) of exponential decay, the system tends to settle in a steady state in which it oscillates at frequencies close to the edges of the continuum; these oscillations correspond to the so-called *edge-modes*, that were first seen numerically in L07 and Gruzinov 2008 and were explained analytically in vH11 (chapter 3 in this thesis). The edge-modes were further observed in the simulations of Gabler et al. (2011a) Colaiuda & Kokkotas (2011) and Gabler et al. (2011b).

In the past half-decade, two distinct computational strategies have been applied to the problem of calculating magnetar oscillations. (1) Several groups employed general relativistic MHD grid codes to simulate the dynamics of magnetized neutron stars. Sotani et al. 2007; Colaiuda et al. 2009 and Cerdá-Durán et al. 2009 were able to reproduce continuum Alfvén modes in the purely fluid stars with axisymmetric poloidal magnetic field, which provided important benchmark tests for the ability of the codes to handle complex MHD oscillations. Building on this, Gabler et al. (2011a), Colaiuda & Kokkotas (2011) and Gabler et al. (2011b) included a crust in their neutron star models and were thus able to study the coupled dynamics of the crust and the core. (2) Our group (L07 and vHL11) and Lee (2008) decomposed the motion of a magnetar into a set of basis functions and studied the dynamics of the coefficients of these series expansion; we shall refer to this strategy as the "spectral method". This framework is able to handle both the dynamical simulations and the stationary eigenmode problem; the latter reduces to solving the eigenvalue problem for a large matrix. L07 and vH11 chose the basis functions so that the crustal motion is decomposed into the normal modes of the free crust and the core motion is decomposed into the sum of core Alfvén modes and a separate contribution of the core's "dc" displacements in reaction to the motion of the crust. We refer the reader to Sections 3.2 of L07 and 3.4.2 and 4.4.2 of this thesis for technical details. This choice of basis functions casts the dynamics of magnetars as a problem of coupled harmonic

oscillators, in which the discrete modes of the crust are coupled to the Alfvén modes in the core. The computations of vH11 have been performed using Newtonian equations of motion and in the limit of a thin crust.

In this chapter we improve on the previous chapter in two ways: (1) We adopt a realistic crust of finite thickness, threaded with a strong magnetic field. (2) We employ fully relativistic equations governing the motion of axial perturbations in the crust and the core. Our spectral method has several practical and conceptual advantages: (1) it is numerically inexpensive, making long simulations of the magnetar dynamics implemented on an ordinary workstation possible. (2) It allows one to sample the stellar structure at high spatial resolution. (3) It does not suffer from the problem of numerical viscosity that occurs in some finite difference schemes (scaling with the grid size) and it is able to handle arbitrary axisymmetric poloidal fields and not just those that are the solutions of the Grad-Shafranov Equations[1]

The plan of this chapter is as follows. In section 4.2 we derive relativistic equations describing the magnetic forces acting on axial perturbations inside a neutron star with an axi-symmetric poloidal magnetic field. We construct a coordinate system which has one of its axes parallel to the fieldlines. The equations thus obtained will be discussed in later sections when we calculate elasto-magnetic modes of the crust and when we calculate the Alfvén continuum in the core.

In section 4.3.1 we introduce a formalism which allows us to calculate general relativistic elasto-magnetic eigenmodes of the crust by expanding the elasto-magnetic equations of motion in a set of basisfunctions. This reduces the eigenmode problem of the crust to a matrix eigenvalue problem. In sections 4.3.2 and 4.3.3 we work out the relativistic equations describing the magnetic and elastic restoring-force densities in the curved space-time of the neutron star crust. In section 4.3.4 we apply these equations to the formalism

[1] The approach developed by Sotani et al (2007) and used in Colaiuda et al. (2009, 2011) casts the MHD equations in the core into a particularly simple form. This transformation is possible if the poloidal field is the solution of the Grad-Shafranov (GS) equation. There is, however, no compelling reason why the GS equation should hold, since neutron stars feature very strong stable stratification due to the radial gradients in proton-to-neutron ratios (Goldreich & Reisenegger 1992, Mastrano et al., 2011)

of section 4.3.1 in order to find free crustal eigenmodes and -frequencies.

In section 4.4, we find the core continuum Alfvén modes in full general relativity and we calculate their coupling to the crustal modes of section 4.3. The magnetar model constructed in this way, qualitatively shows the same features of the model in chapter 3, i.e. above the fundamental Alfvén frequency of ~ 20 Hz, the frequency domain is covered by the core continuum which effectively acts to damp crustal motion. For particular choices of the field configuration, the continuum may contain a number of gaps, generally well below 200 Hz. These gaps give rise to the characteristic 'edge-modes' of chapter 3. Moreover, the crustal modes that reside inside gaps remain undamped. In appendix 4.A we revisit the problem of crustal mode damping due to the presence of an Alfvén continuum, by analytically calculating damping rates according to Fermi's golden rule.

4.2 Relativistic MHD equations

Magnetic coordinates

We consider strongly sub-equipartition $B \ll 10^{18}$ G magnetic fields, so that the physical deformation of the star is very small and the space-time is spherically-symmetric with respect to the star's center. The metric can be written in the standard Schwarzschild-type coordinates r, θ and ϕ. It is natural, in analogy with the Newtonian treatments, to introduce the flux coordinate system in which one of the axes is parallel to the magnetic field lines (the precise meaning of this construction in relativity is described below). In the axisymmetric poloidal field geometry the magnetic field lines are located in planes of constant azimuthal angle ϕ, which allows us to define the two 'magnetic' coordinates $\chi(r,\theta)$ and $\psi(r,\theta)$, such that the (covariant) vectors $\boldsymbol{e}_\phi = \partial/\partial\phi$ and $\boldsymbol{e}_\chi = \partial/\partial\chi$ are orthogonal to $\boldsymbol{e}_\psi = \partial/\partial\psi$. In the flux coordinate system the metric is given by

$$\begin{aligned} ds^2 = &-g_{tt}dt^2 + g_{\chi\chi}d\chi^2 + g_{\psi\psi}d\psi^2 \\ &+2g_{\psi\chi}d\chi d\psi + g_{\phi\phi}d\phi^2, \end{aligned} \tag{4.1}$$

while the magnetic-field vector is given by

$$\boldsymbol{B} = B^{\chi}\boldsymbol{e}_{\chi}. \tag{4.2}$$

Here $\boldsymbol{B}$ is the 4-vector whose components are given by

$$B^{\mu} = \frac{1}{2}\epsilon^{\mu\nu\alpha\beta}F_{\alpha\beta}v_{\nu}, \tag{4.3}$$

and v_{ν} is the 4-velocity vector which for the stationary star is given by $v_t = g_{tt}v^t = \sqrt{-g_{tt}}$, $v_i = 0$. Clearly, g_{tt} and $g_{\phi\phi}$ are identical to the corresponding Schwarzschild metric terms,

$$\begin{aligned} g_{tt} &= 1 - \frac{2m(r)}{r} \\ g_{\phi\phi} &= r^2\sin^2\theta \end{aligned} \tag{4.4}$$

Maxwell's equations

The evolution of the magnetic field is described by Maxwell's equations. In curved space-time these read

$$F_{\mu\nu;\lambda} + F_{\lambda\mu;\nu} + F_{\nu\lambda;\mu} = 0 \tag{4.5}$$

In the ideal MHD limit, the electric field $E_{\mu} = v^{\nu}F_{\mu\nu}$ vanishes so that the only contribution to the electromagnetic tensor comes from the magnetic field:

$$F_{\mu\nu} = -\epsilon_{\mu\nu\lambda\sigma}v^{\lambda}B^{\sigma} \tag{4.6}$$

After some manipulation, the relations (4.5) and (4.6) yield the MHD equations for the magnetic field:

$$\left(v^{\mu}B^{\nu} - v^{\nu}B^{\mu}\right)_{;\mu} = 0. \tag{4.7}$$

This equation entails both magnetic induction, which describes the flux freezing that characterizes magnetic fields in the ideal MHD approximation and Gauss' law for magnetic fields, i.e. $\left(v^{\mu}B^{t} - v^{t}B^{\mu}\right)_{;\mu} = 0$. For a static equilibrium, i.e. $v_t = \sqrt{-g_{tt}}$ and $v_i = 0$ (where the index i runs over the spatial indices), Gauss' law can be expressed in the more familiar form

$$B^{i}_{;i} = \frac{1}{\sqrt{g}}\left(\sqrt{g}B^{i}\right)_{,i} = 0 \tag{4.8}$$

where $g \equiv \det(g_{ij})/g_{tt}$. This expression provides the basis for a convenient map between magnetic fields of Newtonian and relativistic stars. In the Newtonian case, the flux coordinates χ and ψ are functions of r and θ; we keep this functional form for the relativistic versions of χ and ψ. The expression in Eq (4.8) is valid both in the curved space-time and in the flat Euclidean space (with g_{ij} replaced by the Euclidean metric terms) of the Newtonian star. We can therefore use Eq (4.8) to convert the values of the Euclidean field, B_E, to the correct values of the magnetic field in curved space-time, B_S (the subscript E stands again for *Euclidean*, S for *Schwarzschild*): Eq. (4.8) gives $\left(\sqrt{g_S}B_S^i\right)_{,i} = \left(\sqrt{g_E}B_E^i\right)_{,i} = 0$. We thus obtain

$$B_S^\chi = \frac{\sqrt{g_E}}{\sqrt{g_S}} B_E^\chi = \frac{1}{\sqrt{g_{rr}}} B_E^\chi \tag{4.9}$$

which results in the relativistic poloidal magnetic field which is tangent to the flux surfaces $\psi = const$ and which satisfies the Gauss' law. (In the following we will drop the subscript S.) In this work, for concreteness, we use the Newtonian configuration of the magnetic field generated by a current loop inside the neutron star (see discussion in section 3.4). Other Newtonian configurations are readily mapped onto the relativistic configurations using the procedure that is specified above.

Euler equations

The equations of motion are obtained by enforcing conservation of momentum, i.e. by projecting the conservation of energy-momentum 4-vector on the space normal to the 4-velocity v^λ

$$h^\lambda{}_\mu T^{\mu\nu}{}_{;\nu} = 0 \tag{4.10}$$

where the projection tensor $h^\lambda{}_\mu$ is given by

$$h^\lambda{}_\mu = \delta^\lambda{}_\mu + v^\lambda v_\mu \tag{4.11}$$

$T^{\mu\nu}$ is the stress-energy tensor for a magnetized fluid in the ideal MHD approximation and can be expressed as

$$T^{\mu\nu} = \left(\rho + P + \frac{B^2}{4\pi}\right) v^\mu v^\nu + \left(P + \frac{B^2}{8\pi}\right) g^{\mu\nu} - \frac{B^\mu B^\nu}{4\pi} \tag{4.12}$$

Here, ρ and P are the mass-density and pressure and $B^2 = B^\mu B_\mu$ is the square of the magnetic field, where $B_\mu = \frac{1}{2}\epsilon_{\mu\nu\lambda\sigma}u^\nu F^{\lambda\sigma}$ is the covariant component of the Lorentz invariant magnetic field 4-vector ($\epsilon_{\mu\nu\lambda\sigma}$ is the four dimensional Levi-Civita symbol and $F^{\lambda\sigma}$ is the electromagnetic tensor). The equations of motion become

$$\left(\rho + P + \frac{B^2}{4\pi}\right) v^\mu{}_{;\nu} v^\nu = h^{\mu\lambda}\left(P + \frac{B^2}{8\pi}\right)_{;\lambda} + h^\mu{}_\sigma \left(\frac{B^\sigma B^\lambda}{4\pi}\right)_{;\lambda} \tag{4.13}$$

Here we have used the relation $v_\nu v^\nu = g_{\mu\nu}v^\mu v^\nu = -1$. Eq. (4.13) together with equation (4.7) provides a full description of (incompressible) motion of the magnetized fluid in a neutron star.

Perturbation equations

We are now ready to derive equations that describe the linearized motion of a small Lagrangian fluid displacement ζ^μ about the static background equillibrium of the star. The perturbed components of the velocity and the magnetic field 4-vectors, $v^\mu_{\rm pert}$ and $B^\mu_{\rm pert}$ are

$$\begin{aligned} v^\mu_{\rm pert} &= v^\mu + \delta v^\mu = v^\mu + \frac{\partial \zeta^\mu}{\partial \tau} \\ B^\mu_{\rm pert} &= B^\mu + \delta B^\mu \end{aligned} \tag{4.14}$$

where the first terms on the right hand side denote the unperturbed equillibrium quantities and the second terms on the right hand side denote the Eulerian perturbations associated with the displacement ζ^μ. In our 'magnetic' coordinates the only non-zero component of the unperturbed magnetic field is $B^\chi = B/\sqrt{g_{\chi\chi}}$ and because the equillibrium star is static and non-rotating the only non-zero component of the 4-velocity is $v^t = 1/\sqrt{-g_{tt}}$. Restricting ourselves to axi-symmetric torsional oscillations of the star, we introduce a small incompressible axisymmetric displacements ζ^ϕ. This implies that $v^\mu_{\rm pert\ ;\mu} = \delta v^\mu{}_{;\mu} = \delta v^t{}_{;t}$ and that the perturbations in pressure δP and mass-density $\delta\rho$ vanish. Technically, a full description of the linearized motion of a neutron star would involve perturbations of the metric $g_{\mu\nu}$, requiring one to augment the above equations of motion with the perturbed Einstein equations. However, since we're considering incompressional axial oscillations only, the metric perturbations are dominated by the current dipole moment.

One can show that this causes perturbations in the off-diagonal elements of the metric tensor of order $(\delta v)^2$, so that the metric perturbations can be safely ignored (the so-called Cowling approximation). Taking these considerations into account, we linearize Eq's (4.13) and (4.7) and after some work we obtain

$$\left(\rho + P + \frac{B^2}{4\pi}\right)\frac{\partial^2 \zeta^\phi}{\partial t^2} = \sqrt{\frac{g_{tt}}{g_{\chi\chi}}}\frac{B}{4\pi g_{\phi\phi}}\frac{\partial}{\partial \chi}\left(g_{\phi\phi}\sqrt{-g_{tt}}\delta B^\phi\right) \tag{4.15}$$

and

$$\delta B^\phi = \frac{B}{\sqrt{g_{\chi\chi}}}\frac{\partial \zeta^\phi}{\partial \chi} \tag{4.16}$$

These equations can be combined into a single one. After restoring a factor of c^2, we find

$$\left(\rho + \frac{P}{c^2} + \frac{B^2}{4\pi c^2}\right)\frac{\partial^2 \xi}{\partial t^2} = \sqrt{\frac{g_{tt}}{g_{\chi\chi}}}\frac{B}{4\pi c^2\sqrt{g_{\phi\phi}}}\frac{\partial}{\partial \chi}\left[\sqrt{\frac{g_{tt}}{g_{\chi\chi}}}g_{\phi\phi}B\frac{\partial}{\partial \chi}\left(\frac{\xi}{\sqrt{g_{\phi\phi}}}\right)\right] \tag{4.17}$$

where $\xi = \sqrt{g_{\phi\phi}}\zeta^\phi$ is the physical displacement (in the ϕ-direction) in unit length. This equation describes Alfvén waves, traveling along magnetic field lines in the curved space-time of a magnetar. We checked that in the non-relativistic limit Eq. (4.17) reduces to the correct expression for Alfvén waves in self-gravitating magnetostatic equillibria (Poedts et al., 1985).

4.3 Modes of a magnetized crust in General Relativity

In this section we will describe a formalism that allows us to calculate relativistic eigenmodes and -frequencies of a neutron star crust of finite thickness and realistic equation of state, threaded with an arbitrary magnetic field. By considering a crust of finite thickness, we will obtain high frequency radial harmonics that are not present in the crust model of chapter 3 but which should be taken into account in view of the observed high frequency QPO's.

In the past several authors carried out theoretical analyses of torsional oscillations of neutron stars with a magnetized crust. Piro (2005), Glampedakis et al. (2006) and Steiner & Watts (2009) considered horizontal shear waves in a plane-parallel crust threaded by a vertical magnetic field, whereas Sotani et al. (2007 and 2008), Gabler et al. (2011a and 2011b) and Colaiuda & Kokkotas (2011), performed grid-based simulations of spherical, relativistic stars with dipole magnetic fields. Lee (2008) on the other hand, studied the Newtonian dynamics of spherical magnetic neutron stars, by decomposing the perturbed quantities into a set of basis functions and following the dynamics of the expansion coefficients. In this section we follow a strategy which is closely related to that of Lee (2008). We consider normal modes of the 'free' magnetized neutron star crust, i.e. in the absence of external forces. The idea is to decompose the perturbed quantities into a set of orthogonal basis functions. By substituting this expansion in the equation of motion, we obtain equations for the evolution of the expansion coefficients. The solutions of the crustal eigenmode problem, are in this way reduced to a matrix eigenvalue problem. The hydromagnetic coupling of the crust normal modes to the core Alfvén modes, will be discussed in section 4.4.

Formalism for finding crustal eigenmodes

In a magnetized and elastic crust, the motion of a small torsional Lagrangian displacement away from equillibrium $\bar{\boldsymbol{\xi}}(\boldsymbol{x}, t)$ (we use the same notation as in chapter 3; $\bar{\xi}$ denote crustal displacements, ξ denote displacements in the core), is restored both by elastic and magnetic forces,

$$\frac{\partial^2 \bar{\boldsymbol{\xi}}}{\partial t^2} = \boldsymbol{L}_{\rm el}(\bar{\boldsymbol{\xi}}) + \boldsymbol{L}_{\rm mag}(\bar{\boldsymbol{\xi}}) \tag{4.18}$$

where $\boldsymbol{L}_{\rm el}$ and $\boldsymbol{L}_{\rm mag}$ are the accelerations due to the elastic and magnetic forces acting on the displacement field. Expressions for $\boldsymbol{L}_{\rm el}$ and $\boldsymbol{L}_{\rm mag}$ are given and discussed in the next sub-section. Augmented with no-tangential-stress conditions $\delta T_{r\phi} = \delta T_{r\theta} = 0$ on the inner- and outer boundaries, this equation describes the free oscillations of a magnetized neutron star crust. Our procedure for solving Eq. (4.18) is as follows:

First, we decompose the crustal displacement field $\bar{\boldsymbol{\xi}}(t, \boldsymbol{x})$ into an arbitrary set of basis functions $\boldsymbol{\Psi}_i(\boldsymbol{x})$,

$$\bar{\boldsymbol{\xi}}(t, \boldsymbol{x}) = \sum_{i=1}^{\infty} a_i(t) \boldsymbol{\Psi}_i(\boldsymbol{x}). \tag{4.19}$$

The functions $\boldsymbol{\Psi}_i$ form an orthonormal basis for a Hilbert space with inner product

$$\langle \boldsymbol{\eta} \mid \boldsymbol{\zeta} \rangle = \int_{\mathcal{V}} w(\boldsymbol{x})\ \boldsymbol{\eta} \cdot \boldsymbol{\zeta}\ d^3x \tag{4.20}$$

where $\boldsymbol{\eta}$ and $\boldsymbol{\zeta}$ are arbitrary functions defined in the volume $\mathcal{V}$ of the crust and $w(\boldsymbol{x})$ is a weight function. Orthonormality of $\boldsymbol{\Psi}_i(\boldsymbol{x})$ implies that $\langle \boldsymbol{\Psi}_i \mid \boldsymbol{\Psi}_j \rangle = \delta_{ij}$, where δ_{ij} is the Kronecker delta. The coefficients a_i of the expansion of Eq. (4.19) are then simply $a_i(t) = \langle \bar{\boldsymbol{\xi}}(t, \boldsymbol{x}) \mid \boldsymbol{\Psi}_i(\boldsymbol{x}) \rangle$.

The next step is to decompose the acceleration field of Eq. (4.18) into basis functions $\boldsymbol{\Psi}_i$ according to Eq. (4.19) and calculate the matrix elements $\langle \partial^2 \bar{\boldsymbol{\xi}} / \partial t^2 \mid \Psi_j \rangle$. This yields equations of motion for $a_i(t)$:

$$\ddot{a}_j = M_{ij}\ a_i, \tag{4.21}$$

where the double dot denotes double differentiation with respect to time and where

$$M_{ij} = \left[\langle \boldsymbol{L}_{\mathrm{el}}(\boldsymbol{\Psi}_i) \mid \boldsymbol{\Psi}_j \rangle + \langle \boldsymbol{L}_{\mathrm{mag}}(\boldsymbol{\Psi}_i) \mid \boldsymbol{\Psi}_j \rangle \right],$$

Clearly, a crustal eigenmode with frequency ω_m (i.e. $a_{m,i} \propto e^{i\omega_m t}$ for all i), is now simply an eigenvector of the matrix M with eigenvalue $-\omega_m^2$

$$-\omega_m^2 a_{m,j} = M_{ij}\ a_{m,i}. \tag{4.22}$$

The index m is used to label the different solutions to the above equation. In practical calculations, one truncates the series of Eq. (4.19) at a finite index $i = N$, so that one obtains a total number of N eigensolutions. The eigenvalue problem of Eq. (4.21) with finite $(N \times N)$ matrix M can be solved by means of standard linear algebra methods. Given a set of suitable basis functions,

the eigenvectors and eigenvalues (or crustal eigenfrequencies) converge to the correct solutions of Eq. (4.18) for sufficiently large N (see the discussion of section 4.3.5).

Orthogonality relation for elasto-magnetic modes

In the limit of $N \to \infty$, the elasto-magnetic eigenfunctions are

$$\bar{\boldsymbol{\xi}}_m(\boldsymbol{x}) = \sum_i a_{m,i} \boldsymbol{\Psi}_i(\boldsymbol{x}), \tag{4.23}$$

where we omitted the time-dependent part $e^{i\omega_m t}$, on both sides. The eigenfunctions $\bar{\boldsymbol{\xi}}_m$ will form a new basis for a Hilbert space of crustal displacements. We can introduce an inner product $\langle ... | ... \rangle_{\rm em}$ in which this basis is orthogonal as follows: Consider a deformation $\bar{\boldsymbol{\xi}}(\boldsymbol{x}, t)$ of the crust, decomposed into a sum of eigenfunctions

$$\bar{\boldsymbol{\xi}}(\boldsymbol{x}, t) = \sum_m b_m(t) \bar{\boldsymbol{\xi}}_m(\boldsymbol{x}), \tag{4.24}$$

where we incorporated the harmonic time dependence in the coefficients $b_m(t)$. Since $\bar{\boldsymbol{\xi}}_m$ are the eigenmodes of the crust, the kinetic energy of the displacement field $K(\bar{\boldsymbol{\xi}})$ must be equal to the sum of kinetic energies of the individual modes $K(b_m \bar{\boldsymbol{\xi}}_m)$

$$K\left(\bar{\boldsymbol{\xi}}(\boldsymbol{x}, t)\right) = \sum_m K\left(b_m(t) \bar{\boldsymbol{\xi}}_m(\boldsymbol{x})\right). \tag{4.25}$$

How do we find the correct quadratic form for the kinetic energy? In the static Schwarzschild space-time of the neutron star, the conjugate time-like momentum $p_t = -E$ is a constant of geodesic motion (see e.g. Misner, Thorne & Wheeler (1973), §25.2). In terms of the locally measured energy $E_{\rm L} = \sqrt{-g_{tt}} p^t$, the conserved "redshifted" energy is $E = -p_t = \sqrt{-g_{tt}} E_{\rm L}$. Similarly, the kinetic energy K in terms of the locally measured kinetic energy K_L is

$$\begin{aligned} K\left(\bar{\boldsymbol{\xi}}\right) &= \sqrt{-g_{tt}} K_L\left(\bar{\boldsymbol{\xi}}\right) \\ = \frac{1}{2} \int_{\mathcal{V}} \sqrt{-g_{tt}} \tilde{\rho} \left| \frac{\partial \bar{\boldsymbol{\xi}}}{\partial \tau} \right|^2 d\tilde{V} &= \frac{1}{2} \int_{\mathcal{V}} \frac{\tilde{\rho}}{\sqrt{-g_{tt}}} \left| \frac{\partial \bar{\boldsymbol{\xi}}}{\partial t} \right|^2 d\tilde{V} \\ &\equiv \frac{1}{2} \langle \partial \bar{\boldsymbol{\xi}} / \partial t \mid \partial \bar{\boldsymbol{\xi}} / \partial t \rangle_{\rm em} \end{aligned} \tag{4.26}$$

where $\tilde{\rho} = \left(\rho + P/c^2 + B^2/4\pi c^2\right)$ is the mass-density in a local Lorentz frame and $d\tilde{V} = \sqrt{g_{rr}g_{\phi\phi}g_{\theta\theta}}\; dr\; d\phi\; d\theta$ is the locally measured space-like volume element. By substituting this expression for the kinetic energy into Eq. (4.25), one finds that the cross-terms, $\langle \partial\bar{\boldsymbol{\xi}}_m/\partial t \mid \partial\bar{\boldsymbol{\xi}}_k/\partial t\rangle_{\rm em} = \omega_m\omega_k\langle\bar{\boldsymbol{\xi}}_m \mid \bar{\boldsymbol{\xi}}_k\rangle_{\rm em}$ with $m \neq k$, vanish. After normalizing the eigenfunctions $\bar{\boldsymbol{\xi}}_m$, so that $K(b_m\bar{\boldsymbol{\xi}}_m) = 1/2\omega_m^2 b_m^2$, we obtain the orthogonality relation:

$$\langle\bar{\boldsymbol{\xi}}_m \mid \bar{\boldsymbol{\xi}}_k\rangle_{\rm em} = \int_{\mathcal{V}} \frac{\tilde{\rho}}{\sqrt{-g_{tt}}}\bar{\boldsymbol{\xi}}_m\cdot\bar{\boldsymbol{\xi}}_k d\tilde{V} = \delta_{mk}. \tag{4.27}$$

The coefficients $b_m(t)$ are now simply obtained by taking the inner product between the displacement field $\bar{\boldsymbol{\xi}}(\boldsymbol{x},t)$ and the eigenfunctions $\bar{\boldsymbol{\xi}}_m(\boldsymbol{x})$:

$$b_m(t) = \langle\bar{\boldsymbol{\xi}}(\boldsymbol{x},t) \mid \bar{\boldsymbol{\xi}}_m(\boldsymbol{x})\rangle_{\rm em}. \tag{4.28}$$

In the next two sections we give expressions for $\boldsymbol{L}_{\rm mag}$ and $\boldsymbol{L}_{\rm el}$ and we discuss our choice of basis functions $\boldsymbol{\Psi}_i$ and the resulting boundary forces (due to the no-stress boundary conditions) at the end of section 4.3.2. In section 4.3.3 we set up a realistic model of the magnetar crust and we calculate the corresponding elasto-magnetic modes in section 4.3.4, where we apply the formalism described above. In the remainder of this chapter, we focus solely on axi-symmetric azimuthal displacement fields, i.e. $\bar{\boldsymbol{\xi}} = \bar{\xi}\;\hat{\boldsymbol{e}}_\phi$ (where $\hat{\boldsymbol{e}}_\phi$ is the unit vector in the azimuthal direction and $\bar{\xi}$ is the displacement amplitude) and $\partial\bar{\xi}/\partial\phi = 0$.

4.3.1 Magnetic force density in the free crust

While the equations of section 4.2 hold at arbitrary locations in the star, we will now consider magnetic forces acting on axi-symmetric, azimuthal perturbations $\bar{\boldsymbol{\xi}}(r,\theta) = \bar{\xi}(r,\theta)\hat{\boldsymbol{e}}_\phi$ in the 'free' crust, i.e. a crust with no external stresses acting on it. This implies that to Eq. (4.17) we have to add boundary force terms arising from this no-external-stress condition. The tangential forces per unit area on both boundaries are given by

$$\begin{aligned} T_{\rm mag}(r_{\rm in}+\epsilon) - T_{\rm mag}(r_{\rm in}-\epsilon) &= T_{\rm mag}(r_{\rm in}+\epsilon) \\ T_{\rm mag}(r_{\rm out}+\epsilon) - T_{\rm mag}(r_{\rm out}-\epsilon) &= -T_{\rm mag}(r_{\rm out}-\epsilon) \end{aligned} \tag{4.29}$$

where $T_{\rm mag}(r)$ is the magnetic stress at r and ϵ is an infinitesimal number. Adding the boundary terms, we obtain

$$L_{\rm mag}(\bar{\xi}) = \sqrt{\frac{g_{tt}}{g_{\chi\chi}}}\frac{B}{4\pi c^2\tilde{\rho}\sqrt{g_{\phi\phi}}}\frac{\partial}{\partial\chi}\left[\sqrt{\frac{g_{tt}}{g_{\chi\chi}}}g_{\phi\phi}B\frac{\partial}{\partial\chi}\left(\frac{\bar{\xi}}{\sqrt{g_{\phi\phi}}}\right)\right] + \frac{1}{\tilde{\rho}}T_{\rm mag}\left[\delta(r-r_0)-\delta(r-r_1)\right] \tag{4.30}$$

where the δ's are Dirac delta functions. The magnetic stress $T_{\rm mag}$ is derived by linearizing Eq. (4.12) and retaining first order terms. One obtains

$$T_{\rm mag} = \frac{\sqrt{g_{tt}g_{\phi\phi}}}{g_{\chi\chi}}\cos\alpha\frac{B^2}{4\pi}\frac{\partial}{\partial\chi}\left(\frac{\bar{\xi}}{\sqrt{g_{\phi\phi}}}\right) \tag{4.31}$$

4.3.2 Relativistic equations for elastic forces

In the following we use relativistic equations describing the elastic force density acting on axial perturbations in the crust as derived by Schumaker & Thorne (1983) (see also Karlovini & Samuelsson 2007), and presented in a convenient form by Samuelsson & Andersson (2007, SA) (for more details on the derivation of the following equations we refer the reader to these papers). As shown in SA, the equation of motion for axial perturbations in a purely elastic crust, i.e. $\partial^2\bar{\boldsymbol{\xi}}/\partial t^2 = \boldsymbol{L}_{\rm el}(\bar{\boldsymbol{\xi}})$, can be solved by expanding the displacement field $\bar{\boldsymbol{\xi}}(r,\theta,\phi)$ into vector spherical harmonics $\bar{\boldsymbol{\xi}}_{{\rm H},lm}(\theta,\phi) \propto \boldsymbol{r}\times\boldsymbol{\nabla}Y_l^m$ (where Y_l^m is a spherical harmonic of degree l and order m) and corresponding radial- and time-dependent parts $\bar{\xi}_{\rm R}(r)$ and $f_T(t)$ of the displacement field. Rewriting Eq. (2) of SA gives

$$\boldsymbol{L}_{\rm el}\left(\bar{\boldsymbol{\xi}}\right) = \frac{1}{\tilde{\rho}}\left[\frac{1}{r^3}\sqrt{\frac{g_{tt}}{g_{rr}}}\frac{d}{dr}\left(\sqrt{\frac{g_{tt}}{g_{rr}}}r^4\mu\frac{d}{dr}\left(\frac{\bar{\xi}_{\rm R}}{r}\right)\right) - \mu g_{tt}\frac{(l-1)(l+2)}{r^2}\bar{\xi}_{\rm R}\right]\bar{\boldsymbol{\xi}}_{{\rm H},lm}\, f_T \tag{4.32}$$

where the metric terms g_{tt} and g_{rr} are the standard Schwarz-schild metric terms and $\mu(r)$ is the (isotropic) shear modulus. The expansion of $\bar{\boldsymbol{\xi}}$ into

vector spherical harmonics, leads to a particularly simple stress-free boundary condition for the radial function $\bar{\xi}_{\rm R}$:

$$\frac{d}{dr}\left(\frac{\bar{\xi}_{\rm R}}{r}\right) = 0 \tag{4.33}$$

which is valid on the inner- and outer boundaries of the neutron star crust, $r = r_0$ and $r = r_1$.

We are now ready to select our basis functions $\mathbf{\Psi}_i$ in order to solve Eq. (4.18). It is convenient to seperate $\mathbf{\Psi}_i$ into angular and radial parts, i.e. $\mathbf{\Psi}_i = \mathbf{\Psi}_{{\rm H},i}\, \Psi_{{\rm R},i}$. Although our particular choice of basis is technically arbitrary, in view of the above discussion a natural choice for the angular part $\mathbf{\Psi}_{{\rm H},i}$ are vector spherical harmonics of order $m = 0$ and $l = 2, 4, 6...$ *etc.* (we consider axi-symmetric perturbations which are anti-symmetric with respect to the equator),

$$\mathbf{\Psi}_{{\rm H},l}(\theta) = \sqrt{\frac{4\pi}{l(l+1)}}\left(\boldsymbol{r}\times\boldsymbol{\nabla}Y_l^0\right) = \sqrt{\frac{4\pi}{l(l+1)}}\frac{dY_l^0}{d\theta}\hat{\boldsymbol{e}}_\phi \tag{4.34}$$

which are orthonormal with respect to the following inner product:

$$\langle \mathbf{\Psi}_{{\rm H},l} \mid \mathbf{\Psi}_{{\rm H},l'}\rangle = \int_0^\pi \mathbf{\Psi}_{{\rm H},l}\cdot\mathbf{\Psi}_{{\rm H},l'}\sin\theta d\theta = \delta_{ll'} \tag{4.35}$$

One tempting choice for the radial function is to use the radial eigenmodes of Eq. (4.33), $\bar{\xi}_{{\rm R},n}$, (where n is the number of radial nodes) as basis functions, i.e. $\Psi_{{\rm R},n} = \bar{\xi}_{{\rm R},n}$. It turns out however, that the expansion of the elasto-magnetic displacement field [see Eq. (4.19)] into elastic eigenfunctions is very inefficient. We found that better convergence is realized with

$$\Psi_{{\rm R},n}(r) = r\sqrt{\frac{2}{r_1-r_0}}\cos\left(\frac{\pi n(r-r_0)}{r_1-r_0}\right) \quad \text{for} \quad n{=}1,2,...$$
$$\Psi_{{\rm R},n}(r) = r\sqrt{\frac{1}{r_1-r_0}} \quad \text{for} \quad n{=}0 \tag{4.36}$$

which obey Eq. (4.33), so that no extra boundary terms in $\boldsymbol{L}_{\rm el}$ are needed to preserve the stress-free condition. The basis functions of Eq. (4.36) are orthonormal with respect to the following inner-product:

$$\langle \Psi_{{\rm R},n} \mid \Psi_{{\rm R},n'}\rangle = \int_{r_0}^{r_1} \Psi_{{\rm R},n}\,\Psi_{{\rm R},n'}\frac{1}{r^2}dr = \delta_{nn'} \tag{4.37}$$

Combining Eq's (4.34) and (4.37) gives us a series of basis functions that we use in the next section to calculate elasto-magnetic modes of the crust

$$\mathbf{\Psi}_{ln}(r,\theta) = \Psi_{\mathrm{R},n}(r)\ \mathbf{\Psi}_{\mathrm{H},l}(\theta) \tag{4.38}$$

which are orthonormal

$$\langle \mathbf{\Psi}_{ln} \mid \mathbf{\Psi}_{l'n'} \rangle = \int_{r_0}^{r_1} \int_0^{\pi} \frac{\sin\theta}{r^2} \mathbf{\Psi}_{ln} \cdot \mathbf{\Psi}_{l'n'}\ d\theta dr = \delta_{ll'}\delta_{nn'} \tag{4.39}$$

Note that the weight function w of Eq. (4.20) takes the form $w(r,\theta) = \sin\theta/r^2$.

4.3.3 The neutron star model

We assume that our star is non-rotating and neglect deformations due to magnetic pressure, which are expected to be small. Therefore, we adopt a spherically symmetric background stellar model that is a solution of the Tolman-Oppenheimer-Volkoff equation (TOV equation). We calculate the hydrostatic equillibrium using a SLy equation of state (Douchin & Haensel, 2001; Haensel & Potekhin, 2004; Haensel, Potekhin & Yakovlev, 2007) (see *http://www.ioffe.ru/astro/NSG/NSEOS* for a tabulated version). The model that we use throughout this chapter has a mass of $M_* = 1.4\ M_\odot$, a radius $R_* = 1.16\cdot 10^6$ cm, a crust thickness $\Delta R = 7.9\cdot 10^4$ cm, a central density $\rho_c = 9.83\cdot 10^{14}$ g cm^{-3} and cental pressure $P_c = 1.36\cdot 10^{35}$ dyn cm^{-2}. The crustal shear modulus μ is given by (Strohmayer et al., 1991)

$$\mu = \frac{0.1194}{1 + 0.595(173/\Gamma)^2} \frac{n(Ze)^2}{a} \tag{4.40}$$

where n is the ion density, $a = (3/4\pi n)^{1/3}$ is the average spacing between ions and $\Gamma = (Ze)^2/ak_BT$ is the Coulomb coupling parameter. We evaluate μ in the limit $\Gamma \to \infty$.

To the spherical star we add a poloidal magnetic field, which we generate as follows: We start with an Euclidean (flat) space into which we place a circular current loop of radius $r_{\mathrm{cl}} = 0.55\ R_*$ and current I and calculate

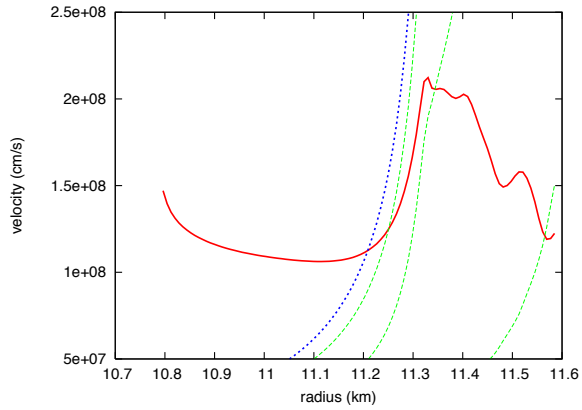


Figure 4.1: *Shear velocity* $c_s = \sqrt{\mu/\rho}$ *(solid line) versus Alfvén velocity* $c_A = \sqrt{B^2/4\pi\rho}$ *for a poloidal field strength of* 10^{15} G *(dotted line). The dashed lines are the radial components of the Alfvén velocity,* $c_{A,\mathrm{rad}} = c_A \cos\alpha$*, evaluated at (from left to right)* $\theta = 69^\mathrm{o}$*,* 79^o *and* 89^o*. Closer to the poles (smaller* θ*), the field becomes nearly radial and* $c_{A,\mathrm{rad}} \sim c_A$*. The* c_A*-curve shown in this plot is evaluated at the pole (*$\theta = 0^\mathrm{o}$*), but varies negligibly as a function of* θ*.*

the magnetic field generated by the loop (see e.g. Jackson, 1998). Then we map this field onto the curved space-time of the neutron star, as discussed in section 4.2. The field is singular near the current loop, however all the field lines which connect to the crust (and thus are physically related to observable oscillations) carry finite field values. This particular field configuration is chosen as an example; there is an infinite number of ways to generate poloidal field configurations. In figure 4.1 we plot resulting shear- and Alfvén velocities in the crust as a function of radial coordinate r.

4.3.4 Results

We now use the formalism and equations of the previous sections to calculate elasto-magnetic modes of the magnetar crust. We construct a basis from N_n radial functions $\Psi_{\mathrm{R},n}(r)$ (see Eq. (4.36)) with index $n = 0, 1, ..., N_n - 1$ and N_l angular functions $\mathbf{\Psi}_{\mathrm{H},l}(\theta)$ (see Eq. (4.34)) with even index $l = 2, 4, ..., 2N_l$.

These functions provide a set of $N_n \times N_l$ linearly independent basisfunctions $\mathbf{\Psi}_{ln}$. Using this basis, we solve the matrix equation (4.22) and reconstruct the normal modes according to Eq. (4.19).

Radial and horizontal cross-sections of a selection of eigenmodes are plotted in figures 4.2 and 4.3 and table 4.1 contains a list of frequencies. These

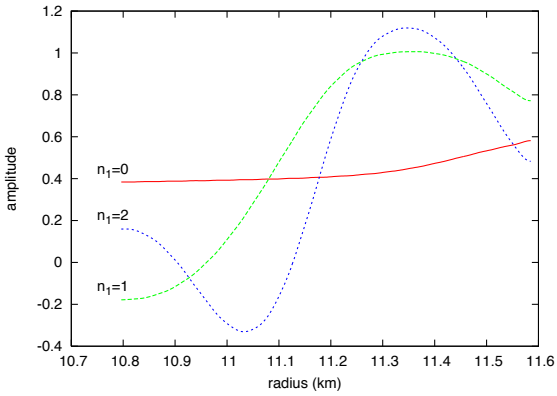


Figure 4.2: *Radial profiles of $l_1 = 2$ elasto-magnetic modes, evaluated at $\theta = 81^o$. The vertical scale of individual curves is adapted for visual convenience.*

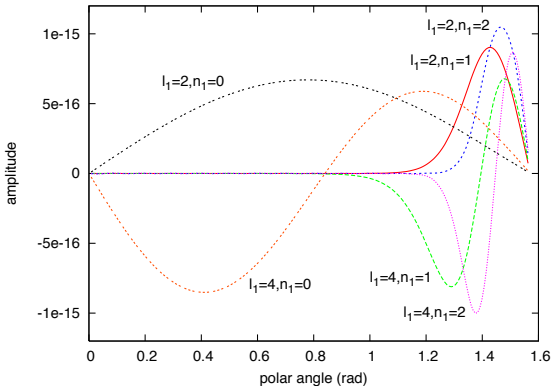


Figure 4.3: *Elasto-magnetic eigenmodes for $B_p = 10^{15}$ G (where B_p is field strength at the magnetic pole), as a function of the polar angle θ, evaluated at the crust-core interface. The $n_1 = 0$ modes are nearly unaffected by the magnetic field, whereas the $n_1 > 0$ modes are affected strongly by the magnetic field and are confined to regions near the equator.*

results are based on a stellar model with a poloidal field strength of 10^{15} G at the magnetic pole. For the calculation we used $N_n = 35$ radial basis functions and $N_l = 35$ angular basis functions. We labeled the modes with

integer indices $n_1 = 0, 1, 2...$ and $l_1 = 2, 4, 6, ...$, where n_1 is defined as the number of nodes along the r-axis and $l_1 + 1$ is the number of nodes along the θ-axis (including the poles). Note that the index l_1, in contrast to l, does not signify a spherical harmonic degree since the angular dependence of the elasto-magnetic modes differs from pure spherical harmonics. However, there is a connection between the two indices: the elasto-magnetic mode of degree l_1 and order n_1, can be interpreted as the magnetically perturbed elastic mode of the same order and (spherical harmonic-) degree. More precisely, if one gradually increases the magnetic field strength, the n, l elastic mode transforms into the elasto-magnetic mode of the same indices, $n_1 = n$ and $l_1 = l$ (see fig. 4.6). It is interesting to note (see fig's 4.6 and 4.3) that as the field strength increases, modes with $n_1 > 0$ become more and more confined to a narrow region near the equator (a similar effect was recently observed in the grid-based simulations of Gabler et al. 2011b). In the equatorial regions, the horizontal field creates a magnetic tension-free cavity for modes with radial nodes, which are reflected back towards the equator at higher lattitudes where the field becomes more radial[1]. The $n_1 = 0$ modes however, having no radial nodes, are virtually insensitive to the magnetic field and are therefore not confined to low lattitudes. The field strength-dependence of the eigenfrequencies, illustrated in figure 4.5, is qualitatively similar to results obtained by other authors (see Carroll et al., 1986; Piro, 2005; Sotani et al., 2007). As we increase the field strength, we find that the increase in frequency $\delta\omega$ for $n_1 = 0$ modes scales weakly with B, i.e. $\delta\omega \propto B^2$. For modes with $n_1 > 0$, $\delta\omega \propto B^2$ if $B < 5 \cdot 10^{13}$ G and $\delta\omega \propto B$ if $B > 5 \cdot 10^{13}$ G. As a test, we compared the eigenfrequencies and eigenmodes for zero field, $B = 0$ G, to those obtained by a direct integration of the elastic equation of motion (Eq. 4.33).[2] We find that both frequencies and wavefunctions obtained by the series expansion-method

[1] A similar effect is well-known from the study of waveguides: as the waveguide gets narrower (i.e. as its transverse frequency increases), the propagating wave may become evanescent in the longitudinal direction and be reflected

[2] The latter works as follows: One starts by assuming harmonic time depence for the displacement $\bar{\xi}$, so that $L_{\rm el}(\bar{\boldsymbol{\xi}}) = -\omega^2 \bar{\boldsymbol{\xi}}$. Dropping the angular- and time-dependent parts of $\bar{\boldsymbol{\xi}}$ on both sides of the equation, one is left with an equation for $\bar{\xi}_{\rm R}$, which is integrated from the bottom of the crust, with corresponding boundary condition, to the surface. This is repeated for different ω until the surface boundary condition is satisfied; one has found an eigenmode. By repeating this procedure with gradually increasing ω, one obtains a series of eigenmodes and -frequencies.

mode indices	elastic modes ($B = 0$ G)	elasto-magnetic modes ($B = 10^{15}$ G)
$n_1 = 0$, $l_1 = 2$	27.42 Hz	27.61 Hz
$n_1 = 0$, $l_1 = 4$	58.16 Hz	59.14 Hz
$n_1 = 0$, $l_1 = 6$	86.69 Hz	88.13 Hz
$n_1 = 0$, $l_1 = 8$	114.7 Hz	116.5 Hz
$n_1 = 1$, $l_1 = 2$	895.9 Hz	954.1 Hz
$n_1 = 1$, $l_1 = 4$	897.4 Hz	985.7 Hz
$n_1 = 1$, $l_1 = 6$	899.7 Hz	1001.4 Hz
$n_1 = 1$, $l_1 = 8$	902.8 Hz	1003.4 Hz
$n_1 = 2$, $l_1 = 2$	1474.6 Hz	1607.1 Hz
$n_1 = 2$, $l_1 = 4$	1475.7 Hz	1664.4 Hz
$n_1 = 2$, $l_1 = 6$	1477.5 Hz	1708.1 Hz
$n_1 = 2$, $l_1 = 8$	1479.9 Hz	1740.4 Hz

Table 4.1: *The eigenfrequencies of the non-magnetic crust (second column) versus the eigenfrequencies of the magnetized crust (third column), with a magnetic field of* 10^{15} G *at the polar surface. The elasto-magnetic frequencies were calculated using a basis of* 35×35 *basisfunctions* Ψ_{ln}.

converge rapidly[1] to the real values, obtained by integration of Eq. (4.33). E.g. for $N_n = 10$, $n_1 = 0$ elastic frequencies have a typical error of 0.02%, while frequencies for modes $n_1 < 4$ are well within 1% accuracy. In figure 4.4 we plot elastic eigenfunctions, obtained by both methods. The solutions from the series-expansion method with $N_n = 10$ radial basis functions are nearly indistinguishable from the solutions obtained by direct integration.

For the full elasto-magnetic equation of motion, Eq. (4.18) with a magnetic field strength of 10^{15} G at the pole, we tested the convergence of resulting eigenfrequencies by increasing the number of basis functions N_n and N_l (see figure 4.7). We find that, compared to the non-magnetic case, a significant number N_n of radial functions and N_l angular functions is required to get acceptable convergence to stable results. The large number of required radial

[1] Note that in the purely elastic case, l is a good quantum number and the angular basis functions $\mathbf{\Psi}_{\mathrm{H},l}(\theta)$ are already solutions to the elastic eigenmode equation. Therefore, for a given $l_1 = l$ only the series with the radial basis-functions needs to be considered.

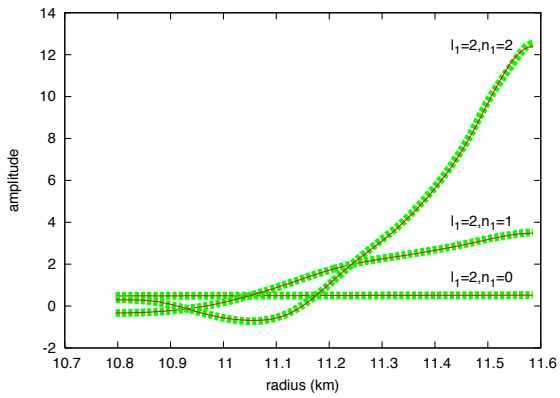


Figure 4.4: *Elastic crustal modes obtained through integration of the elastic equation of motion (thick dashed curves) and the same modes obtained by the series-expansion method (overplotted by the thin solid curve), using $N_n = 10$ radial basis functions.*

basis functions can be understood from the fact that the magnetic acceleration L_B (Eq. (4.31)) contains delta-functions, arising from the boundary terms. Obviously, one needs many radial basis functions to obtain an acceptable sampling of these singular boundary terms. The number of computational operations however, is a steep function of the number of basis functions (approximately $\propto (N_l \times N_n)^3$), so that computations with large N_l and N_n ($> 30 - 40$) can become unpractical on ordinary workstations. Although this limits the number of basisfunctions in our calculations, we find that for $N_l, N_n \sim 35$, the scatter in frequencies is typically $\lesssim 1\%$ for most modes (figure 4.7) and the eigenfunctions $\bar{\xi}_m$ reproduce the orthogonality relation of Eq. (4.27) with good precision.

4.4 Core continuum and the coupling between crust and core

4.4.1 The continuum

The equation of motion is in this case simply the Alfvén wave equation:

$$\frac{\partial^2 \xi(\psi,\chi)}{\partial t^2} = L_{\rm mag}\left[\xi(\psi,\chi)\right], \tag{4.41}$$

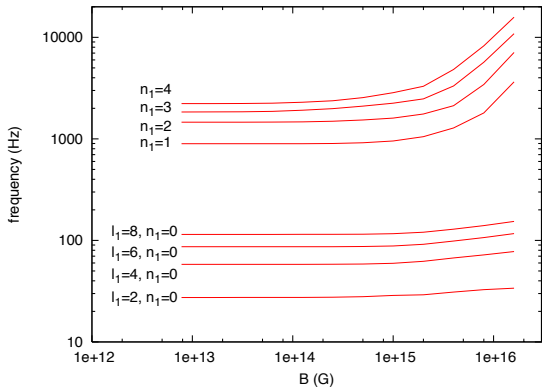


Figure 4.5: *Frequencies as a function of B. For $n_1 > 0$, the frequencies of (low) l_1-modes nearly coincide and are therefore collectively indicated with their n_1-value, i.e. $n_1 = 1$, $n_1 = 2$, etc. Note that high field strengths, the $n_1 > 0$ frequencies collectively behave as $\omega \propto B$.*

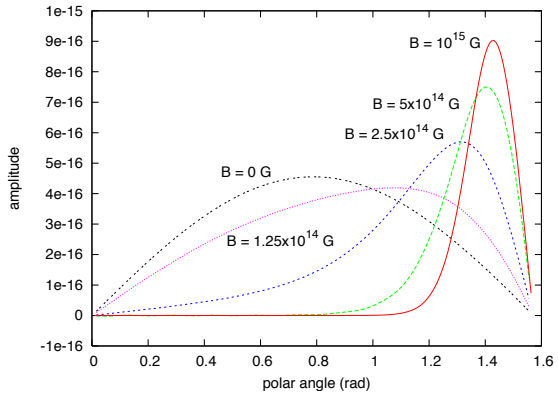


Figure 4.6: *Angular geometry of the $l_1 = 2$, $n_1 = 1$ crustal mode, as a function of the magnetic field strength. For zero magnetic field, the curve is identical to the $l = 2$ vector spherical harmonic $\Psi_{\mathrm{H},l}(\theta)$. As the field strength increases, the crustal motion becomes gradually more confined towards the equator.*

where t denotes the Schwarzschild time-coordinate. The operator L_{mag} is given in Eq. (4.17), which we repeat here for convenience

$$L_{\mathrm{mag}}\left[\xi(\psi,\chi)\right] = \frac{1}{\tilde{\rho}c^2}\sqrt{\frac{g_{tt}}{g_{\chi\chi}}}\frac{B}{4\pi\sqrt{g_{\phi\phi}}}\frac{\partial}{\partial\chi}\left[\sqrt{\frac{g_{tt}}{g_{\chi\chi}}}g_{\phi\phi}B\frac{\partial}{\partial\chi}\left(\frac{\xi}{\sqrt{g_{\phi\phi}}}\right)\right] \quad (4.42)$$

Here g_{tt}, $g_{\chi\chi}$ and $g_{\phi\phi}$ are the metric terms corresponding to the system of coordinates defined in section 4.2.

For determining the spectrum of the core continuum, the appropriate boundary conditions are $\xi(\chi = \chi_c) = 0$, where $\chi_c(\phi)$ marks the location of the crust-core interface. The full significance of this boundary condition will become apparent later in this section when we develop the analysis for the

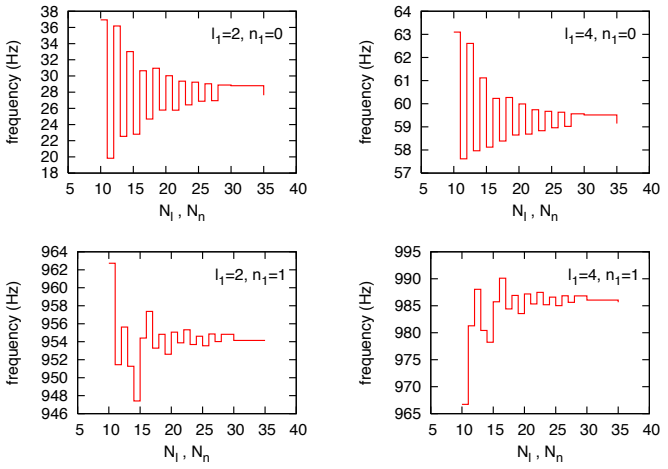


Figure 4.7: *Demonstration of convergence for elasto-magnetic frequencies for low-order, low-degree modes as a function of N_n and N_l, where we took $N_n = N_l$. The actual number of basisfunctions, $N = N_n \times N_l$, is the square of the value along the x-axis.*

crust-core interaction; see also section 3.4.2. With this boundary condition, Equation (4.41) constitutes a Sturm-Liouville problem on each separate flux surface ψ. Using the stellar structure model and magnetic field configuration described in section 4.3.3, we can calculate the eigenfunctions and eigenfrequencies for each flux surface ψ. The reflection symmetry of the stellar model and the magnetic field with respect to the equatorial plane assures that the eigenfunctions of equation (4.41) are either symmetric or anti-symmetric with respect to the equatorial plane. We can therefore determine the eigenfunctions by integrating equation (4.41) along the magnetic field lines from the equatorial plane $\chi = 0$ to the crust-core interface $\chi = \chi_c(\psi)$. Let us consider the odd modes here for which $\xi(0) = 0$ and solve equation (4.41) with the boundary condition $\xi(\chi_c) = 0$ at the crust-core interface; for even modes, the boundary condition is $d\xi(0)/d\chi = 0$. We find the eigenfunctions by means of a shooting method; using fourth order Runge-Kutta integration we integrate from $\chi = 0$ to $\chi = \chi_c$. The correct eigenvalues σ_n and eigenfunctions $\xi_n(\chi)$ are found by changing the value of σ until the boundary condition at

ξ_n is satisfied. In this way we gradually increase the value of σ until the desired number of harmonics is obtained. In figure 4.8 we show a typical resulting core-continuum. The continuum is piece-wise and covers the domains $\sigma = [41.8, 67.5]$ Hz and $\sigma = [91.4, \infty)$ Hz. Gaps, such as the one between 67.5 Hz and 91.4 Hz in fig. 4.8, are a characteristic feature for the type of poloidal field that we employ in this chapter and typically occur at low frequencies (i.e. $\sigma < 150$ Hz). As we discuss in section 4.4.3, they may give rise to strong low frequency QPOs; see also vHL11 (section 3.4) and Colaiuda & Kokkotas 2011. According to Sturm-Liouville theory the normalized eigenfunctions ξ_n of equation (4.41) form an orthonormal basis with respect to the following inner product:

$$\langle \xi_m, \xi_n \rangle = \int_0^{\chi_c} r(\chi)\, \xi_m(\chi)\, \xi_n(\chi)\, d\chi = \delta_{m,n} \tag{4.43}$$

Where $\delta_{m,n}$ is the Kronecker delta. Noting that the operator $L_{\rm mag}(\xi)$ is in Sturm-Liouville form, one reads off the weight-function $r(\chi)$:

$$r = \sqrt{\frac{g_{\chi\chi}}{g_{tt}}} \frac{4\pi\tilde{\rho}}{B_\chi}. \tag{4.44}$$

We have checked that the solutions $\xi_n(\chi)$ satisfy the orthogonality relations.

4.4.2 Equations of motion for the coupled crust and core

We are now ready to compute the coupled crust-core motion. In contrast to L07 and vHL11 (chapter 3), where the crust was assumed to be an infinitely thin spherical elastic shell, we shall here adopt a crust of finite thickness with realistic structure. We label the lattitudinal location by the flux surface ψ intersecting the crust-core interface and consider the crustal axisymmetric displacements $\bar{\xi}_\phi(\psi, r)$, where r is the radial Schwarzschild-coordinate. In the MHD approximation, the magnetic stresses enforce a no-slip boundary condition at the crust-core interface (at $r = r_0$ in the Schwarzschild coordinates of the crust, or χ_c in the flux-coordinates of the core), such that

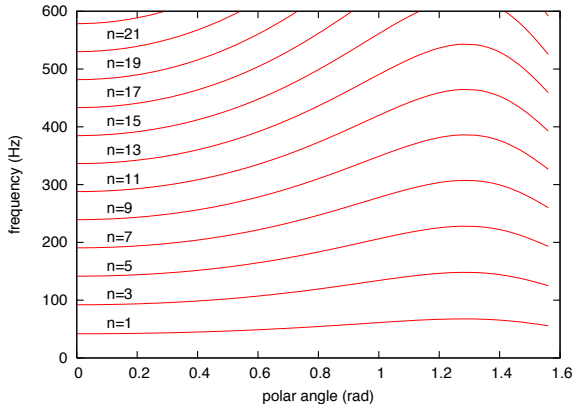


Figure 4.8: *The curves show the Alfvén frequencies σ_n as a function of the angle $\theta(\psi)$, the polar angle at which the flux surface ψ intersects the crust. Since we are only considering odd crustal modes, the only Alfvén modes that couple to the motion of the star are the ones with an odd harmonic number n. This particular continuum was calculated using a poloidal field with a surface value of $B = 10^{15}$ G at the poles.*

$\xi(\psi, \chi_c) = \bar{\xi}(\theta(\psi), r_0)$ instead of $\xi(\psi, \chi_c) = 0$. It is useful to make the following substitution

$$\zeta(\psi, \chi) \equiv \xi(\psi, \chi) - \bar{\xi}(\theta(\psi), r_0)\, w(\psi, \chi) \tag{4.45}$$

where we choose the function $w(\psi, \chi)$ so that (1) it corresponds to the static displacement in the core and hence satisfies $L_{\rm mag}(w(\psi, \chi)) = 0$ and (2) $w(\psi, \chi_c) = 1$. From the definition of the operator F it follows that for the odd modes

$$w(\psi, \chi) = \sqrt{g_{\phi\phi}} \int_0^{\chi} \sqrt{\frac{g_{\chi\chi}}{g_{tt}}} \frac{K(\psi)}{g_{\phi\phi} B(\psi, \chi')} d\chi' \tag{4.46}$$

Here the constant $K(\psi)$ is chosen such that $w(\psi, \chi_c) = 1$. The new quantity ζ from Eq. (4.45) now satisfies the boundary condition $\zeta(\psi, \chi_c) = 0$ and can be expanded into the Alfvén normal modes ξ_n which satisfy the same boundary conditions.

We now proceed by substituting equation (4.45) into equation (4.41) thus

obtaining a simple equation of motion for ζ

$$\frac{\partial^2 \zeta\left(\psi,\chi\right)}{\partial t^2} - L_{\rm mag}\left(\zeta\left(\psi,\chi\right)\right) = -w\left(\psi,\chi\right)\frac{\partial^2 \bar{\xi}\left(\theta(\psi),r_0\right)}{\partial t^2} \tag{4.47}$$

We expand ζ and w into a series of ξ_n's:

$$\zeta\left(\psi,\chi,t\right) = \sum_n a_n\left(\psi,t\right)\xi_n\left(\psi,\chi\right) \tag{4.48}$$

$$w\left(\psi,\chi\right) = \sum_n c_n\left(\psi\right)\xi_n\left(\psi,\chi\right). \tag{4.49}$$

Using these expansions, equation (4.47) reduces to the following equations of motion for the eigenmode amplitudes a_n

$$\frac{\partial^2 a_n\left(\psi\right)}{\partial t^2} + \sigma_n^2\left(\psi\right)a_n\left(\psi\right) = -c_n\left(\psi\right)\frac{\partial^2 \bar{\xi}(\psi,r_0)}{\partial t^2} \tag{4.50}$$

These equations show how the core Alfvén modes are driven by the motion of the crust. To close the system, we must address the motion of the crust driven by the hydromagnetic pull from the core:

$$\frac{\partial^2 \bar{\xi}}{\partial t^2} = L_{\rm crust}\left(\bar{\xi}\right) - \frac{1}{\tilde{\rho}}\left[\frac{g_{tt}}{g_{\chi\chi}}\frac{\sqrt{g_{\phi\phi}}B^2}{4\pi c^2}\cos\alpha\frac{\partial}{\partial\chi}\left(\frac{\xi}{\sqrt{g_{\phi\phi}}}\right)\right]\delta(r-r_0) \tag{4.51}$$

The expression between the square brackets is the hydro-magnetic stress from stellar core acting on the crust, α is the angle between the magnetic field line and the radial coordinate of the star and $L_{\rm crust}\left(\bar{\xi}\right) = L_{\rm mag}\left(\bar{\xi}\right) + L_{\rm el}\left(\bar{\xi}\right)$ is the acceleration of the crustal displacement due to magnetic- and elastic stress (see section 4.3). We can rewrite this in terms of the coefficients, using Eq. (4.45), the definition of w and the expansions and orthogonality relations of Eq's (4.27) and (4.29), as:

$$\frac{\partial^2 b_j}{\partial t^2} + \Omega_j^2 b_j = -\int_0^\pi \frac{\sqrt{g_{rr}g_{tt}}}{g_{\chi\chi}}\frac{B^2}{2c^2}\cos\alpha\left(\sum_n a_n\frac{\partial\xi_n}{\partial\chi} + \sqrt{\frac{g_{\chi\chi}}{g_{tt}}}\frac{K}{B\sqrt{g_{\phi\phi}}}\sum_i b_i\bar{\xi}_i\right)\bar{\xi}_j\Bigg|_{r=r_0} r_0^2\sin\theta d\theta \tag{4.52}$$

where the coefficients $b_j(t)$ are crustal mode amplitudes defined in Eq's (4.24) and (4.29). Up to this point the derived equations of motion for the crust

and the fluid core are exact. Note that, as a consequence of the crust-core coupling, equation (4.53) describing the evolution of $b_j(t)$ contains a term proportional to b_j on the right hand side. This term enters due to the static fluid displacement $w\bar{\xi}$ corresponding to the j-th crustal mode and effectively loads this mode with tension. The 'tension-loaded' frequency $\tilde{\Omega}_j$ of the j-th crustal mode is obtained by moving the term proportional to b_j to the left-hand side of Eq. (4.53)

$$\tilde{\Omega}_j^2 = \Omega_j^2 + \int_0^\pi \sqrt{\frac{g_{rr}}{g_{\chi\chi}}} \frac{BK}{2c^2} \cos\alpha \; \bar{\xi}_j^2 \; r \Big|_{r=r_0} d\theta \tag{4.53}$$

In the appendix we use these 'tension-loaded' frequencies to calculate theoretical damping rates of crustal modes.

We are now ready to discretize the continuum by converting the integral of equation (4.51) into a sum over N points θ_i. In order to avoid the effect of phase coherence (see section 4.3) which caused drifts in the results of L07, we sample the continuum randomly over the θ-interval $[0, \pi/2]$. In the following, functional dependence of the coordinate ψ or $\theta\,(\psi)$ is substituted by the discrete index i which denotes the i-th flux surface.

$$\frac{\partial^2 b_j}{\partial t^2} + \Omega_j^2 b_j = -\sum_i \frac{\sqrt{g_{rr,i} g_{tt,i}}}{g_{\chi\chi,i}} \frac{B_i^2}{2c^2} \cos\alpha_i \left(\sum_{n,i} a_{n,i} \frac{\partial \xi_{n,i}}{\partial \chi} + \sqrt{\frac{g_{\chi\chi,i}}{g_{tt,i}}} \frac{K_i}{B_i \sqrt{g_{\phi\phi,i}}} \sum_m b_m \bar{\xi}_{m,i} \right) \bar{\xi}_{j,i} \Big|_{r=r_0} r_0^2 \sin\theta_i \Delta\theta_i \tag{4.54}$$

$$\frac{\partial^2 a_{nk}}{\partial t^2} + \sigma_{nk}^2 a_{nk} = -c_{nk} \sum_j \frac{\partial^2 b_j}{\partial t^2} \bar{\xi}_{j,k} \tag{4.55}$$

These are the equations that fully describe dynamics of our magnetar model. As with the toy model from section 3.2 we integrate them using a second order leap-frog scheme which conserves the total energy to high precision. As a test we keep track of the total energy of the system during the simulations. Further we have checked our results by integrating equations (4.55) and (4.55)

with the fourth-order Runge-Kutta scheme for several runs and found good agreement with the leap-frog integration.

4.4.3 Results

Based on the results of chapter 3, we expect the following dynamical characteristics to occur; (1) Crustal modes with frequencies that are inside the continuum should undergo resonant absorption, i.e. if such a mode couples efficiently to continuum Alfvén modes of the core with similar frequencies, its motion will be damped on rather short time-scales. In appendix 4.A we analytically investigate the efficiency of this coupling and the resulting damping time scales. (2) Late-time behavior of the system will show oscillations near the edges of the continuum; the edge modes. (3) Gaps, as present in the continuum of fig. 4.8 will give rise two types of QPOs. First, crustal modes which are inside these gaps will remain undamped, although slightly shifted in frequency due to the interaction with the continuum.[1] Second, edge modes near the edges of the gaps may occur. All of these characteristics were observed in simulations of chapter 3 and we expect them to occur in this work.

We consider 16 crustal modes, i.e. $(n,l) = (0,2)$, $(0,4)$, $(0,6)$, $(0,8)$, $(0,10)$, $(0,12)$, $(0,14)$, $(0,16)$, $(0,18)$, $(0,20)$, $(1,2)$, $(1,4)$, $(1,6)$, $(1,8)$, $(1,10)$ and $(1,12)$. We couple these crustal modes to 9000 continuum oscillators, i.e. 300 different flux surfaces, each with 30 Alfvén overtones. We start the simulation by initializing the crustal mode amplitudes $b_j = 1$ for all crustal modes, while keeping the continuum oscillators relaxed ($a_{ni} = 0$). We evolve the system for 52s in time.

In table 4.2 we list the 'free' crustal frequencies Ω and 'tension-loaded' frequencies $\tilde{\Omega}$ for the 16 modes considered in our simulation. The last column of table 4.2 contains the corresponding theoretically calculated damping rates (see appendix). In figure 4.9 we show the power spectrum which was calculated using the data of the last 26 s of the simulation.

[1] The presence of 'gap modes' like the ones found in section 3.4, was recently confirmed by Colaiuda & Kokkotats, 2011.

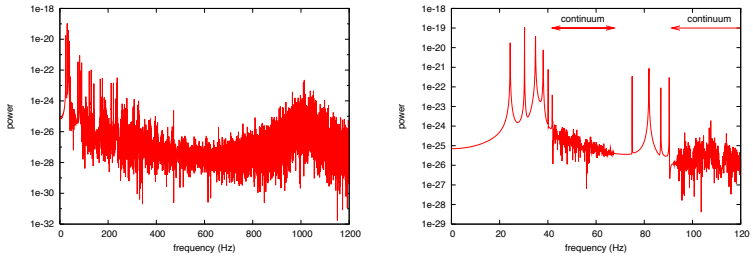


Figure 4.9: *Power spectrum of the crustal motion. The zoomed in version in the right panel shows the location of the core-continuum.*

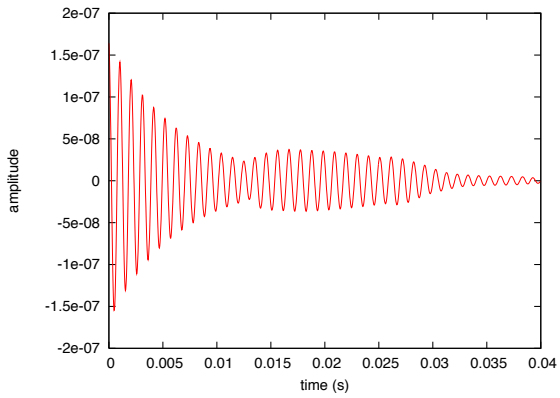


Figure 4.10: *Displacement of the* $l_1 = 2$, $n_1 = 1$ *mode. The theoretically calculated damping time is* $\tau_d = 5.8 \cdot 10^{-3}$ s. *Note the transient increase in the mode amplitude. This is due to the initial Alfvén wave train, which is reflected at the equator.*

mode indices	crustal frequencies Ω	tension-loaded frequencies $\tilde{\Omega}$	damping time τ_d
$n_1 = 0$, $l_1 = 2$	27.61 Hz	71.10 Hz	∞ ms
$n_1 = 0$, $l_1 = 4$	59.14 Hz	86.49 Hz	∞ ms
$n_1 = 0$, $l_1 = 6$	88.13 Hz	107.6 Hz	6.2 ms
$n_1 = 0$, $l_1 = 8$	116.5 Hz	131.6 Hz	0.47 ms
$n_1 = 0$, $l_1 = 10$	144.7 Hz	157.0 Hz	0.53 ms
$n_1 = 0$, $l_1 = 12$	172.7 Hz	183.0 Hz	287 ms
$n_1 = 0$, $l_1 = 14$	200.6 Hz	209.5 Hz	0.67 ms
$n_1 = 0$, $l_1 = 16$	228.5 Hz	236.3 Hz	1.3 ms
$n_1 = 0$, $l_1 = 18$	256.3 Hz	263.3 Hz	0.97 ms
$n_1 = 0$, $l_1 = 20$	284.1 Hz	290.4 Hz	0.83 ms
$n_1 = 1$, $l_1 = 2$	954.1 Hz	955.0 Hz	5.8 ms
$n_1 = 1$, $l_1 = 4$	985.7 Hz	986.7 Hz	11.4 ms
$n_1 = 1$, $l_1 = 6$	1001.4 Hz	1002.4 Hz	1.4 ms
$n_1 = 1$, $l_1 = 8$	1003.4 Hz	1004.5 Hz	3.3 ms
$n_1 = 1$, $l_1 = 10$	1006.5 Hz	1007.5 Hz	2.7 ms
$n_1 = 1$, $l_1 = 12$	1010.5 Hz	1011.6 Hz	2.5 ms

Table 4.2: *Frequencies of the 'free' crustal modes Ω (2nd column) and 'tension-loaded' frequencies $\tilde{\Omega}$ due to the crust-core coupling (3rd column; see Eq. (4.53)). The resonant damping time-scales τ_d (see appendix), are given in the 4th column. The $n_1 = 0$, $l_1 = 2, 4$ modes are shifted into the 'gap' (in the interval $\sigma = [67.5, 91.4]$ Hz) and are therefore undamped. The long damping time of the $n_1 = 0$, $l_1 = 12$ crustal mode is due to the fact that the only resonant Alfvén layer coincides nearly with a crustal node.*

4.5 Discussion

In this chapter we have laid out the spectral formalism for computation of general-relativistic torsional magnetar oscillations. This method is efficient; a typical simulation of 50 seconds of the magnetar dynamics (i.e., up to tens of thousands of the oscillatory periods) takes only a few hours or an ordinary workstation. The second-order symplectic leap-frog scheme ensures that the energy of the system is conserved with very high accuracy. Our simulations allow us to investigate which of the oscillatory behavior is long-lived enough (~ 100 s) to be relevant to the observations of QPOs in the tails of giant SGR flares (Israel et al. 2005, Strohmayer & Watts 2006).

The results from the simulations in this chapter are qualitatively in agreement with earlier results in chapter 3. In particular the presence of undamped crustal motion in gaps of the Alfvén continuum was obtained both analytically and in our numerical simulations, in contrast to recent results by Gabler et al. (2011b), where the authors report in some detail the strong damping of an elastic crustal mode inside a gap. We argue that this discrepancy might be due to the fact that Gabler et al., while considering stronger magnetic fields, couple the entire core mass, including the neutrons to the Alfvén modes. As a result the effective mass of the Alfvén modes is a factor of $\sim 20 - 40$ greater than ours, imposing a frequency shift on the crustal mode which may well push it out of the gap.

One of the puzzling features of the observations are several high-frequency QPOs above 600 Hz (Watts & Strohmayer 2006). The thin-crust models of vH11 had strongly suggested that crustal modes of such high frequency should be subject to the strong resonant absorption in the core, even if the core's Alfvén modes do not form a mathematical continuum[1]. In accordance with results of Gabler et al. (2011b), we found that some crustal modes are confined to the regions in the crust where the magnetic field is nearly horizontal. Because of this, the coupling to the Alfvén modes in the core is reduced relative to the coupling strength estimated in chapter 3, however, the coupling is still

[1] This is because the frequencies of even discrete Alfvén modes form a grid, whose characteristic spacing is much less than 600 Hz. At such high frequencies, the grid acts dynamically as a continuum. See vH11 for a more detailed discussion

large enough for the mode energy to be drained on a time-scale small compared to the observed QPOs ($\tau_d \ll 100$ s). Thus it is still hard to understand the high frequency QPOs (> 600 Hz) in terms of axial oscillations of the star. An interesting alternative might be to consider polar Alfvén oscillations. The polar oscillations studied by Sotani & Kokkotas (2009) form a discrete set of modes with frequencies of several hundreds of Hz and may be interesting candidates for high frequency QPOs if their coupling to other Alfvén modes turns out to be weak.

Acknowledgements

This research was supported, in part, by the Leiden Observatory and the Lorentz Institute through internal grants. We thank the referee, Prof. Kostas Kokkotas, for making valuable comments and suggestions. MvH thanks Monash School of Physics, where part of this research was completed, for hospitality during his extensive visit.

Appendix 4.A: Damped modes

Now we explore the phenomenon of resonant absorption which occurs in a system where a harmonic oscillator is coupled to a continuum of oscillators. Our aim is to find an analytic estimate for the rate at which the energy of such an oscillator is transferred to the continuum. The objective of this section and the method that we follow, are analogous to a derivation of the quantum mechanical Fermi's Golden Rule, which gives the transition rate from one quantum mechanical eigenstate into a continuum of states.

Consider the coupled crust-core dynamics of section 4.4. The forced motion of the core Alfvén modes due to the acceleration of the crust, is

$$\ddot{a}_n(\psi) + \sigma_n^2(\psi) a_n(\psi) = -c_n(\psi)\ \ddot{\bar{\xi}}(\psi, r_0) \tag{4.56}$$

where $a_n(\psi)$ is the displacement of the n-th core Alfvén harmonic on the flux-surface ψ with frequency σ_n, $\ddot{\bar{\xi}}(\psi, r_0)$ is the acceleration of the crust at the location where the flux surface ψ intersects the crust and $c_n(\psi) = \langle w(\psi,\chi), \xi_n \rangle$ is a coupling constant (see Eq. (4.49)). Suppose that we keep the system initially fixed in a position where the crust is displaced with amplitude $b_{m,0}$ according to the m-th eigenmode, i.e. $\bar{\xi} = b_{m,0}\bar{\xi}_m$ and the continuum oscillators are relaxed; $a_n(\psi) = 0$. At time $t = 0$ we release the crust which starts oscillating at frequency $\tilde{\Omega}_m$. Suppose that the damping timescale $\tau_{d,m}$ of the crustal mode is much larger than its period $\tau_m = 2\pi/\tilde{\Omega}_m$, then the crust oscillates at roughly constant amplitude, i.e. $b_m(t) \approx b_{m,0}\cos\tilde{\Omega}_m t$. This motion forces the Alfvén oscillators according to

$$\ddot{a}_n(\psi) + \sigma_n^2(\psi) a_n(\psi) = c_n(\psi)\ \tilde{\Omega}_m^2 b_{m,0}\ \bar{\xi}_m(\psi, r_0)\cos\tilde{\Omega}_m t \tag{4.57}$$

One can solve the time-evolution of the oscillator $a_n(t)$ using standard techniques (see e.g. Landau & Lifshitz, Mechanics §22). After a time t the energy per flux surface $\mathcal{E}_n(\psi) = 1/2(\dot{a}_n^2 + \sigma_n^2 a_n^2)$ absorbed by the oscillator is

$$\mathcal{E}_n(\psi, t) = \frac{1}{2} c_n^2(\psi)\ \tilde{\Omega}_m^4 b_{m,0}^2\ \bar{\xi}_m^2(\psi, r_0) \left| \int_0^t \cos\tilde{\Omega}_m t' e^{-i\sigma_n t'} dt' \right|^2 \tag{4.58}$$

It is easy to verify that at late times the term between the vertical brackets in Eq. (4.58) becomes narrowly peaked around $\sigma_n = \tilde{\Omega}_m$, so that the bulk

of energy is transported to oscillators which are in (near) resonance with the crust. The average rate of energy (per flux surface) transfer $\langle \dot{\mathcal{E}}_n(\psi,t)\rangle$ from the crust to the to the flux surface ψ at time t is $\mathcal{E}_n(\psi,t)/t$. For sufficiently large t one finds

$$\langle \dot{\mathcal{E}}_n(\psi,t)\rangle \approx \frac{\pi}{4} c_n^2(\psi)\ \tilde{\Omega}_m^4 b_{m,0}^2\ \bar{\xi}_m^2(\psi,r_0)\delta(\tilde{\Omega}_m-\sigma_n) \tag{4.59}$$

where $\delta(\tilde{\Omega}_m-\sigma_n)$ is a Dirac delta function. This expression is exact in the limit of $t\to\infty$. The total rate of energy transfer $\dot{E}$ from the crust to the Alfvén continuum is then obtained simply by integrating Eq. (4.59) over ψ and summing over all n

$$\dot{E} = \sum_n \int_{\psi_{\min}}^{\psi_{\max}} \langle \dot{\mathcal{E}}_n(\psi)\rangle d\psi = \sum_{n,k} \frac{\pi}{4} c_n^2(\psi_k)\ \tilde{\Omega}_m^4 b_{m,0}^2\ \bar{\xi}_m^2(\psi_k,r_0)\ \left.\frac{d\psi}{d\sigma_n}\right|_{\psi=\psi_k} \tag{4.60}$$

here ψ_k denotes flux surfaces that are in resonance with the crustal motion, $\sigma_n(\psi_k)=\tilde{\Omega}_m$. Since for a given n, the crustal mode may be in resonance with Alfvén modes in several flux surfaces ψ_k, the total energy transfer is obtained by summing over the index k. Eq. (4.60), which is the analog of the quantum physics' Fermi's Golden Rule, leads to a simple expression for the energy damping timescale $\tau_{E,m}$ $(=1/2\ \tau_{d,m})$ of the crustal mode

$$\tau_{E,m} \sim \frac{E(t=0)}{\dot{E}} = \left[\sum_{n,k} \frac{\pi}{2}\tilde{\Omega}_m^2 c_n^2(\psi_k)\bar{\xi}_m^2\ \left.\frac{d\psi}{d\sigma_n}\right|_{\psi=\psi_k}\right]^{-1} \tag{4.61}$$

where $E(t=0)=1/2\tilde{\Omega}_m^2 b_{m,0}^2$ is the initial energy of the m-th crustal mode. Using numerical simulations, we verified the correctness of Eq. (4.61). Even for very short damping times, i.e. $\tau_d=2\tau_E\sim 2\pi/\tilde{\Omega}_m$, Eq. (4.61) proves remarkably accurate.

Bibliography

References

Abadie, J., et al., (LIGO Scientific Collaboration, VIRGO), 2010, arXiv1011.4079

Abbott, B. P., et al., 2008, ApJ, 681, 1419

Abbott, B. P., et al., 2009a, Reports on Progress in Physics, 72, 076901

Abbott, B. P., et al., 2009b, ApJ Letters, 701, L68

Acernese, F., et al., 2008, Classical and Quantum Gravity, 25, 114045

Alladio, F. & Micozzi, P., 1996, Phys. Plasmas, 3, 72

Alpar, M. A., Langer, S. A. & Sauls, J. A., 1984, ApJ, 282, 533

Andersson, N. & Kokkotas, K. D., 1996, Phys. Rev. Letters, 77, 4134

Andersson, N. & Kokkotas, K. D., 2001, IJMPD, 10, 381A

Andersson, N., Comer, G.L. & Glampedakis, K., 2005, Nucl. Phys. A 763, 212

Andersson, N., Glampedakis, K. & Samuelsson, L., 2009, MNRAS, 396, 894

Barat, C., et al., 1983, A&A, 126, 400

Bekarevich, I. L. & Khalatnikov, I. M., 1961, Sov. Phys. JETP, 13, 643

Braithwaite, J. & Spruit, H. C., 2004, Nature, 431, 819

Braithwaite, J. & Nordlund, A., 2006, A&A, 450, 1077

Braithwaite, J., 2008, MNRAS, 386, 1947

Bryson, B., 2003, *A Short History of Nearly Everything*, (Black Swan (UK))

Carroll, B. W., Zweibel, E. G., Hansen, C. J., McDermott, P. N., Savedoff, M. P., Thomas, J. H. & van Horn, H. M., 1986, ApJ, 305, 767C

Cerdá-Durán, P., Stergioulas, N. & Font, J., 2009, MNRAS, 397, 1607

Chandrasekhar, S., 1970 Phys Rev L., 24, 611
Christensen-Dalsgaard, J., 2003, *Lecture Notes on Stellar Oscillations, 5-th ed.*, (available online at: http://users-phys.au.dk/jcd/oscilnotes/)
Colaiuda, A., Beyer, H. & Kokkotas, K.D., 2009, MNRAS, 396, 1441
Colaiuda, A. & Kokkotas, K. D., 2011, MNRAS, 414, 3014C
Corsi, A. & Owen, B., 2011, arXiv1102.3421
Cox, J. P., 1980, *Theory of Stellar Pulsation*, (Princeton University Press)
Cutler, C & Lindblom, L., 1987, ApJ, 314, 234
DeGrasse Tyson, N. & Soter S., 2001, *Cosmic Horizons: Astronomy at the Cutting Edge*, (The new press)
Donnelly, R. J., 1991, *Quantized Vortices in Helium, Vol. II*, (Cambridge University Press)
Douchin, F. & Haensel, P., 2001, A&A, 380, 151D
Duncan, R. C. & Thompson, C., 1992, ApJ, 392L, 9D
Duncan, R. C., 1998, ApJ Letters, 498, 45
Easson, I. & Pethick, C. J., 1977, Phys. Rev. D., 16, 265
Easson, I. & Pethick, C. J., 1979, ApJ, 227, 995
Evans, W. D. et al., 1980, ApJ, 237L, 7E
Flowers, E. & Itoh, N., 1979, ApJ, 230, 847
Friedman, J. L. & Schutz, B. F., 1978, ApJ, 222, 881
Gabler, M., Cerdá Durán, P., Font, J. A., Müller, E. & Stergioulas, N., 2011a, MNRAS, 410L, 37G
Gabler, M., Cerdá Durán, P., Stergioulas, N., Font, J. A. & Müller, E., 2011b, arXiv: 1109.6233 [astro-ph]
Gill, R. & Heyl, J. S., 2010, MNRAS, 407, 1926
Glaberson, W. I., Johnson, W. W. & Ostermeier, R. M., 1974, Phys. Rev. Lett., 33, 1197
Glampedakis, K., Samuelsson, L. & Andersson, N., 2006, MNRAS, 371, L74
Glampedakis, K., Andersson, N. & Jones, D. I., 2007, Phys. Rev. Lett., 100h1101G (GAJ1)
Glampedakis, K., Andersson, N. & Jones, D. I., 2009, MNRAS, 394, 1908G (GAJ2)
Goedbloed, J. P. & Poedts, S., 2004, *Principles of Magnetohydrodynamics*,

(Cambridge University Press)
Goldreich, P. & Reisenegger, A., 1992, ApJ, 395, 250G
Gruzinov, A., 2008a, arXiv: 0801.4032 [astro-ph]
Gruzinov, A., 2008b, arXiv: 0812.1570 [astro-ph]
Gruzinov, A., 2009, arXiv: 0905.0911 [astro-ph]
Haensel P. & Pichon, B., 1994, A&A, 283, 313
Haensel P. & Potekhin A. Y., 2004, A&A, 428, 191
Haensel P., Potekhin A. Y. & Yakovlev D. G., 2007. *Neutron Stars 1: Equation of State and Structure*, (New York: Springer)
Hall, H. E. & Vinen, W. F., 1956, Proc. R. Soc. Lond., A238, 204
Hollweg, J. V., 1987, ApJ, 312, 880
http://www.physics.mcgill.ca/∼pulsar/magnetar/main.html
Hurley K. et al., 1999, Nature, 397, 41
Hurley K. et al., 2005, Nature, 434, 1098
Ionson, J. A. 1978, ApJ, 226, 650
Israel G. L. et al., 2005, ApJ, 628, L53
Jackson, J. D., 1998, *Classical Electrodynamics*, 3rd edition, (Wiley)
Kalmus, P., Cannon, K. C., Marka, S. & Owen, B., 2009, Phys. Rev. D, 80, 042001
Karlovini, M. & Samuelsson, L., 2007, CQGra, 24, 3171K
Kashiyama, K. & Ioka, K., 2011, Phys. Rev. D, 83h1302K
Kinney, J. B. & Mendell, G., 2003, Phys. Rev. D., 67b4032
Kirshner, R. P., 2002, *The Extravagant Universe*, (Princeton science library)
Kouveliotou, C., et al., 1999, ApJ, 510L, 115K
Landau, L. D., 1932, Phys. Z. Sowjetunion 1: 285-288
Landau, L. D., 1938, Nature, 141, 333L
Landau, L. D. & Lifshitz, E. M., 1976, *Mechanics*, (Pergamon press)
Lander, S. K. & Jones, D. I., 2011a, MNRAS, 412, 1394L
Lander, S. K. & Jones, D. I., 2011b, MNRAS, 412, 1730L
Laros et al., 1987, ApJ, 320, L111
Lee, U., 2008, MNRAS, 385, 2069
Levin, Y., 1998, Phys. Rev. D., 57, 659
Levin, Y., 2006, MNRAS Letters, 368, 35 (L06)

Levin, Y., 2006, MNRAS Letters, 410, 37
Levin, Y., 2007, MNRAS, 357, 159 (L07)
Levin, Y. & D'Angelo, C., 2004, ApJ, 6163, 1157
Levin, Y. & van Hoven, M.B., 2011, MNRAS, 418, 659
Link, B., 2003, Phys. Rev. Lett., 91, 101101
Link, B., 2007, Ap&SS, 308, 435
Lorimer, D. R. & Kramer, M., 2004, *Handbook of Pulsar Astronomy*, (Cambridge University Press)
Lyutikov, M., 2003, MNRAS, 346, 540
Lyutikov, M., 2006, MNRAS, 367, 1594
Mastrano, A., Melatos, A., Reisenegger, A. & Akgün, T., 2011, MNRAS, tmp, 1462M
Mazets E. P., Golenetskii S. V., Ilinskii V. N., Aptekar R. L. & Guryan I. A., 1979, Nature, 282, 587
Mazets, E. P. & Golenetskii, S. V.,1981, Ap&SS, 75, 47
Mendell, G., 1991, ApJ, 380, 515
Mendell, G., 2001, Phys. Rev. D., 64d4009
Melatos, A. & Peralta, C., 2007, ApJ Letters, 662, 99
Mereghetti S., 2008, Astron. Astrophys. Rev., 15, 225
Misner, C. W., Thorne, K. S. & Wheeler, J. A., 1973, *Gravitation*, (W.H. Freeman & Co., San Francisco)
Paczyński, B., 1992, Acta Astron., 42, 145
Palmer, D. M., et al., 2005, Nature, 434, 1107
Pavlov, G. G., Sanwal, D. & Teter, M. A., 2004, IAUS, 218, 239P
Pedlosky, J., 1979, *Geophysical fluid dynamics*, (New York, Springer)
Peralta, C., Melatos, A., Giacobello, M. & Ooi, A., 2005, ApJ, 635, 1224 (PMGO5)
Peralta, C., Melatos, A., Giacobello, M. & Ooi, A., 2006, ApJ, 651, 1079 (PMGO6)
Piro, A., 2005, ApJ, 634, L153
Poedts, S., Hermans, D. & Goossens, M., 1985, A&A, 151, 16 (P85)
Rasetti, F., 1929, Nature, 124, 792R
Reisenegger, A. & Goldreich, P., 1992, ApJ, 395, 250

Ruderman, M., Zhu, T. & Chen, K., 1998, ApJ, 492, 267
Samuelsson, L. & Andersson, N., 2007, MNRAS, 374, 256S
Schumaker, B. L. & Thorne, K. S., 1983, MNRAS, 203, 457S
Sedrakian, A., Wasserman, I. & Cordes, J.M., 1999, ApJ, 524, 341
Sidery, T., Andersson, N. & Comer, G. L., 2008, MNRAS, 385, 335S (SAG)
Shaham, J., 1977, ApJ, 214, 251
Shapiro, S.L. & Teukolsky, S.A., 1983, *Black holes, white dwarfs, and neutron stars: the physics of compact objects*, (New York, Wiley-Interscience)
Sotani, H., Kokkotas, K. D. & Stergioulas, N., 2007, MNRAS, 375, 261S
Sotani, H., Kokkotas, K. D. & Stergioulas, N., 2008, MNRAS Letters, 385, 5
Sotani, H. & Kokkotas, K. D., 2009, MNRAS, 395, 1163
Spitkovsky, A., 2006, ApJ, 648L, 51S
Steiner W. & Watts A. L., 2009, Phys. Rev. Letters, 103r1101S
Strohmayer, T.E. & Watts, A.L., 2005, ApJ, 632, L111
Strohmayer, T.E. & Watts, A.L., 2006, ApJ, 653, 594
Thompson, C. & Duncan, R. C., 1993, ApJ, 408, 194
Thompson, C. & Duncan, R.C., 1995, MNRAS, 275, 255
Thompson, C. & Duncan, R. C., 2001, ApJ, 561, 980
Thompson, C., Lyutikov, M. & Kulkarni, S. R., 2002, ApJ, 574, 332
Unno, W., Osaki, Y., Ando, H., Saio, H. & Shibahashi, H., 1989, *Non-radial Oscillations of Stars*, (University of Tokyo Press, Tokyo)
Usov, V. V., 1992, Nature, 357, 472
van Hoven, M.B. & Levin, Y., 2008, MNRAS, 391, 283
van Hoven, M.B. & Levin, Y., 2011a, MNRAS, 410, 1036V (vHL11)
van Hoven, M.B. & Levin, Y., 2011b, ArXiv:1110.2107v1
Watts, A. L. & Strohmayer T. E., 2006, ApJ, 637, L117
Watts, A. L. & Reddy, S., 2007, MNRAS Letters, 379, 63
Woods P. M. & Thompson C., 2006, *Soft gamma repeaters and anomalous X-ray pulsars: magnetar candidates*, (Cambridge University Press)

Nederlandstalige samenvatting

Het proefschrift dat u in handen hebt, bevat de resultaten van een promotieonderzoek in de sterrenkunde dat de afgelopen vierenhalf jaar heeft plaatsgevonden aan de Universiteit van Leiden. De basis van het werk dat in dit boek wordt gepresenteerd, bestaat uit een viertal gepubliceerde wetenschappelijke artikelen met als gemeenschappelijk onderwerp de *seismologie van magnetars*. De hoofdstukken 1, 2, 3 en 4 in dit boek zijn geheel of deels op deze artikelen gebaseerd.

Omdat het voor de niet-specialistische lezer geheel onduidelijk kan zijn wat er nu precies wordt bedoeld met 'seismologie van magnetars', volgt er in deze Nederlandstalige samenvatting een uitgebreide uitleg over dit onderwerp. In het kort is 'seismologie van magnetars' te vertalen als: de wetenschap van trillingen of bevingen van zeer sterk magnetische neutronensterren. De ervaring leert dat een dergelijke beschrijving meer vragen oproept dan beantwoordt, bijvoorbeeld: wat zijn neutronensterren? of: waarom zou je trillingen bestuderen? In de praktijk blijkt het moeilijk, zo niet onmogelijk te zijn om op dergelijke vragen korte én begrijpelijke antwoorden te geven. Op de vraag wat neutronensterren nu eigenlijk zijn, zou een antwoord bestaande uit enkele regels immers even onbevredigend als incompleet zijn. Aan de andere kant zou een complete uitleg van het onderwerp een onredelijke hoeveelheid kennis van de fundamentele natuur- en wiskunde vereisen. Om deze redenen beperken we ons tot de grote lijnen, ten koste van de vele details. Daarom vervolgen we in de geest van Einstein: "Zo eenvoudig mogelijk, maar niet eenvoudiger!"

Om het een en ander in het juiste perspectief te plaatsen, wordt eerst een beeld geschetst van het universum zoals dat bestaat in de huidige wetenschap. Vervolgens komen sterren ter sprake, met de nadruk op de levensloop en dood van sterren en de daaruit volgende geboorte van neutronensterren. Hierna wordt gesproken over neutronensterren en magnetars, en komt de inhoud van dit proefschrift specifieker aan bod.

Het heelal in een notendop

Ons beeld van de hemel op een willekeurige heldere nacht wordt gedomineerd door enkele duizenden gloeiende gasbollen die we met het blote oog kunnen onderscheiden. Deze schijnbaar statische constellatie van sterren aan de nachthemel vormt in werkelijkheid niet meer dan een kleine selectie 'nabije' buren van onze Zon. Dat wil zeggen, nabij in vergelijking tot andere sterren en sterrenstelsels in het heelal. Afstanden zijn immers relatief wanneer men bedenkt dat zelfs onze meest nabije buur, de ster α Centauri, bijna 300.000 maal verder weg staat dan onze eigen Zon, terwijl de Zon alweer zo'n 400 maal verder weg staat dan de Maan (zie tabel 1). Als men zich de beide sterren, α Centauri en de Zon, voorstelt als golfballetjes en men plaatst de Zon in Nederland, zal α Centauri in de buurt van de Franse Riviera te vinden zijn. Het opmerkelijke is dat de gigantische ruimte die zich tussen deze en andere sterren bevindt, vrijwel helemaal leeg is. Zou men, ware het mogelijk, van ster naar ster reizen, dan zou men niets maar dan ook niets tegenkomen dan lege ruimte.

Wie in een donkere, heldere nacht goed naar de hemel kijkt, ontdekt een vage, lichtende band die zich uitstrekt van horizon tot horizon. Dit is de Melkweg, een verzameling van enkele honderden miljarden sterren waarvan de Zon deel uitmaakt, in de vorm van een reusachtige pannenkoek. De afstanden zijn enorm; doet het licht van de Zon er overdag zo'n acht minuten over om ons te bereiken, het licht van een gemiddelde ster in de Melkweg is tienduizenden jaren onderweg om uiteindelijk een beeld op ons netvlies te vormen. Alhoe-

Tabel 1: *Astronomische afstanden*

object, afstand in:	kilometers	astronomische eenheden	lichtjaren
Maan	384.000	$0,0026$	$4,1 \times 10^{-8}$
Zon	$1,5 \times 10^{8}$	1	$1,6 \times 10^{-5}$
Saturnus	$1,4 \times 10^{9}$	9,5	$1,5 \times 10^{-4}$
α Centauri (dichtstbijzijnde ster na de Zon)	$4,1 \times 10^{13}$	270.000	4,3
Sagittarius A* (centrum van de Melkweg)	$2,6 \times 10^{17}$	$1,7 \times 10^{9}$	27.000
Andromeda (naburig sterrenstelsel)	$2,1 \times 10^{19}$	$1,4 \times 10^{11}$	$2,2 \times 10^{6}$
Virgo (nabij cluster van sterrenstelsels)	$4,8 \times 10^{20}$	$3,2 \times 10^{12}$	$5,1 \times 10^{7}$
Verst verwijderde objecten	$1,3 \times 10^{23}$	$8,7 \times 10^{14}$	$13,7 \times 10^{9}$

Tabel 1: *De afstanden tot verschillende objecten in het heelal in verschillende eenheden. Een astronomische eenheid (*AE*) komt overeen met de afstand van de Aarde tot de Zon. Een lichtjaar is de afstand die het licht in één jaar aflegt (licht plant zich voort met een snelheid van zo'n 300.000 kilometer per seconde). Om de leesbaarheid te bevorderen, hebben we de getallen gegeven in machten van 10, bijvoorbeeld:* 10^6 *is gelijk aan een 1 met 6 nullen, ofwel een miljoen. En* 10^{-5} *betekent 1 gedeeld door* 10^5*, ofwel éénhonderdduizendste.*

wel een aanblik van de sterrenhemel anders doet vermoeden, is dit geheel van hemellichamen allesbehalve statisch. De onderlinge gravitatie tussen de sterren in de Melkweg maakt dat zij voortdurend in beweging zijn en gemiddeld met zo'n tweehonderd kilometer per seconde rondom het centrum van de schijf snellen. Als we een kleine honderdduizend jaar de tijd hadden, zouden we de sterren ten opzichte van elkaar langzaam van positie zien veranderen. Dit dy-

namische stelsel van sterren staat niet op zichzelf, maar vormt op zijn beurt samen met enkele tientallen naburige melkwegstelsels (of sterrenstelsels) een groep waarvan de leden onderling zwaartekracht op elkaar uitoefenen. Een van deze naaste buren, de Andromedanevel, bevindt zich zelfs op ramkoers met de Melkweg, de verwachting is dat deze twee stelsels over enkele honderden miljoenen jaren op ruwe wijze met elkaar zullen versmelten om zo uiteindelijk één groot systeem van sterren te vormen. De mogelijkheid dat daarbij de Zon in botsing zou komen met een andere ster is overigens vrijwel uitgesloten; gezien de enorme leegte waarin de relatief minuscule sterren zich bevinden, is de kans nihil dat individuele hemellichamen fysiek met elkaar in aanraking komen.

Interacties tussen sterrenstelsels zoals de Melkweg en Andromeda zijn daarentegen een veelvoorkomend fenomeen. Naar welke uithoek aan de hemel we de telescoop ook richten, als we goed genoeg kijken, vinden we er sterrenstelsels in diverse soorten en maten, vele daarvan verwikkeld in een sierlijke dans met hun naaste buren. Deze complexe dynamiek is het gevolg van het feit dat de materie op deze kosmische schaal de neiging heeft om samen te klonteren. De structuur van het heelal is dientengevolge verre van gelijkmatig, maar heeft eerder iets weg van een spons. Holle leegtes van vele miljoenen lichtjaren in doorsnede worden omgeven door een fijnmazig web van filamenten en clusters bestaande uit soms duizenden sterrenstelsels.

Wanneer we verder uitzoomen, krijgen we een overzicht van het gehele voor ons zichtbare heelal. Op deze schaal is de materie, bestaande uit clusters en filamenten, zeer gelijkmatig verdeeld; het lijkt erop dat er geen structuur in de vorm van verdichtingen en leegtes te vinden is. Het opmerkelijke hierbij is dat, alhoewel clusters en filamenten zich lijken samen te trekken onder invloed van de zwaartekracht, de structuur op de allergrootste schaal een tegenovergestelde trend vertoont. Ver verwijderde sterrenstelsels blijken van elkaar af te bewegen in plaats van naar elkaar toe getrokken te worden, met een snelheid die groter is naarmate de stelsels verder van elkaar verwijderd zijn: het heelal dijt uit als een ballon die opgeblazen wordt. Ver verwijderde sterrenstelsels moeten zich dus in het verleden dichter bij elkaar bevonden



Figuur 1: *Sterrenstelsels in verschillende soorten en maten in het cluster Abell S0740, op een afstand van zo'n 460 miljoen lichtjaar van de Aarde. Op enkele sterren na die zich op de voorgrond bevinden, zijn alle objecten in dit plaatje sterrenstelsels. Het grote, eivormige stelsel bestaat uit honderden miljarden sterren en heeft een doorsnede van ongeveer 100.000 lichtjaar. (NASA, ESA, and The Hubble Heritage Team (STScI/AURA))*

hebben. Wie in gedachten de tijd 13,7 miljard jaar terugdraait, komt op een punt waarop de ruimte zich in een toestand van onnoemelijke massadichtheid en temperatuur bevindt en in explosief tempo expandeert. Dit is het moment waar het heelal zijn oorsprong vond en het spoor dat deze gewelddadige geboorte naliet, is tot op heden meetbaar als een gelijkmatig aan de hemel verdeelde warme nagloed.

Hoe het heelal zich in de loop der geschiedenis heeft ontwikkeld tot wat wij er nu van waarnemen, blijft een onderwerp van voortdurend wetenschappelijk onderzoek. Aan de basis van dit vraagstuk ligt echter vaak de zoektocht naar inzicht in de fundamentele eigenschappen van de natuur. Wat is het karakter van ruimte en tijd? Wat is de aard van de verschillende fundamentele natuurkrachten? Hoe gedraagt materie zich onder de extreme omstandigheden die zich voordoen in het heelal? Om op dergelijke vragen antwoorden te vinden,

zijn astronomische waarnemingen, naast vele natuurkundige laboratoriumexperimenten, een onontbeerlijke bron van kennis en inzicht. De sterrenhemel biedt in veel gevallen omstandigheden die men in het laboratorium onmogelijk kan nabootsen. Zo zijn er sterren met extreme gravitatievelden, processen met extreme temperaturen, explosies met extreme energieën, objecten met extreme magnetische velden en ga zo maar door. We zullen zien dat het in dit proefschrift uitvoerig besproken object, een type neutronenster dat we magnetar noemen, ook in deze categorie van extreme objecten valt.

Het leven en sterven van een ster

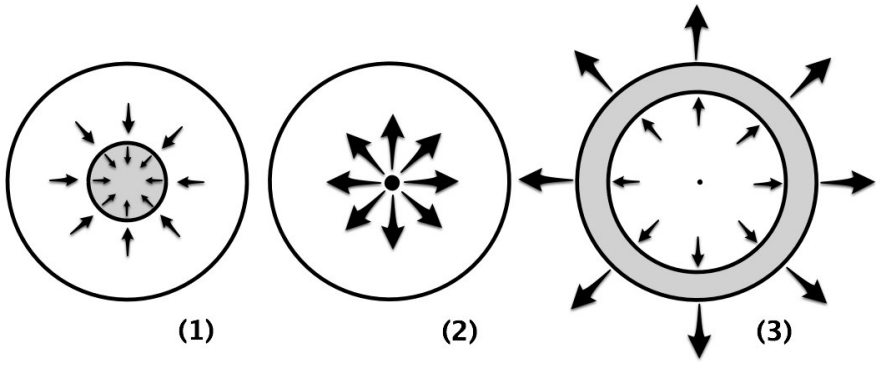
Wat sterren onderscheidt van andere hemellichamen zoals planeten, asteroïden of kometen, is dat sterren door de buitengewoon hoge druk en temperatuur in hun binnenste, spontaan tot verbranding komen. Het extreme klimaat dat zich in het binnenste van sterren voordoet, is het directe gevolg van de grote hoeveelheid massa waar zij uit bestaan. Een doorsnee ster zoals de Zon, is niets minder dan een ophoping van enkele honderdduizenden aardmassa's aan gas, bijeengehouden door de zwaartekracht die zij op zichzelf uitoefent. Ware het mogelijk een duik naar het binnenste van de Zon te maken, dan zou men, op zo'n zevenhonderdduizend kilometer diepte, aankomen in een gebied waar niet alleen een verzengende temperatuur heerst van ruim vijftien miljoen graden Celsius, maar ook een druk waarbij iedere vingertop verpletterd zou worden onder een gewicht vergelijkbaar met dat van vijftig miljoen volwassen Afrikaanse olifanten. Hier, in het centrum van de Zon, zijn de omstandigheden zodanig dat individuele deeltjes, voornamelijk atoomkernen van het element waterstof, met elkaar versmelten om het zwaardere element helium te vormen. Deze verbranding door *kernfusie* is, in tegenstelling tot de verbranding die we kennen van het openhaardvuur, niet van chemische aard, maar van nucleaire aard. De energieopbrengst van deze nucleaire verbranding verhoudt zich dientengevolge tot die van een alledaagse verbranding, als een atoombom zich verhoudt tot dynamiet. Het is deze nucleaire energie die de Zon uiteindelijk uitstraalt in de vorm van licht. En tegelijkertijd levert deze

energie de druk die ervoor zorgt dat de Zon niet bezwijkt onder haar eigen gewicht. Wanneer na enkele miljarden jaren het moment komt waarop alle waterstof in het centrum van de Zon is opgebrand en omgevormd tot helium, zal haar binnenste inkrimpen onder het grote gewicht van alle bovenliggende massa. Als gevolg van de verhoogde druk die zo ontstaat, stijgt vervolgens de temperatuur weer, totdat deze een hoogte bereikt die toestaat dat heliumkernen met elkaar fuseren om zodoende wederom energie vrij te maken en het nog zwaardere element koolstof te vormen. Dergelijke opeenvolging van cycli, waarbij nucleaire reacties in het interne van de ster geleidelijk steeds zwaardere elementen vormen, is karakteristiek voor de levensloop van sterren. Voor de Zon echter leidt de episode van heliumverbranding het eindstadium van haar bestaan in. Haar buitendelen expanderen totdat de planeten Mercurius en Venus zijn verzwolgen onder haar oppervlak en de Aarde veranderd is in een gloeiend hete, verschroeide woestijn. Hierna krimpt de Zon geleidelijk terwijl zij als een nachtkaars uitgaat.

Voor sterren die een aantal maal massiever zijn dan de Zon, betekent de vorming van koolstof echter niet het einde, maar gaat de verbranding van de elementen in onheilspellend tempo door totdat er ijzer gevormd wordt. Elementen zwaarder dan ijzer hebben de ongunstige eigenschap dat hun vorming uit lichtere elementen energie kost, in plaats van energie oplevert. Met andere woorden: ijzer is het as van de nucleaire verbranding, de brandstof is op! Het onvermijdelijke effect is dat, binnen enkele dagen (!) nadat zich ijzer begint te vormen in de sterkern, er niet voldoende energie meer geleverd wordt om de ster te behoeden voor instorting onder zijn eigen gewicht. Het gevolg is een catastrofe van ongeëvenaarde proporties.

Tijdens de implosie, die zich voltrekt in een fractie van een seconde, worden de nucleaire bestanddelen van ijzer en andere aanwezige elementen rap omgezet in neutronen en neutrino's.[1] De hoeveelheid energie die gedragen wordt door neutrino's is equivalent aan 10^{32} Hiroshima-bommen (een 1 met

[1] Neutronen vormen samen met (positief geladen) protonen de bestanddelen van atoomkernen. Deze atoomkernen worden omgeven door een gas van (negatief geladen) elektronen. Wanneer, tijdens de implosie van de sterkern, de verschillende deeltjes met grote kracht samengeperst worden, beginnen de protonen in de atoomkernen elektronen in te vangen. Bij deze reactie komen deeltjes vrij die neutronen en neutrino's genoemd worden.



Figuur 2: *Schematische weergave van de opeenvolgende gebeurtenissen in een ster tijdens de eerste paar seconden van een supernova.* (**1**) *Onder het gewicht van de bovenliggende massa begint de kern van de ster (grijs) te imploderen.* (**2**) *Tijdens de implosie worden neutronen en neutrino's gevormd. De neutronen zijn zeer massief en hopen zich op in de kern (zwarte stip), de lichte neutrino's (pijlen) bewegen met hoge snelheid naar buiten.* (**3**) *De buitenliggende lagen van de ster (grijs) worden door de hoog energetische neutrino's versneld en worden op deze manier met een explosieve schok verstoten. In het centrum blijft een neutronenster over (stipje).*

32 nullen). Neutrino's zijn elementaire deeltjes die weinig interactie hebben met hun omgeving en daardoor gemakkelijk aan de imploderende kern van de ster kunnen ontkomen. Op hun weg naar buiten echter, geven deze neutrino's een fractie van hun energie af aan buiten liggende schillen van de ster, wat voldoende is om deze op explosieve wijze te verstoten; het begin van een van de krachtigste explosies in het heelal, een supernova. De restanten van wat ooit de buitenlagen van een massieve ster waren, worden met hoge snelheid de ruimte ingeschoten en verrijken zodoende het interstellaire medium met alle 'zware' chemische elementen die de ster in zijn verbranding produceerde.[1] Terwijl de buitendelen van de ster gedurende deze fractie van een seconde tot hoge snelheid versneld worden, komt de implosie van de sterkern, die inmiddels

[1] De vele elementen waaronder zuurstof, stikstof en koolstof, die op Aarde zo prominent aanwezig zijn en het leven mogelijk maken, zijn alle afkomstig uit zware sterren die, lang voordat ons zonnestelsel zich vormde, explodeerden. Ons eigen lichaam, dat opgebouwd is uit deze chemische elementen, is dus in de letterlijke zin van het woord sterrenstof.

voornamelijk uit neutronen bestaat, abrupt tot een einde. De massadichtheid van de sterkern is op dat moment zo hoog opgelopen, dat individuele neutronen met elkaar in aanraking komen, waardoor verdere instorting een halt wordt toegeroepen.[1] Met een grote schok komt de invallende materie tot stilstand; de geboorte van een neutronenster (zie figuur 2 voor een schematische weergave van de opeenvolgende gebeurtenissen tijdens de vorming van een neutronenster).



Figuur 3: *Het restant van de supernova N49 in de Grote Magellaanse Wolk, op een afstand van 170.000 lichtjaar. De zichtbare structuur bestaat uit heet gas dat afkomstig is van een massieve ster die aan het eind van zijn leven explodeerde, ongeveer 5.000 jaar geleden. De ingestorte sterkern heeft zich gevormd tot een extreem magnetische neutronenster; een magnetar met de naam 'SGR 0526-66'. (NASA, ESA, and The Hubble Heritage Team (STScI/AURA))*

[1] Hier wordt de vorming van een neutronenster bescheven. Bij een implosie van nog zwaardere sterren is de instorting niet te stoppen. In dat geval wordt er een zwart gat gevormd; een object waar zelfs het licht niet aan de zwaartekracht kan ontsnappen.

Neutronensterren

De geïmplodeerde sterkern, die voornamelijk bestaat uit neutronen, is een bol met een doorsnede van niet meer dan 25 kilometer. Alhoewel de grootte van een neutronenster naar astronomische maatstaven minuscuul genoemd kan worden, is de hoeveelheid massa binnen deze kleine ruimte bijna anderhalf maal zo groot als die van onze Zon. De zwaartekracht op het oppervlak van de ster is bijgevolg zo intens, dat men er verpletterd zou worden onder zijn of haar eigen gewicht, dat ter plekke meer dan honderd miljard maal zo hoog is als op Aarde. Het komt erop neer dat de materie van een neutronenster zó sterk is samengeperst door de zwaartekracht, dat een brok ter grootte van een suikerklontje ongeveer zoveel massa bevat als de gehele menselijke wereldbevolking.

Gegeven de zeer kleine afmetingen van neutronensterren zou men kunnen verwachten dat het buitengewoon moeilijk moet zijn om deze objecten met een telescoop te observeren. Immers, het waarnemen van een neutronenster op een afstand van zo'n 1.000 lichtjaar (wat relatief dichtbij is) is vergelijkbaar met het waarnemen van een enkele zandkorrel op de planeet Mars! Om deze reden achtten de meeste astronomen het, tot zo'n vijfenveertig jaar geleden, onmogelijk om ooit een neutronenster te observeren. Dit veranderde in 1967 toen Jocelyn Bell, promovenda aan de Universiteit van Cambridge, een opmerkelijke ontdekking deed. Met behulp van een primitieve radiotelescoop vond Bell een bron aan de hemel die iedere 1,3 seconden een korte puls van radiostraling uitzond. Omdat het pulseren zó regelmatig was, en omdat een dergelijk fenomeen onbekend was in de sterrenkunde, dachten Bell en haar promotiebegeleider Anthony Hewish in eerste instantie dat het signaal veroorzaakt werd door lokale radiozenders of andere storende invloeden. Toen na herhaalde experimenten het signaal aanwezig bleef, werd het duidelijk dat de pulserende bron daadwerkelijk een kosmische oorsprong had. Na de bekendmaking van het nieuwe en raadselachtige object, door Hewish 'pulsar' genoemd, gingen sterrenkundigen koortsachtig op zoek naar mogelijke verklaringen voor het fenomeen. In eerste instantie werd zelfs de mogelijkheid van buitenaards leven ('little green men') geopperd, maar al vrij snel werd het overduidelijk dat de bron een neutronenster moest zijn die werkte als een soort

vuurtoren; de ster zond een smalle bundel licht uit, die iedere 1,3 seconden dat de ster een wenteling om zijn as maakte, even in de richting van de Aarde scheen. Direct na de ontdekking van Bell begonnen andere onderzoeksgroepen pulserende radiobronnen te zoeken, en vonden sterren die in duizelingwekkend tempo pulseerden, sommige zelfs enkele honderden malen per seconde.[1]

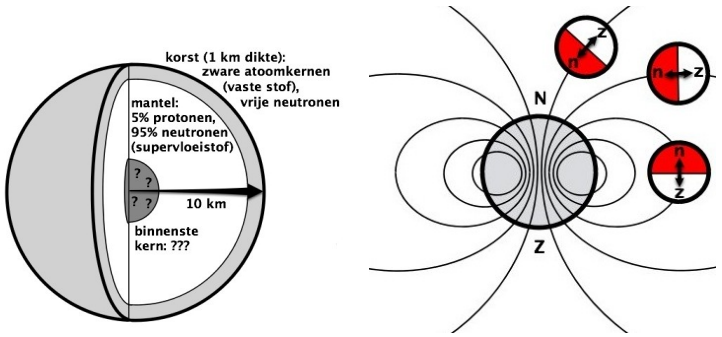
Eén van de overtuigende argumenten dat pulsars inderdaad neutronensterren moeten zijn, is de hoge rotatiesnelheid die afgeleid wordt uit de waargenomen pulsen. Men kan zich voorstellen dat op een object dat snel om zijn as draait, enorme middelpuntvliedende krachten (centrifugaalkrachten) werken. Deze krachten, die de massa van een roterende ster naar buiten willen slingeren[2], moeten tegengewerkt worden door de aantrekkende werking van de zwaartekracht. Als de zwaartekracht van een ster niet sterk genoeg is, vliegt de ster simpelweg uit elkaar. Om deze reden kan een ster als onze Zon nooit of te nimmer sneller om zijn as draaien dan zo'n één rotatie per halfuur.[3] Het feit dat pulsars zich honderden malen per seconden om hun as wentelen, betekent dus dat we te maken hebben met een object dat een geweldig sterke zwaartekracht moet hebben. Daarbij komt dat de hoge rotatiesnelheid direct verklaard kan worden met de catastrofale implosie waaruit neutronensterren worden gevormd. Dit effect wordt wel *de wet van behoud van impulsmoment* genoemd, en het werkt als volgt: zoals de meeste hemellichamen, beweegt de ster vóór de implosie langzaam om zijn as. Wanneer de ster aan het einde van zijn leven implodeert, begint deze sneller te roteren naargelang zijn massa meer en meer naar binnen valt. Dit is vergelijkbaar met de manier waarop een ijsdanseres haar pirouette versnelt door massa (armen en benen) naar binnen te trekken. Het verschil met de ijsdanseres is echter dat de massa van een imploderende sterkern zó sterk geconcentreerd raakt in het centrum, dat de rotatiesnelheid bij de geboorte van een neutronenster kan oplopen tot enkele

[1] In 1974 ontving Bell's promotiebegeleider Anthony Hewish, samen met Sir Martin Ryle van de Universiteit van Cambridge, de Nobelprijs voor de ontdekking van de eerste pulsar. Het feit dat Jocelyn Bell niet meedeelde in de prijs zorgde begrijpelijkerwijs voor enige publieke opschudding.

[2] Via hetzelfde principe werkt een centrifuge of een wasmachine. Hoe sneller de trommel roteert, hoe krachtiger de inhoud naar buiten geslingerd wordt.

[3] Hetzelfde argument geldt ook voor de Aarde. De rotatieperiode van de Aarde (een dag) zou in theorie nooit lager kunnen worden dan ongeveer 13 minuten. Bij een snellere rotatie zou de centrifugaalkracht sterker worden dan de zwaartekracht, en de Aarde zou in losse stukken uiteen vliegen.

honderden omwentelingen per seconde.



Figuur 4: *Schematische weergaven van een neutronenster. Het linkerplaatje laat een dwarsdoorsnede van een neutronenster zien, met de bijbehorende afmeting en chemische samenstelling. Over de samenstelling van het binnenste deel van de kern (donkergrijs) bestaat onzekerheid. Het rechterplaatje laat een (sterk vereenvoudigd) magnetisch veld zien. De gekromde lijnen geven de magnetische veldlijnen weer. Hoe dichter de lijnen bij elkaar staan, hoe sterker het magnetisch veld. Men zou in theorie de richting van de veldlijnen kunnen bepalen met een kompas; de kompasnaald staat altijd parallel aan het magnetisch veld.*

Sinds de ontdekking van pulsars zijn neutronensterren niet meer weg te denken uit de astronomie. Hun extreme fysische eigenschappen zoals de enorme massadichtheden en zwaartekracht, maken dat deze objecten een fundamenteel puzzelstuk vormen in de ontwikkeling van ons begrip van de natuur. De omstandigheden die zich voordoen op deze sterren zijn niet alleen extreem, maar ook uniek in die zin dat vele verschijnselen in en rondom neutronensterren geen equivalent kennen op Aarde, en zelfs in de meest geavanceerde laboratoria niet nagebootst kunnen worden. Zo bevindt het binnenste van neutronensterren zich mogelijk in een staat van superfluïditeit; een vloeistofvorm waarin geen frictie (viscositeit) bestaat (zie figuur 4). Aan de andere kant is het waarschijnlijk dat er een veelheid aan exotische natuurkundige deeltjes voorkomt, en dat de ster zich in een staat van supergeleiding bevindt. Het leidt te ver om al deze bijzondere eigenschappen hier te bespreken, maar het moge duidelijk zijn dat er nog zeer veel te leren valt van en over deze sterren.

Magnetars

Dankzij de grote vooruitgang van astronomische waarneemtechnieken in de afgelopen decennia, is het nu mogelijk om vrijwel alle uithoeken van de hemel te observeren in vrijwel alle mogelijke soorten licht. Deze recente ontwikkelingen hebben het mogelijk gemaakt om objecten in het heelal waar te nemen die anders voor het menselijke oog altijd onzichtbaar gebleven zouden zijn.[1] Zo heeft de komst van een generatie ruimtetelescopen die gevoelig zijn voor de hoog energetische röntgen- en gammastraling er in de afgelopen jaren aan bijgedragen dat een groot aantal tot dan toe onbekende typen objecten ontdekt werd. Tot deze nieuwe ontdekkingen behoort onder meer de klasse van magnetars; neutronensterren met een zeer sterk magnetisch veld.[2] De mogelijkheid dat, onder bijzondere omstandigheden, een neutronenster geboren kan worden met een extreem sterk magnetisch veld, was in het begin van de jaren negentig al voorspeld door de theoretische astrofysici Robert Duncan en Chris Thompson. In een serie belangrijke wetenschappelijke artikelen deed het duo uitvoerig uitleg over hoe een dergelijke ster gevormd zou kunnen worden, en wat zijn fysische eigenschappen zouden zijn. Een aantal jaren bleef het idee van magnetars een puur theoretische hypothese. Maar tegen het eind van de jaren negentig begonnen de observationele bewijzen zich op te stapelen dat een tot dan toe onbegrepen klasse van röntgen- en gammabronnen, inderdaad magnetars moesten zijn. De waargenomen eigenschappen van deze objecten voldeden in vrijwel alle opzichten aan de kenmerken die Duncan en Thompson voorspeld hadden voor magnetars: (1) De sterren waren zeer helder in röntgen- en gammastraling. (2) Ze waren zeer actief, wat wil zeggen dat hun helderheid voortdurend veranderde en dat er zo nu en dan sterke uitbarstingen plaatsvonden. (3) In veel gevallen viel de locatie van deze objecten samen met die van het restant van een relatief jonge supernova (zie figuur 3). (4)

[1] Het zichtbare licht dat wij met onze ogen kunnen waarnemen, beslaat slechts een klein deel van het elektromagnetisch spectrum. Niet voor het oog zichtbaar zijn bijvoorbeeld radiostraling, infrarood, ultraviolet, röntgenstraling, gammastraling etc. Veel moderne (ruimte)telescopen zijn gevoelig voor deze 'onzichtbare' straling, en kunnen het voor ons onzichtbare heelal in kaart brengen.

[2] Alle neutronensterren hebben naar Aardse maatstaven zeer sterke magnetische velden; gemiddeld zo'n tien miljard maal sterker dan een typische koelkastmagneet. De magnetische velden van magnetars daarentegen zijn nog eens duizend maal sterker.

De sterren hadden een hele trage rotatie en leken geleidelijk aan iets trager te gaan roteren.[1]

Hoewel de meeste neutronensterren, en dus ook magnetars, geboren worden met een zeer snelle rotatie, neemt deze snelheid in de loop van hun leven geleidelijk af. De oorzaak hiervan is de aanwezigheid van een sterk magnetisch veld (zie figuur 4), dat effectief werkt als een soort rem. Hoe sterker het magnetisch veld, des te sneller zal de rotatie vertragen. Het interessante is nu, dat men met behulp van de waargenomen pulsen (zoals die van Bell en Hewish), zowel de rotatiesnelheid als de mate van afremming van de ster heel nauwkeurig kan bepalen. Met deze gegevens kan men vervolgens een zeer goede schatting maken van de sterkte van het magnetisch veld van de ster. Zodoende was de constatering dat de raadselachtige röntgenbronnen een relatief langzame rotatie hadden en bovendien in hoog tempo vertraagden, een duidelijke aanwijzing dat de objecten neutronensterren moesten zijn met extreem sterke magnetische velden. Precies zo sterk als Duncan en Thompson voorspeld hadden voor de tot dan toe hypothetische magnetars.

Magnetars zijn buitengewoon rusteloze objecten. Het intense magnetische veld in deze sterren is onderhevig aan de sterke aantrekkende en afstotende magnetische krachten die magnetars tot bijzonder dynamische en temperamentvolle sterren maken. Omdat de magnetische veldlijnen langzaam van positie veranderen, worden sterke elektrische stromen aangedreven in de *magnetosfeer*[2], waarbij intense straling vrijkomt die de ster voor onze ruimtetelescopen zichtbaar maakt als een bron van röntgenstraling. Het continue 'verschuiven' van magnetische veldlijnen laat de ster niet onberoerd. De reden hiervoor is dat de veldlijnen als het ware verankerd zijn in de vaste korst van de ster, waardoor deze een sterke trekkracht ondervindt wanneer de veldlijnen verschuiven. Omdat de korst opgebouwd is uit een sterke vaste stof, biedt het van nature veel weerstand tegen deze magnetische trekkracht. Wanneer echter in de loop der tijd de magnetische spanningen steeds sterker wor-

[1] De beschrijving van magnetars die Duncan en Thompson gaven, is een stuk langer en gedetailleerder dan de vier punten die in de tekst genoemd worden. Hun voorspellingen bleken opmerkelijk correct te zijn.

[2] Met 'magnetosfeer' wordt de ruimte buiten de ster bedoeld die gekarakteriseerd wordt door de aanwezigheid van het sterke magnetische veld van de ster.

den, bestaat de mogelijkheid dat op een gegeven moment ofwel de korst het begeeft en breekt, ofwel het magnetisch veld het begeeft, waarbij een enorme hoeveelheid energie in een krachtige klap vrijkomt.[1] Dit soort uitbarstingen is karakteristiek voor jonge magnetars, en varieert sterk in krachtigheid. De allerkrachtigste van deze evenementen kunnen de sterren letterlijk doen schudden op hun grondvesten.

Oscillaties van sterren

In het voorgaande is het een en ander opgemerkt over de inwendige structuur en processen in sterren, met name toen de levensloop van sterren besproken werd. Men kan zich echter afvragen hoe het mogelijk is om überhaupt iets te weten te komen over de interne structuur van sterren. Immers wat we van sterren waarnemen, zelfs met de meest geavanceerde telescopen, is over het algemeen niet meer dan een minuscuul lichtpuntje aan de hemel. Zelfs in het geval van onze Zon, waarvan we weliswaar een gedetailleerder beeld hebben, lijkt het onmogelijk om verder te kijken dan wat zich aan haar oppervlak laat zien; de rest ligt verborgen onder dikke lagen gloeiend gas. Als het niet mogelijk is om dwars door een ster heen te kijken, hoe kunnen we dan iets te weten komen over zijn binnenste? Het antwoord op deze vraag is tweeledig.

Allereerst is het mogelijk om puur op theoretische gronden modellen op te stellen die op basis van bekende (of veronderstelde) natuurwetten de sterstructuur beschrijven. De ingrediënten van een dergelijk model zijn wiskundige vergelijkingen die beschrijven hoe fysische eigenschappen als druk, massadichtheid en temperatuur van elkaar afhangen in de ster. Het resultaat is vaak een reeks gedetailleerde stermodellen met variërende stermassa's, die voorspellingen doen over meetbare eigenschappen van de ster, zoals de lichtkracht en

[1] Men kan zich dit voorstellen door het magnetisch veld van een magnetar te vergelijken met de strak gespannen snaren op een gitaar, en de vaste korst van de ster met de klankkast waarop de snaren bevestigd zijn. Door processen die zich in het interne van een magnetar afspelen, worden als het ware de snaren steeds strakker gespannen. Dit gaat zo geleidelijk door, totdat op een catastrofaal moment, ofwel de snaren breken, ofwel de brug op de klankkast breekt. Alle energie die men van het begin af gebruikt had om de snaren te spannen, komt er met een grote klap uit.

de temperatuur, en als zodanig aan de waarnemingen getoetst kunnen worden. De procedure is dus als volgt: men produceert een serie stermodellen van verschillende massa's en vervolgens selecteert men het model dat het best overeenkomt met de waargenomen lichtkracht en temperatuur van de ster. Dit model bevat een gedetailleerde beschrijving van de interne structuur van de ster en als bonus heeft men ook nog eens de massa bepaald. Het vraagstuk lijkt hiermee dus opgelost te zijn. Echter, het probleem met een dergelijke benadering is dat we blind hebben moeten vertrouwen op de correctheid van de theoretische aannames waarop ons stermodel berustte. We hebben deze aannames immers *zelf* niet getest. Het is bovendien niet ondenkbaar dat onze waarneming prima verklaard kan worden met een heel ander model. De vraag rijst dus: hoe testen we de correctheid van onze theorie?[1]

Tot dusver ligt het probleem erin dat we er nog niet in geslaagd zijn om op *directe* wijze de interne structuur van de ster te bepalen. Ware het mogelijk geweest om met een röntgenbril naar binnen te kijken, dan konden we bepalen of ons theoretisch model al dan niet een juiste beschrijving van de ster geeft. Helaas is het zo dat röntgenstraling noch enige andere soort van straling, ons een beeld kan geven van het binnenste van sterren.[2] Er bestaat echter een alternatieve, directe methode om de interne structuur te bestuderen. Dit is de studie van waargenomen trillingen (oscillaties) van sterren; *asteroseismologie*. Deze oscillaties, die het stellaire equivalent zijn van aardbevingen, zijn niks anders dan golven die zich door de ster voortbewegen. Afhankelijk van de trillingssnelheid (frequentie) en golflengte dringt zo'n golf dieper of minder diep door in het inwendige van de ster. Op deze manier bevat iedere trilling informatie over de structuur op een bepaalde diepte in het inwendige, en door op slimme manier deze trillingen te analyseren, is het mogelijk om op een directe manier het binnenste van sterren in kaart te brengen. Dit mag ingewikkeld klinken voor lezers die niet vertrouwd zijn met de basisprincipes van de seismologie, toch heeft iedereen hier een intuïtief begrip voor. Gaat

[1] Anders gezegd: hoe testen we de correctheid van onze ideeën over de natuur van de ster?

[2] Een uitzondering vormt straling in de vorm van neutrino's. Zoals al eerder is opgemerkt, hebben neutrino's zeer weinig interactie met andere deeltjes, waardoor de meeste neutrino's ongestoord het binnenste van de Zon kunnen verlaten. Dit betekent dat waargenomen neutrino's een direct beeld kunnen geven van de structuur in het binnenste van de Zon, maar het betekent tevens dat het zeer moeilijk is om neutrino's waar te nemen.

u maar na hoe u door met uw vinger op een wijnglas te tikken, aan de hand van het geluid kunt bepalen of de kelk uit een dikke laag glas bestaat of juist een dun laagje, of het glas vol is of leeg. Het geluid dat u hoort, is immers niets anders dan de trilling van het glas. Wanneer dus uw tafelgenoot aan de linkerzijde beweert dat uw glas leeg is, en uw tafelgenoot aan de rechterzijde meent het tegendeel, hoeft u het glas niet gezien te hebben om te bepalen of deze moet worden bijgevuld of niet. Op analoge wijze is het mogelijk om informatie af te leiden over de inhoud van sterren en over de correctheid van theorieën die sterren trachten te beschrijven.[1]

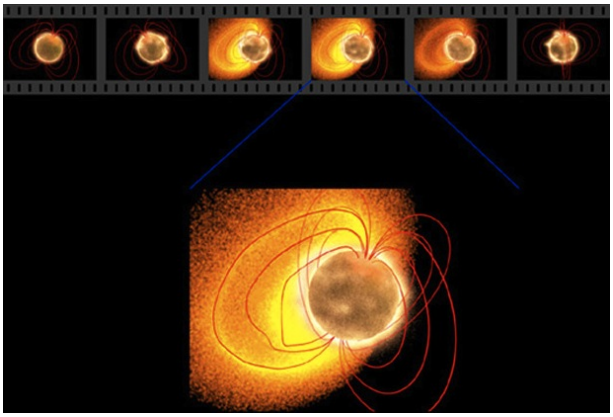
Willen we iets te weten komen over de interne structuur van een ster, of willen we onze theoretische ideeën toetsen, dan komt het er dus op aan om steroscillaties waar te nemen. En dat is in de praktijk waar de moeilijkheden beginnen. Het is immers nog maar de vraag of deze oscillaties wel aanwezig zijn, en als dat al zo is: zijn ze sterk genoeg om waargenomen te worden? Het moge duidelijk zijn dat hier een grote uitdaging ligt voor de observerende astronoom, die beperkt wordt door de gevoeligheid van zijn of haar telescoop. In sommige gevallen ligt de beperking in het feit dat bepaalde oscillaties uiterst zeldzaam zijn, zodat men simpelweg niet anders kan dan het moment afwachten dat zij zich voordoen. Dit is in het bijzonder het geval voor de trillingen van magnetars; het onderwerp van dit proefschrift.

Seismologie van magnetars

De omstandigheden waarbij magnetaroscillaties in sterke mate veroorzaakt worden, doen zich zó sporadisch voor, dat tot op heden slechts 3 gebeurtenissen zich voordeden (sinds 1979) waarbij de ster waarneembaar natrilde. Kort gezegd komt het erop neer dat, om een neutronenster zoals een magnetar te laten trillen, een gigantische kracht nodig is. Om een wijnglas te laten trillen,

[1] Een ander voorbeeld waarin het verband tussen trillingen en de fysieke eigenschappen van materie duidelijk wordt, doet zich voor bij het bespelen van een snaarinstrument zoals een gitaar. In het geval dat men een enkele snaar bespeelt, wordt de hoogte van de toon (de snelheid van de trilling) bepaald door de positie waarop de snaar wordt ingedrukt, ofwel de lengte van de snaar. Anderzijds hangt de toonhoogte af van de spanning en de massa (dikte) van de snaar.

is een tikje met de vingers voldoende en om een gong te laten trillen, is een behoorlijke klopper nodig, maar om een neutronenster te laten trillen, zijn krachten nodig die het voorstellingsvermogen te boven gaan. Zulke krachten zijn echter, zoals al eerder opgemerkt, latent aanwezig in de enorme magnetische velden van magnetars, en het is vaak slechts een kwestie van tijd totdat deze in volle hevigheid vrijkomen. Een dergelijke uitbarsting van energie werd



Figuur 5: *Een artistieke interpretatie van een magnetar giant flare. In een fractie van een seconde vormt zich een 'vuurbal' in het magnetisch veld buiten de ster. In de loop van enkele minuten dooft deze vuurbal uit. (Illustratie van Robert Mallozzi)*

waargenomen op 27 december 2004, toen een magnetar met de obscure naam *SGR 1804-20*, in een heldere flits de aarde belichtte met intense, maar voor het oog onzichtbare röntgen- en gammastraling. Deze gebeurtenis, die een *Giant Flare* (reuzenuitbarsting) genoemd wordt, was in werkelijkheid zó krachtig dat er in een fractie van een seconde meer energie vrijkwam dan de totale energie die de Zon uitstraalt in honderdduizend jaar. Gedurende enkele minuten na de uitbarsting bleef de ster helder nagloeien, waarna de stralingsintensiteit weer terugkeerde naar het niveau van voor de uitbarsting. Bij nadere inspectie van de meetgegevens van deze nagloed, bleek de intensiteit van het waargenomen licht in zeer hoog tempo te fluctueren.

Een voor de hand liggende verklaring voor dit periodieke helderder en minder helder worden van de magnetar (tientallen tot honderden malen per seconde), is dat dit verschijnsel wordt veroorzaakt door hevige trillingen in de korst van de ster, vergelijkbaar met aardbevingen op Aarde. Een belangrijke aanwijzing die dit idee bevestigt, is dat de snelheid van de helderheids-

fluctuaties, ook wel 'quasiperiodieke oscillaties' (QPO's) genoemd, vrij goed overeenkomt met de trillingssnelheid die men zou verwachten van de korst van een neutronenster. Daarbij komt, zoals we in hoofdstuk 2 van dit proefschift aantonen, dat het precies dìt soort 'korsttrillingen' zijn, waarvan men verwacht dat ze ontstaan tijdens een reuzenuitbarsting. De vraag die zich voordoet, is dus wat de quasiperiodieke oscillaties ons kunnen vertellen over de interne structuur van neutronensterren. Om deze vraag adequaat te kunnen beantwoorden, moeten we allereerst, vanuit een theoretisch standpunt, een idee hebben van de natuurkundige aard van deze trillingen. Dit is het onderwerp dat in dit proefschrift behandeld wordt. De vragen die aan bod komen, zijn onder andere:

Hoe planten golven zich voort in een supervloeistof zoals die bestaat binnen in een neutronenster? (Hoofdstuk 1) Hoe en hoe sterk trilt een magnetar na een reuzenuitbarsting? (Hoofdstuk 2) Wat is het effect van het sterke magnetische veld op de trillingen van de korst? En hoe kunnen we 'sterbevingen' van magnetars het beste simuleren? (Hoofdstukken 3 en 4) De onderwerpen van de verschillende hoofdstukken zijn hieronder kort uiteengezet.

Hoofdstuk 1: Golven in de kern van een neutronenster

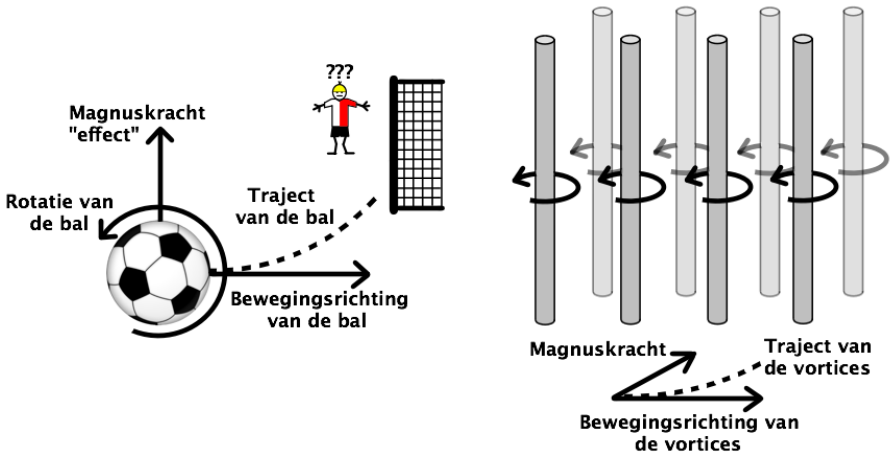
In hoofdstuk 1 wordt het fysische karakter van golven (trillingen) in de vloeibare kern van een neutronenster onder de loep genomen. Een factor die bepalend is voor de eigenschappen van een golf, is de staat waarin het medium zich bevindt. Zo gedragen golven in een vaste stof zich over het algemeen heel anders dan golven in een vloeistof of een gas.[1] Op dezelfde manier is de toestand van de materie binnen in een neutronenster bepalend voor het karakter van de golven die de ster doen trillen. Vanuit een theoretisch standpunt

[1] Een fundamenteel verschil tussen golven in een vloeistof en golven in een vaste stof, is dat een vaste stof, in tegenstelling tot een vloeistof, weerstand biedt tegen zogenaamde 'shear motion' ofwel schuifbeweging. Deze schuifbewegingen kan men zich voorstellen als auto's op de linkerrijbaan van een snelweg die auto's op de rechterrijbaan proberen in te halen. In een vaste stof zou dit 'inhalen' onmogelijk zijn, omdat de deeltjes (auto's) als het ware aan elkaar vastzitten. In een vloeistof is dit niet het geval en bewegen de deeltjes vrij langs elkaar.

verwacht men dat de neutronen in het binnenste van een neutronenster zich in een zeldzame staat van vloeibaarheid bevinden; superfluïditeit. Wat een supervloeistof bijzonder maakt ten opzichte van een normale vloeistof (zoals water), is dat het volledig vrij is van viscositeit (stroperigheid) en dat een supervloeistof als geheel niet kan roteren. Zou men, bij wijze van experiment, een supervloeistof in een theekopje proberen te roeren met een lepel, dan zou de vloeistof als geheel niet gaan roteren zoals thee dat wél zou doen. In plaats hiervan zouden diverse kleine wervelingen ontstaan, ook wel vortices (enkelvoud: vortex) genoemd, die zich verspreiden door de supervloeistof. Deze vortices kan men zich voorstellen als *microscopisch smalle tornado's* (zie figuur 6), die bestaan uit deeltjes die zich *niet* in een toestand van superfluïditeit bevinden en dus *wel* kunnen roteren. Hoe harder men vervolgens roert in het theekopje, hoe meer van dit soort vortices de kop op steken.

Het interessante is nu dat, omdat neutronensterren in het algemeen zeer snel om hun as draaien, de supervloeistof binnen in de ster gevuld is met een soort spaghetti van vortices. Om te begrijpen hoe golven zich in de ster voortplanten, moet men dus een goede beschrijving hebben van de interactie die individuele vortices hebben met elkaar en met andere deeltjes in de ster. Met name de interactie van de vortices met het magnetisch veld speelt een belangrijke rol. In hoofdstuk 1 bestuderen we het het scenario dat vortices sterk beïnvloed worden door magnetische krachten. Het magnetisch veld treedt in dat geval op als een vork die door een bak spaghetti roert: wanneer het magnetisch veld beweegt, trekt het de vortices mee. Het verschil met de slierten spaghetti echter, is dat vortices roteren als een tornado, wat ervoor zorgt dat het zogenaamde 'Magnuseffect' optreedt. Dit effect, dat ook wel bekend is in balsporten (bijvoorbeeld als 'slice' en 'topspin' in het tennis), maakt dat de vortices een sterke tegenkracht geven die vervolgens weer invloed uitoefent op het (bewegende) magnetische veld. De vraag is: hoe sterk beïnvloedt deze 'Magnuskracht' de bewegingen van het magnetisch veld? Kan het magnetisch veld vrij bewegen, of wordt het beperkt door de vortices in de supervloeistof? Ofwel: is de spaghetti stijf en zwaar, zodat het veel kracht kost om erdoorheen te roeren? Of kost dit weinig moeite?

De analyse die in hoofdstuk 1 uiteengezet wordt, wijst uit dat de boven-



Figuur 6: *Schematische weergave van het 'Magnuseffect' dat een belangrijke rol speelt in de dynamica van vortices in een supervloeistof. Het Magnuseffect is een bekend verschijnsel in balsporten. Als een voetbal (of tennisbal, golfbal etc.) geschoten wordt en daarbij een sterke rotatie meekrijgt, wordt het traject van de bal afgebogen door middel van een kracht die 'Magnuskracht' wordt genoemd (linkerplaatje). Hetzelfde effect is ook aanwezig in een supervloeistof (rechterplaatje). De vortices die een intrinsieke rotatie hebben, ondergaan een sterke Magnuskracht wanneer zij voortgestuwd worden door het magnetisch veld. De afbeelding aan de rechterzijde is een sterke vergroting van de werkelijkheid; in een magnetar is de afstand tussen individuele vortices een fractie van een millimeter.*

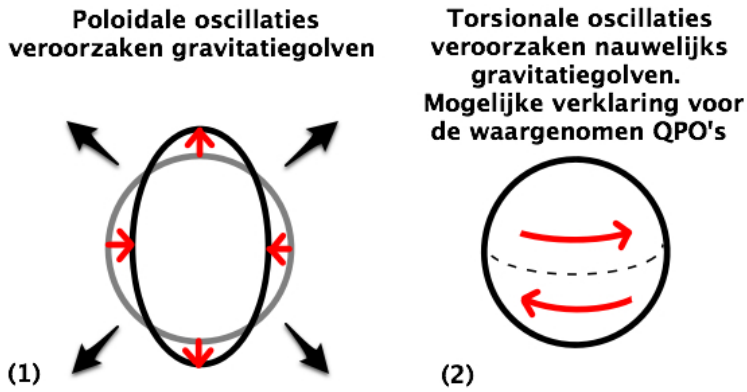
genoemde interactie afhankelijk is van de sterkte van het magnetisch veld en de rotatiesnelheid van de ster. Voor snel roterende neutronensterren kan de interactie tussen het magnetisch veld en de vortices een belangrijke rol spelen met uiteenlopende gevolgen. In het geval van een magnetar echter (zeer sterk magnetisch veld, trage rotatie) is de conclusie dat de vortices nauwelijks invloed uitoefenen op bewegingen (golven) van het magnetisch veld. Met andere woorden: de vortices geven geen noemenswaardige tegenkracht. Dit is een belangrijk resultaat met het oog op de berekeningen en simulaties die uitgevoerd en besproken worden in de volgende hoofdstukken.

Hoofdstuk 2: Het ontstaan van 'magnetarbevingen'

In hoofdstuk 2 wordt onderzocht hoe en hoe sterk verschillende soorten van sterbevingen ontstaan na reuzenuitbarstingen op magnetars. Er worden twee verschillende mechanismen beschouwd die een reuzenuitbarsting en de daaruit volgende sterbevingen (oscillaties) kunnen veroorzaken. In beide scenario's ontstaan de trillingen doordat de enorme druk- en trekkracht die het magnetisch veld al de tijd voor de uitbarsting op de ster uitoefende, plotseling wegvallen. (1) Eén mogelijkheid is dat een reuzenuitbarsting op een magnetar ontstaat ten gevolge van een enorme breuk van de korst. Zo'n breuk is het gevolg van sterke magnetische krachten die van binnenuit de ster de korst onder zúlke hoge druk zetten, dat deze in een grote klap kraakt. Net als op Aarde zou zo'n breuk van de korst gepaard gaan met zeer sterke bevingen. (2) Een tweede mogelijkheid is dat het magnetisch veld buiten de ster (dus in de magnetosfeer), eveneens door grote magnetische spanningen, instabiel wordt en plotseling 'breekt'. Zo'n gebeurtenis gaat gepaard met een enorm krachtige uitstoot van energie die de ster eveneens doet trillen. Het is overigens goed mogelijk dat beide mechanismen tegelijkertijd plaatsvinden tijdens een daadwerkelijke reuzenuitbarsting.

Een belangrijke vraag is welk soort van stertrillingen er ontstaat ten gevolge van beide scenario's. Eén van de onderliggende motivaties voor deze vraag is dat het in theorie mogelijk is om bepaalde steroscillaties in de nabije toekomst waar te kunnen nemen met behulp van 'gravitatiegolfdetectors'.[1] Sommige typen sterbevingen zijn efficiënter in het veroorzaken van gravitatiegolven dan andere. Met name de klasse van *poloïdale* oscillaties, die de ster als geheel vervormen (zie het linkerplaatje van figuur 7), zouden in theorie

[1] Gravitatiegolfdetectors zijn astronomische instrumenten die momenteel in ontwikkeling zijn. Deze detectors zijn gevoelig voor gravitatiegolven en bieden zo, naast conventionele telescopen die licht waarnemen, een totaal nieuwe manier om naar het heelal te kijken. Gravitatiegolven worden voorspeld door Einstens *algemene relativiteitstheorie* en kan men omschrijven als periodieke schommelingen van ruimte en tijd. Deze golven verplaatsen zich net als licht met de lichtsnelheid door de ruimte en zorgen ervoor dat de ruimte lokaal periodiek iets inkrimpt en dan weer uitdijt. Het effect van een gravitatiegolf op een object is dus dat zijn lengte een heel klein beetje fluctueert. Deze schommelingen kunnen in theorie gemeten worden wanneer een gravitatiegolf de Aarde passeert, maar zijn over het algemeen zeer klein en daardoor uiterst moeilijk om waar te nemen. Met de huidige ontwikkelingen (anno 2012) is te verwachten dat gravitatiegolfdetectors binnen enkele jaren gevoelig genoeg zijn om de eerste gravitatiegolven te detecteren.



Figuur 7: *Twee typen oscillaties die onderzocht worden in hoofdstuk 2. Het linkerplaatje* (**1**) *geeft de vervorming van de ster weer t.g.v. een poloïdale oscillatie. De ster wordt periodiek uitgerekt en dan weer afgeplat. Deze beweging veroorzaakt sterke fluctuaties in de ruimtetijd, die in theorie waargenomen zouden kunnen worden in de vorm van gravitatiegolven. De poloïdale oscillaties die ontstaan tijdens uitbarstingen op magnetars zijn echter te zwak om door toekomstige detectors gemeten te worden. Het rechterplaatje* (**2**) *geeft torsionale oscillaties weer. In dit voorbeeld bewegen het noordelijk en het zuidelijk halfrond periodiek in tegenovergestelde richtingen. In tegenstelling tot de poloïdale oscillaties, vervormen de torsionale oscillaties de ster niet. Ondanks het feit dat torsionale oscillaties zeer sterk zijn na een reuzenuitbarsting, veroorzaakt dit type van sterbevingen weinig gravitatiegolven en zal dus niet waarneembaar zijn voor toekomstige gravitatiegolfdetectors.*

waargenomen kunnen worden, mits deze voldoende sterk aangeslagen worden tijdens reuzenuitbarstingen. In theorie bestaat dus de mogelijkheid om seismologie van magnetars te bedrijven met behulp van gravitatiegolfdetectors. Een andere klasse van sterbevingen zijn de *torsionale* oscillaties (zie het rechterplaatje in figuur 7). Deze bevingen zijn relatief traag en laten de ster horizontaal schudden (zoals de meeste aardbevingen op Aarde). Aangezien deze oscillaties de ster niet vervormen, zijn zij inefficiënt in het voortbrengen van gravitatiegolven. Desalniettemin zijn de torsionale sterbevingen zeer interessant vanwege het feit dat hun trillingssnelheid zeer goed overeenkomt met de 'quasiperiodieke oscillaties' (QPO's) die waargenomen werden na reuzenuitbarstingen op magnetars. Het vermoeden bestaat dan ook dat deze QPO's

in werkelijkheid veroorzaakt werden door torsionale oscillaties.

De berekeningen die uitgevoerd worden in hoofdstuk 2 laten zien dat de poloïdale oscillaties van een magnetar na een reuzenuitbarsting te zwak zijn om waargenomen te worden met toekomstige gravitatiegolfdetectors. Dit is jammer, want het sluit de mogelijkheid uit om deze speciale klasse van oscillaties in de nabije toekomst te bestuderen door middel van gravitatiegolven. Dezelfde berekeningen tonen echter aan dat de torsionale oscillaties zeer sterk aangeslagen worden tijdens reuzenuitbarstingen. Dit bevestigt het vermoeden dat zij de oorsprong zijn van de waargenomen QPO's. In de hoofdstukken 3 en 4 wordt dit type van sterbevingen nader onderzocht.

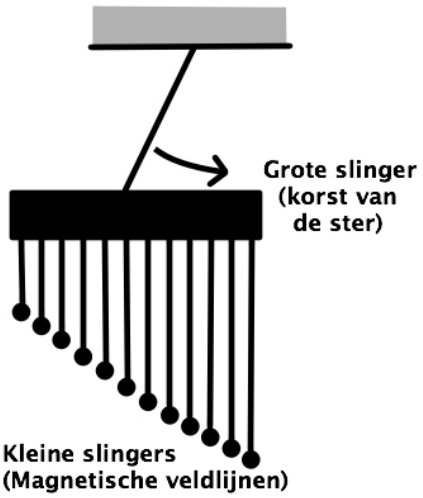
Hoofdstukken 3 en 4: Een dynamisch model van een magnetar

De hoofdstukken 3 en 4 vormen de hoofdmoot van dit proefschrift. In deze hoofdstukken worden de relevante natuurkundige elementen samengevoegd om zo tot een dynamisch model van een magnetar te komen. Dit wil zeggen dat het model in het bijzonder dient om de bewegingen, dus trillingen, van een magnetar te kunnen nabootsen in de computer. De kunst daarbij is om uit deze ingewikkelde mix van natuurkundige bouwstenen (magnetische velden, supervloeistof, vaste korst etc.) een zekere eenvoud en essentie te ontdekken. Immers, wanneer men een probleem tot zijn essentie weet te reduceren, verkrijgt men het grootste inzicht.

In de loop van de jaren zijn er diverse groepen onderzoekers geweest die het probleem van magnetaroscillaties benaderd hebben door middel van de zogenaamde 'brutekrachtmethode'. Deze benadering houdt in dat men een zo realistisch mogelijk model van een magnetar samenstelt, om deze vervolgens te laten doorrekenen met zeer geavanceerde computercodes die vele subtiele fysische processen integraal in rekening nemen. Alhoewel men op die manier zeer indrukwekkende resultaten heeft weten te bereiken, is het probleem van deze benadering dat het in het algemeen moeilijk is om deze goed te interpreteren. De computer geeft immers geen tekst en uitleg, alleen het resultaat.

In dit opzicht vormt het werk dat gepresenteerd wordt in de hoofdstukken 3 en 4 een aanvulling op de 'brutekrachtmethode' in de zin dat het een belangrijk inzicht biedt in de fysische processen die ten grondslag liggen aan het probleem. Daarbij wordt in deze hoofdstukken een alternatief rekenkundig model voor magnetaroscillaties gegeven dat niet onderdoet voor de meer geavanceerde computercodes. De essentie en de kracht van deze methode is dat het, in tegenstelling tot andere benaderingen, de magnetar ontbindt in losse onderdelen en deze individueel analyseert alvorens de afzonderlijke componenten weer samen te voegen. Zo worden de trillingen van de korst afzonderlijk berekend, evenals de trillingen van vele individuele magnetische veldlijnen in de kern van de ster. Vervolgens worden de korst en de magnetische veldlijnen weer samengevoegd en worden hun wederzijdse interacties berekend. Men kan de magnetar dus opvatten als een collectie oscillerende onderdelen die aan elkaar gekoppeld zijn. In figuur 8 is dit principe schematisch uitgebeeld als een grote slinger (korst van de ster) die gekoppeld is aan een groot aantal kleine slingers (magnetische veldlijnen). Aangezien het relatief eenvoudig is om de bewegingen van een systeem van gekoppelde oscillatoren te berekenen, biedt het rekenkundig model van de hoofdstukken 3 en 4 het grote voordeel dat deze het mogelijk maakt om lange en zeer nauwkeurige simulaties van magnetars uit te voeren, zonder dat dit de computer té veel tijd kost. Bovendien zijn bepaalde karakteristieke eigenschappen van een trillende magnetar intuïtief te begrijpen in termen van de trillingen van zijn losse onderdelen, namelijk de korst en het magnetisch veld.

Hoe werkt deze interactie tussen de trillende korst en magnetische kern van de ster? Om het antwoord op deze vraag te begrijpen is het van belang om een intuïtief begrip te hebben van de aard van magnetisme. Uit de dagelijkse praktijk weet men dat de magnetische eigenschappen van een materiaal samenhangen met het vermogen van dit materiaal om elektrische stroom te geleiden. Zo wordt een stuk ijzer (geleider van stroom) sterk aangetrokken tot een magneet, terwijl een stuk plastic (elektrische isolator) geen kracht voelt. De magnetische kracht is in werkelijkheid niets anders dan de aantrekking (of afstoting) van stromen elektrisch geladen deeltjes die zich in een materiaal



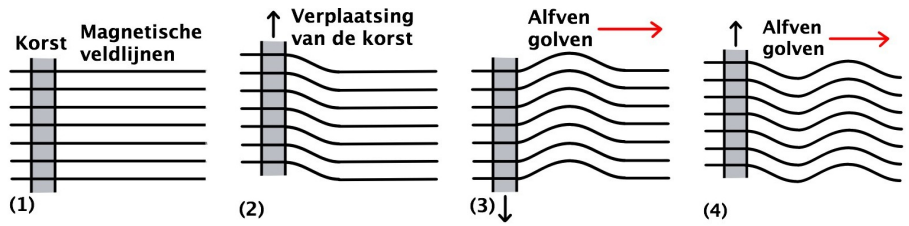
Figuur 8: *Trillingen van een magnetar zijn te vergelijken met de bewegingen van een grote slinger, die de korst van de ster voorstelt en die gekoppeld is aan een groot aantal kleinere slingers, die de magnetische veldlijnen voorstellen. Wanneer de korst (grote slinger) in beweging wordt gebracht, trekt deze de magnetische veldlijnen (kleine slingers) mee, die op hun beurt beginnen te slingeren, ieder op zijn karakteristieke snelheid (kortere magnetische veldlijnen slingeren/trillen van nature sneller dan langere veldlijnen). De trillende veldlijnen beïnvloeden op hun beurt de beweging van de korst.*

bevinden. Zo is het ook in een magnetar, waar zeer sterke elektrische stromen een gigantisch sterk magnetisch veld voortbrengen (een voorbeeld van een magnetisch veld van een magnetar is gegeven in figuur 4). De magnetische krachten die zo ontstaan, houden de geladen deeltjes die in de ster voorkomen, voornamelijk elektronen en protonen, als het ware in een houdgreep. Deze deeltjes kunnen namelijk vrij bewegen langs de magnetische veldlijnen, maar ondervinden een sterke magnetische tegenkracht wanneer ze hiervan afwijken en zijn op deze manier gebonden aan de veldlijnen als kralen aan een ketting. Dit effect is bijzonder sterk in neutronensterren, die uitstekende elektrische geleiders zijn[1]. Het gevolg is tevens dat de magnetische veldlijnen gebonden zijn aan de vaste materie van de korst en de vloeibare materie van de kern van de ster. Wanneer de korst in beweging komt worden de veldlijnen, zowel in de korst als in de kern, meegetrokken. Deze veldlijnen gedragen zich min of meer als de gespannen snaren op een gitaar en worden door de snelle

[1] Zoals al eerder is opgemerkt voorspelt de theorie dat de protonen in neutronensterren een supergeleider vormen. Supergeleiders geleiden elektrische stroom zonder weerstand, zodat de protonen zeer sterk gebonden zijn aan de magnetische veldlijnen.

beweging van de korst aan het trillen gebracht (zie figuur 9), ieder op zijn eigen, karakteristieke trillingssnelheid. Deze magnetische golven verplaatsen zich langs de magnetische veldlijnen door ster, komen na korte tijd aan de andere kant van de ster aan bij de korst en leveren op hun beurt weer een sterke trekkracht die de beweging van de korst weer beïnvloedt. Op deze manier ontstaat er een ingewikkeld samenspel tussen de bewegingen van de korst en die van de magnetische veldlijnen in de kern van de ster. Het uiteindelijke resultaat in de meeste gevallen, is dat de korst zijn bewegingsenergie op vrij korte termijn overdraagt aan de magnetische sterkern en zijn initiële trillingssnelheid verliest. In plaats daarvan wordt de beweging van de korst vrijwel geheel bepaald door de bewegingen van de vele magnetische veldlijnen. Een belangrijk punt hierbij, is dat deze magnetische veldlijnen allemaal een unieke trillingssnelheid hebben die variëert van veldlijn tot veldlijn. Het gevolg is dat de korst op een willekeurig moment in verschillende richtingen getrokken wordt door de veldlijnen. Deze tegengerichte krachten tellen op tot een nettokracht van vrijwel nul en het resultaat is dat de korst vrijwel tot stilstand komt. Dit principe wordt in vaktermen ook wel *resonante absorptie* of *Landau damping* genoemd en vormt de belangrijkste eigenschap van magnetar oscillaties. Deze *resonante absorptie* vindt alleen plaats wanneer de trillingssnelheid van de korst gelijk is (in resonantie is) aan de trillingssnelheid van een aantal magnetische veldlijnen in de kern van de ster. Als dit niet het geval is, dempt de trilling van de korst niet of nauwelijks. Dit leidt tot de conclusie dat de verschillende waargenomen trillingen (QPO's) in feite duiden op de afwezigheid van magnetische veldlijnen met overeenkomende trillingssnelheden.

De resultaten van het rekenkundig model dat in de hoofdstukken 3 en 4 beschreven wordt, alsmede de numerieke resultaten van andere groepen wetenschappers, geven een gedeeltelijke verklaring voor de waargenomen oscillaties van magnetars. Een aantal van de sterkste 'quasi periodieke oscillaties' komt zeer goed overeen met de uitkomst van numerieke berekeningen. Er is echter een klein aantal uitzonderingen op dit positieve resultaat. Met name de zeer 'snelle' QPO's, de waargenomen trillingen met de hoogste trillingssnelheden, lijken moeilijk verklaard te kunnen worden met het model. Dit kan



Figuur 9: *Hoe ontstaan magnetische golven (Alfvéngolven) in het interne van een magnetar? In deze vier plaatjes wordt schematisch afgebeeld hoe bewegingen in de korst van een magnetar magnetische golven lanceren in de ster. De plaatjes laten een close-up zien van een deel van de korst en een aantal magnetische veldlijnen.* (**1**) *Zowel de korst als de magnetische veldlijnen zijn in een rusttoestand. Op een gegeven moment* (**2**) *raakt de korst in beweging. Doordat de magnetische veldlijnen vastzitten aan de korst, worden deze meegetrokken wanneer de korst zich verplaatst. De korst schudt heen en weer en veroorzaakt magnetische (Alfvén)golven die zich langs de veldlijnen in het binnenste van de ster voortplanten* (**3**) *en* (**4**).

erop duiden dat de huidige ideeën over de interne structuur van magnetars aangepast moeten worden. De berekeningen zijn immers gebaseerd op een gedetailleerd stermodel, waar op zich nog enige onzekerheid over bestaat. Zo is het goed mogelijk dat de huidige aannames over de structuur van de binnenste kern van neutronensterren niet correct zijn en het is daarom van groot belang in de toekomst alternatieve stermodellen te bestuderen.

Curriculum Vitae

Op 7 juni 1981 kwam ik ter wereld in het Academische Ziekenhuis van Leiden (tegenwoordig LUMC) op enkele steenworpen afstand van de huidige Sterrewacht. Ik bracht mijn jeugd door in het mooie dorpje Valkenburg (ZH), waar toegewijde basisschoolmeesters en -juffen mij, zo goed als zij konden, de basisprincipes van de taal en het rekenen bijbrachten. Op mijn twaalfde jaar zette mijn schoolcarrière voort op het atheneum van het Andreas College te Katwijk, alwaar ik een interesse ontwikkelde voor de exacte vakken. Na het VWO eindexamen van 1999 besloot ik de studie sterrenkunde in Leiden te gaan volgen.

Tijdens de studietijd in Leiden was ik actief lid van de studentenverenigingen K.S.R.V. Njord en L.V.V.S. Augustinus en was ik een jaar bestuurslid van het L.A.D. Kaiser. Onder leiding van Prof. dr. Huub Röttgering werkte ik met WSRT data van het cluster Abell 2256 op lage radiofrequenties. Tijdens dit onderzoek kreeg ik de kans om ervaring op te doen in Socorro, New Mexico, alwaar ik met Dr. Chris Carilli GMRT data van radiosterrenstelsels op hoge roodverschuiving analyseerde. Mijn afstudeeronderzoek deed ik onder leiding van Dr. Yuri Levin, over getijdeninteracties tussen hoofdreekssterren en massieve zwarte gaten.

Na het behalen van mijn doctoraalexamen in 2007, begon ik aan mijn promotieonderzoek op het onderwerp van magnetar oscillaties onder supervisie van Dr. Yuri Levin aan de Sterrewacht Leiden en het Lorentz Instituut. Gedurende drie jaar tijdens mijn promotieonderzoek was ik onderwijsassistent bij het college *Inleiding Astrofysica* dat gegeven werd door professor Frank Israel. Ik bezocht verschillende conferenties en workshops in buiten- en binnenland, waaronder verschillende *Nederlandse Astronomen Conferenties*, *Conference*

on Helioseismology, Asteroseismology and MHD Connections in Göttingen, *ILIAS-GW meeting* in Tübingen, *IAU General Conference* in Rio de Janeiro, *NORDITA workshop on Neutron Stars* in Stockholm en *Winter School in Theoretical Physics* in Jeruzalem. Op verschillende van deze gelegenheden heb ik mijn werk mondeling gepresenteerd. Ik bracht ruim acht maanden door als bezoeker op Monash University in Melbourne, de nieuwe werkplek van mijn supervisor.

Ik hoop in de nabije toekomst mijn wetenschappelijke carrière voort te zetten in de theoretische astrofysica.

Nawoord

Deze laatste bladzijden wil ik gebruiken om de mensen te bedanken die voor mij belangrijk zijn geweest bij de totstandkoming van dit proefschrift. Ik heb de afgelopen jaren met veel plezier op de Sterrewacht gewerkt en ben me steeds meer gaan realiseren dat het een groot voorrecht is om deel uit te maken van een instituut dat zo rijk is aan historie, diversiteit en bovenal kwaliteit. Dit alles heeft mijn studie- en promotieperiode tot een prettige en verrijkende ervaring gemaakt.

Dat de Sterrewacht zo'n soepele machine is, is met name te danken aan een toegewijde support staff. Ik wil hiervoor het secretariaat bedanken: Kirsten, Jeanne, Liesbeth en Anita, bedankt! Een instituut als de Sterrewacht kan niet zonder een stabiel draaiend computersysteem. Erik, David, Tycho, Aart en Niels, buiten het feit dat jullie achter de schermen bergen werk verzetten, staan jullie altijd voor iedereen klaar die vragen of computerproblemen heeft. Zonder jullie hulp was er niets van dit proefschrift terechtgekomen. Ik wil Jan en Evelijn bedanken voor hun niet aflatende behulpzaamheid bij financiële zaken.

Ik heb de afgelopen jaren met heel wat mensen een kamer gedeeld: Raymond, Rogier, Ernst, Mario, Maryam, Sweta, Rafael, Mehdi, Rowin en Lynn, bedankt voor jullie dagelijkse gezelschap. Raymond, Ernst en Reinout, de regelmatige lunches en koffiepauzes waren altijd een prettige afleiding van het werk, waarvoor dank! Verscheidene malen heb ik mogen genieten van de welbekende Lub-sigaar. Jan, Frank, Franco, Jelle, Remco, Edo en Rowin, het was een eer! Ik hoop dat deze traditie tot in lengte van dagen voortgezet zal worden.

Of course the theory group: Clovis, Evgenii, Richard, Anders, Dan, Ann-

Marie, Rutger and the numerous MSc students and guests. Your doors were always wide opened for questions and discussions. You guys gave color to the weekly group meetings, and always turned them into a valuable learning experience. In particular I want to thank Rutger and Ann-Marie for the awesome time in Melbourne. Ozzies and Kiwi's: Mario, Jeremy, Elliot, Wan, Katie, Nadia, Jay, Martijn, I will never forget the morning breaks, lunches, dinners, parties, hangovers, morning breaks and lunches that I shared with you. Amanda and Alex, I'm grateful for the time I spent in your company. I could not have asked for better house mates, thank you for making me feel at home. I thank the Levin family for their warm hospitality. I enjoyed the many conversations and fantastic dinners at your home! Of course, my extensive visit to Australia would not have been possible without the hospitality of the Monash School of Physics, at which a significant part of my PhD research was done. I'm especially grateful to Jean Pettigrew and Michael Morgan for their help, and to the astrophysics group for organizing inspiring group meetings and seminars.

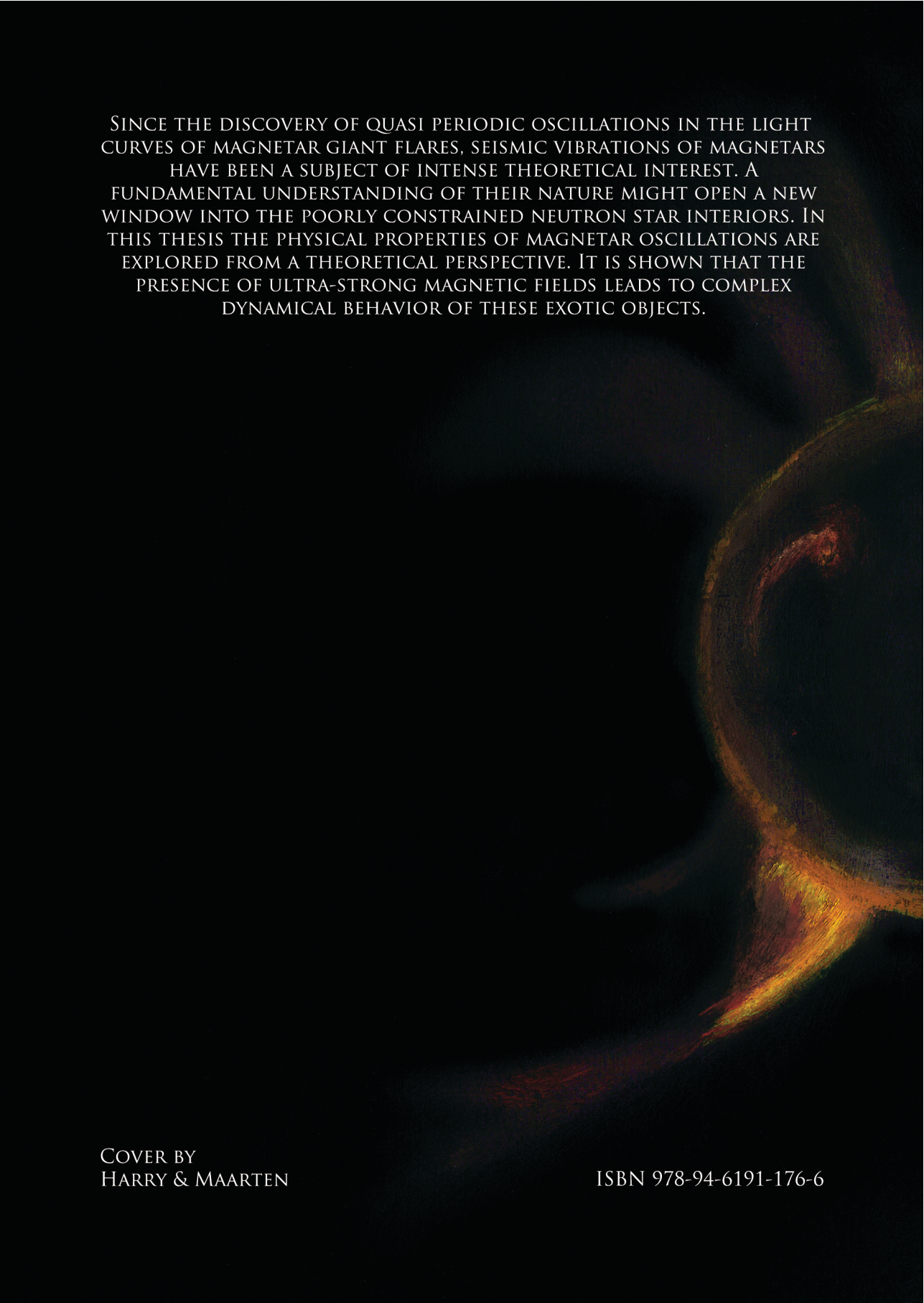
Verder wil ik de vele vrienden bedanken die mij de afgelopen jaren een mooie tijd bezorgd hebben: oud-huisgenoten, cordialgenoten en Valkenburgers. In het bijzonder ben ik dank verschuldigd aan Harry, mijn goede matti en oud-huisgenoot waarmee ik menig nachtelijk uur schilderend en/of filosoferend heb doorgebracht. De cover is s*ck geworden. Thanks! En Rick, mijn beste vriend sinds jaar en dag. Hij heeft zijn kritische, literaire oog laten schijnen over mijn nederlandstalige samenvatting. Duizend dank!

Ik wil mijn ouders, m'n zusjes en broeder bedanken voor hun onvoorwaardelijke steun en liefde. Het lukt jullie altijd weer om me met beide benen op de grond te zetten en dat is soms nodig ook! Ik kan me geen betere familie voorstellen.

En last but not least Gwen. Je hebt me meer gemotiveerd dan je denkt. We gaan een mooie toekomst tegemoet samen! X

Maarten van Hoven
Leiden, januari 2012

Since the discovery of quasi periodic oscillations in the light curves of magnetar giant flares, seismic vibrations of magnetars have been a subject of intense theoretical interest. A fundamental understanding of their nature might open a new window into the poorly constrained neutron star interiors. In this thesis the physical properties of magnetar oscillations are explored from a theoretical perspective. It is shown that the presence of ultra-strong magnetic fields leads to complex dynamical behavior of these exotic objects.



Cover by
Harry & Maarten

ISBN 978-94-6191-176-6